



Spring 2008

Characterizing Surface Deformation from 1981 to 2007 on Mount Baker Volcano, Washington

Brendan E. Hodge

Western Washington University, brendan.hodge@gmail.com

Follow this and additional works at: <https://cedar.wwu.edu/wwuet>



Part of the [Geology Commons](#)

Recommended Citation

Hodge, Brendan E., "Characterizing Surface Deformation from 1981 to 2007 on Mount Baker Volcano, Washington" (2008). *WWU Graduate School Collection*. 666.

<https://cedar.wwu.edu/wwuet/666>

This Masters Thesis is brought to you for free and open access by the WWU Graduate and Undergraduate Scholarship at Western CEDAR. It has been accepted for inclusion in WWU Graduate School Collection by an authorized administrator of Western CEDAR. For more information, please contact westerncedar@wwu.edu.

CHARACTERIZING SURFACE DEFORMATION FROM 1981
TO 2007 ON MOUNT BAKER VOLCANO, WASHINGTON

BY

BRENDAN E. HODGE

Accepted in Partial Completion
of the Requirements for the Degree
Master of Science

~~_____~~
Moheb A. Ghali, Dean of the Graduate School

ADVISORY COMMITTEE

~~_____~~
Chair, Dr. Juliet G. Crider

~~_____~~
Dr. Jackie Caplan-Auerbach

~~_____~~
Dr. Pete Stelling

MASTER'S THESIS

In presenting this thesis in partial fulfillment of the requirements for a master's degree at Western Washington University, I agree that the Library shall make its copies freely available for inspection. I further agree that copying of this thesis in whole or in part is allowable only for scholarly purposes. It is understood, however, that any copying or publication of this thesis for commercial purposes, or for financial gain, shall not be allowed without my written permission.

Signature _____

Date

3/24/08

MASTER'S THESIS

In presenting this thesis in partial fulfillment of the requirements for a master's degree at Western Washington University, I grant to Western Washington University the non-exclusive royalty-free right to archive, reproduce, distribute, and display the thesis in any and all forms, including electronic format, via any digital library mechanisms maintained by WWU.

I represent and warrant this is my original work, and does not infringe or violate any rights of others. I warrant that I have obtained written permissions from the owner of any third party copyrighted material included in these files.

I acknowledge that I retain ownership rights to the copyright of this work, including but not limited to the right to use all or part of this work in future works, such as articles or books.

Library users are granted permission for individual, research and non-commercial reproduction of this work for educational purposes only. Any further digital posting of this document requires specific permission from the author.

Any copying or publication of this thesis for commercial purposes, or for financial gain, is not allowed without my written permission.

Brendan Hodge
February 23, 2018

**CHARACTERIZING SURFACE DEFORMATION FROM
1981 TO 2007 ON MOUNT BAKER VOLCANO,
WASHINGTON**

A Thesis
Presented to
The Faculty of
Western Washington University

In Partial Fulfillment
of the Requirements for the Degree
Master of Science

By

Brendan E. Hodge

March 2008

Abstract

Surface deformation studies at active volcanoes are used to detect changes to magmatic source regions beneath the volcano. At Mount Baker, Washington, continued elevated gas (CO_2 and H_2S) and heat flux from fumaroles in Sherman Crater indicate the presence of a degassing magma reservoir. Campaign geographic positioning system surveys in 2006 and 2007 provide slope distance measurements of all 19 trilateration lines on Mount Baker. These data are compared with previous slope distance measurements acquired in 1981 and 1983 with electronic distance measurement. The results indicate that surface deformation has occurred on Mount Baker during the last quarter century. Slope distances have predominantly shortened around the edifice at rates of less than 2 mm/yr. The greatest slope length change detected (HDLY-RSVT) is -17 ± 4 ppm on the northern flank of the volcano. A nonlinear least-squares regression fits a uniform surface strain-rate model to the weighted slope change data. The strain model results indicate contractional strain accumulation on Mount Baker with an areal dilation rate of -420 ± 140 nanostrain/yr. The observed strain-rate is distinctly different, by at least an order of magnitude, than the expected regional secular strain-rate from tectonic sources.

Elastic dislocation models are used to invert for the location, and strength of a point source at depth. The inversion uses a discrete grid search to find the global minimum of the residuals from a nonlinear least squares algorithm. The optimal model predicts a volume change of $-11 \times 10^6 \text{ m}^3$, located 1500 meters east-northeast of the summit at a depth of 5.4 km (MSL). However, the global minimum is not well defined, resulting in a wide range of suitable source parameters. The model can account for much of the deformation detected, indicating that a spherical source model is appropriate, at least to a first order, for modeling physical changes to the magmatic or hydrothermal system at Mount Baker. These results suggest that the magmatic and hydrothermal system at Mount Baker has depressurized, likely from the combined result of cooling, mass loss, and/or densification, since 1981. This study also provides a new baseline for precise geodetic study of ongoing quiescent degassing at Mount Baker.

Acknowledgments

I thank Juliet Crider for her support of this project, her many helpful discussions and reviews, and for fostering my scientific interests in any way she could. I thank my committee members Jackie Caplan-Auerbach, and Pete Stelling for their reviews and discussions on this thesis. Mike Lisowski gave guidance through the old world of EDM geodesy into the modern world of GPS geodesy and I thank him for processing my GPS data. I thank Mike Poland for his mentorship as a volcano geophysicist and for discussions of this work.

Financial support for this thesis was provided by grants from the Geological Society of America, Mazamas, the Geology Department at Western Washington University, and by the USGS Jack Kleinman fellowship for volcano research. This thesis was also supported by an NSF-EAR geophysics program grant to J. Crider for ongoing geophysical study of Mount Baker.

Field work to collect GPS data on a glaciated volcano can be dangerous and exhausting work. Without the assistance of many skilled and spirited people I would still be collecting data, or worse. Thanks to Melissa Park, Troy Baggerman, Kurt Parker, Soren Cunningham, Owen Callahan, William Benton Amos III, Celestine Mercer, Chuck Park, Juliet Crider, and Dave Tucker for their efforts on and off the mountain.

I thank Asta Miklius for code to develop the inverse model. I thank Allen Remple for Matlab advice. David Schmidt and Paul Wallace provided helpful discussions. Dave Tucker gave discussions of all things Baker related. I thank Celestine Mercer for providing me the space to finish writing.

Last but not least, I thank my family for the support they have given me during this project. Finally, I thank my friends, who have made my time in Bellingham an immense amount of fun. I will miss you all in New Zealand. Cheers!

Table of Contents

ABSTRACT	iv
ACKNOWLEDGMENTS	v
LIST OF FIGURES	viii
LIST OF TABLES	ix
1.0 INTRODUCTION	1
1.1 GEOLOGIC BACKGROUND.....	2
1.2 THE 1975 THERMAL EVENT.....	3
1.3 GEOPHYSICAL AND GEOCHEMICAL MONITORING SINCE 1975.....	5
<i>Geodesy</i>	5
<i>Gas geochemistry</i>	6
<i>Gravity</i>	7
<i>Seismicity</i>	7
1.4 PRINCIPLES OF VOLCANO GEODESY.....	7
<i>InSAR geodesy</i>	8
<i>GPS Geodesy</i>	9
1.5 PREVIOUS GEODETIC STUDIES AT VOLCANOES.....	11
<i>What we have learned with geodetic study of stratovolcanoes</i>	12
<i>Designing a good GPS network</i>	14
2.0 DATA COLLECTION AND DATA REDUCTION	21
2.1 THE EDM NETWORK ON MOUNT BAKER.....	21
2.2 2006 AND 2007 CAMPAIGN GPS RESURVEY METHODS.....	22
2.2.1 <i>Benchmark reoccupation procedure</i>	23
2.3 GPS DATA PROCESSING.....	25
2.3.1 <i>Pre-Processing</i>	26
2.3.2 <i>GPS processing</i>	26
2.4 ERROR ANALYSIS.....	27
2.4.1 <i>EDM line length uncertainty</i>	27
2.4.2 <i>GPS line length uncertainty</i>	30
2.5 UNCERTAINTY IN THE EDM TO GPS COMPARISON.....	32
2.6 GPS VECTOR UNCERTAINTY.....	33
3.0 RESULTS OF GPS RESURVEY	46
3.1 GPS LINE LENGTHS.....	46
3.2 EDM-GPS COMPARISON.....	46
3.3 GPS DISPLACEMENT VECTORS.....	47
4.0 TWO-DIMENSIONAL SURFACE STRAIN ANALYSES	52
4.1 PRINCIPLES OF STRAIN AND DEFORMATION.....	52
4.2 REGIONAL STRAIN ACCUMULATION FROM TECTONIC SOURCES.....	54
4.3 CALCULATING SURFACE STRAIN-RATES FROM 1981 TO 2007.....	56

4.3.1	<i>Mount Baker surface strain rate uncertainty estimation</i>	56
4.3.2	<i>Calculating the surface strain-rate tensor</i>	57
4.4	RESULTS OF SURFACE STRAIN MODEL	58
4.5	DISCUSSION OF SURFACE STRAIN MODEL	59
5.0	MODELING THE SOURCE OF DEFORMATION	66
5.1	ANALYTICAL ELASTIC DISLOCATION SOLUTIONS	67
5.1.1	<i>The point source model and reference system</i>	68
5.1.2	<i>Topographic correction for analytical models</i>	69
5.2	MODEL INVERSION.....	72
5.2.1	<i>Introduction to inverse models</i>	72
5.2.2	<i>Inversion methods for Mount Baker data</i>	73
5.3	INVERSION MODEL RESULTS.....	77
6.0	INTERPRETATION AND DISCUSSION	89
7.0	CONCLUSIONS	97
7.1	FUTURE MONITORING AND GEODETIC STUDY OF MOUNT BAKER	98
8.0	REFERENCES.....	102
9.0	APPENDICES.....	112
A.	MOUNT BAKER CAMPAIGN GPS FIELD GUIDE	112
B.	DIGITAL RESOURCES (ON COMPACT DISC)	124
B.1.	<i>Raw and processed GPS data</i>	124
B.2.	<i>Matlab code used in this thesis</i>	124
B.3.	<i>GIS data</i>	124
B.4.	<i>Copies of figures and thesis</i>	124
B.5.	<i>Field Notes</i>	124
10.	CURRICULUM VITAE.....	125

List of Figures

1.1	Location of Mount Baker in the Cascades arc.....	17
1.2	Interferogram of Mount Baker.....	18
1.3	Trilateration network on Mount Baker.....	19
1.4	Map of existing and proposed benchmarks on Mount Baker.....	20
2.1	In-situ EDM and GPS benchmark examples.....	41
2.2	View of Mount Baker and campaign GPS survey set-up.....	42
2.3	Deming resurvey plot.....	43
2.4	Time series plot of Mount Baker campaign sites.....	44
2.5	Time series plot of regional continuous GPS sites.....	45
3.1	Line length changes from 1981 to 2007.....	50
3.2	GPS velocity plot for repeat GPS surveys on Mount Baker.....	51
4.1	Strain accumulation from 1981 to 2007 on Mount Baker.....	63
4.2	Surface strain rate tensor model results.....	64
4.3	Surface strain rates in Cascadia.....	65
5.1	Coordinate system for elastic dislocation model.....	81
5.2	Analytical solution for a point source.....	82
5.3	Misfit plots.....	83
5.4	Histograms of returned optimal parameter values.....	84
5.5	Reduced Chi square values for model.....	85
5.6	Covariance plots for parameter estimates.....	86
5.7	Comparison of point source model to the observational data.....	87
5.8	Model residuals and observation uncertainties.....	88

List of Tables

2.1	Mount Baker GPS station names and survey times.....	35
2.2	EDM line length measurements.....	36
2.3	GPS determined line length measurements.....	37
2.4	Estimated GPS survey site errors.....	38
2.5	Line-length changes from 1981 to 2007.....	39
2.6	GPS station velocities.....	40
4.1	Surface strain tensor results.....	62
5.1	Optimal model parameters and confidence intervals.....	80

1.0 Introduction

Knowledge of volcanic systems has improved greatly over the past few decades because of the implementation of geodetic studies at active volcanoes (Dzurisin, 2003). Surface deformation studies can reveal important physical constraints on evolving magmatic systems and provide important precursory indicators to volcanic eruptions. At Mount Baker in northern Washington, persistent CO₂ and H₂S gas emissions from fumaroles in Sherman Crater and the Dorr fumarole field indicate a magmatic source at depth. A recent thermal event, which produced elevated gas and heat flux from Sherman Crater in 1975, may indicate the onset of renewed magmatic activity beneath Mount Baker (Frank et al., 1977). Here I present the results of a surface deformation study, which employed portable GPS instruments to collect a modern geodetic dataset at Mount Baker. I compare these data to the previous trilateration survey from 1981 and 1983, to determine a cumulative measure of deformation on Mount Baker since that time. I use an elastic dislocation model to guide interpretations of the source of deformation beneath Mount Baker. The observed deformation is placed in context with other geophysical observations to help interpret the potential magmatic and hydrothermal mechanisms driving unrest at Mount Baker. The results of this study also provide a new baseline for future geodetic monitoring of continued activity at Mount Baker.

1.1 Geologic background

Mount Baker is one of more than a dozen Pleistocene stratovolcanoes in the Cascade magmatic arc of western North America produced by oblique convergence of the Juan de Fuca oceanic plate subducting beneath the North American plate (**Figure 1.1**). The volcano is located 50 km east of Bellingham, Washington, and within sight of the metropolitan areas of Seattle, Washington, and Vancouver, British Columbia. With the exception of Mt. St. Helens, Mount Baker is considered to be the most active volcano in the Cascade arc (Scott et al., 2003). The modern Mount Baker stratovolcano is one of a number of eruptive centers that compose the Mount Baker volcanic field, including: the 3.7 Ma Hannagen Caldera (Tucker et al., 2007), the 1.15 Ma Kulshan Caldera (Hildreth, 1996), and the extinct 0.5 -0.3 Ma Black Buttes stratovolcano (Hildreth et al., 2003). The late Pleistocene composite cone of Mount Baker is thought to be one of the youngest vents in the Cascades, with the majority of edifice construction occurring after 40 ka (Hildreth et al., 2003). Bulk geochemistry on lava flows and breccia deposits indicates that Mount Baker is composed almost entirely of andesite, with few (less than 3%) rocks of other compositions (Hildreth et al., 2003). The volcanic field has been built on a non-volcanic assemblage of mostly Mesozoic meta-sedimentary and plutonic rocks typical of North Cascade terranes (Tabor et al., 2003).

Mount Baker has remained magmatically inactive for most of the Holocene, with the exception of several notable events. An early Holocene extrusive event produced pyroclastic flows, ash and debris flows that moved down Boulder Creek valley (Hyde and Crandell, 1978). Near this same time, a monogenic basaltic cinder cone eruption on the southern flank of the volcano producing tephra fall and lava flows that extended into the

Baker River drainage (Scott et al., 2001). The most recent documented magmatic eruption occurred around 6.5 ka (calibrated radiocarbon years) and came from the currently active Sherman Crater, as indicated by tephra deposits found around the volcano (Scott and Tucker, 2003). More recently, historical accounts indicate that phreatic eruptions have occurred in the mid 19th century from Sherman Crater, which may indicate the start of a new eruption cycle that includes the more recent thermal event of 1975 (Tucker and Scott, 2006).

Late Pleistocene glacial activity has influenced the regional morphology, creating steeply incised glacial valleys that bound the volcano to the north and south. Over a dozen high alpine glaciers cling to the slopes of Mount Baker. The glaciers are dissected by isolated ridges of rock, which are the primary exposures high on the volcano and the location of many of the geodetic benchmarks. Currently, the glacial mass at Mount Baker is second only to Mount Rainier in the Cascades, with a total ice and snow volume of 1.8 km³ (Gardner et al., 1995). The lower elevation flanks of Mount Baker are typically steep and heavily vegetated, providing few outcrops, a dense canopy, and thereby complicating GPS geodesy.

1.2 The 1975 thermal event

In March 1975, large steam plumes emitted from Sherman Crater were seen from Bellingham and the surrounding areas. In response to the renewed activity, the U.S. Geological Survey (USGS) began to monitor Mt. Baker closely with geodetic, seismic, gravity, petrography, and hydro-geochemical studies (Bortleson et al., 1977; Malone and Frank, 1976; Radke et al., 1976). A microgravity survey was conducted between May

1975 and October 1976, which revealed a decrease in gravity (~ 0.33 mgal) beneath Sherman Crater (Malone, 1979). The gravity decrease was interpreted by Malone (1979) to be resulting from loss of mass due to degassing. However, this could not be confirmed because of the lack of geodetic constraints at the crater, which are necessary to rule out inflation as a cause for a decreased gravity signal.

Between July and August 1975, a survey of three spirit-level sites found a slight tilt away from the volcano at two sites (Frank et al., 1977). In August 1975, two continuous borehole tiltmeters were installed at the leveling sites. Continuous monitoring of the tilt sites between August and December 1975 revealed a slight tilt toward the volcano (Frank et al., 1977). These contradicting results and low deformation signal led the USGS to conclude that surface deformation was not significant during that time. One permanent seismometer deployed in 1972 measured no significant seismic activity before and during the thermal event (Frank et al., 1977). Five temporary seismometers installed in the summer of 1975 recorded only one local (ML ~ 1) earthquake, occurring after the 1975 thermal event (Frank et al., 1977).

The rate of steam and gas emissions increased in March 1975, and ejecta deposits were sampled from the glaciers surrounding the crater (Frank et al., 1977). Aerial measurements detected a three-fold increase in the area of thermal emission within Sherman Crater, which culminated in a large, boiling melt-water lake (Frank et al., 1977). Fumarole temperatures increased from 90°C to 128°C and the total heat flux was estimated to have increased from 8 Wm^{-2} before 1975 to 150 Wm^{-2} during the thermal event (Frank et al., 1977). Pyrite particulates were found in the ejected tephra, indicative of hydrothermal remineralization (Frank et al., 1977). However, despite these

observations, petrographic analysis of the 1975 ejecta revealed no evidence of juvenile magma (Frank et al., 1977).

1.3 Geophysical and geochemical monitoring since 1975

Since the 1975 thermal event, geophysical monitoring has occurred intermittently by a few workers, which I summarize here. The only continuous monitoring has been from a single short period seismometer (MBW) operated by the Pacific Northwest Seismic Network, located 5 km west of Mount Baker.

Geodesy

In the early 1980's, the newly founded U.S. Geological Survey Cascade Volcano Observatory (CVO) began a comprehensive volcano monitoring initiative on all major Cascade volcanoes, including geodetic study of Mt. Baker (Chadwick et al., 1985). Electronic distance measurement (EDM) techniques were used to measure line-of-sight distances between stations in the trilateration network (**Figure 1.2**). The results of the initial EDM surveys in 1981 and 1983 found no resolvable surface deformation exceeding EDM errors (Chadwick et al., 1985). This initial dataset provides the baseline that I use in this thesis to characterize surface deformation on Mount Baker since 1981.

In the summer of 2004, a pilot GPS study reoccupied three benchmark stations and determined that two other marks were in good condition (Parker, 2005). The results of this survey determined that one trilateration line (HDLY-THND) had shortened by 6 ± 3 cm over the 22 year period since the EDM survey (Parker, 2005). This effort

determined that a GPS survey was feasible with the equipment available and that detectable surface deformation had occurred since 1981.

Gas geochemistry

Airborne gas measurements indicate that emission rates have decreased from 273 to 187 tonnes/day of carbon dioxide (CO₂) and from 12 to 5.5 tonnes/day of hydrogen sulfide (H₂S) between 1975 and 2001 (McGee et al., 2001). Flux estimates from August 2007 indicate continued degassing of CO₂ (150 tonnes/day minimum) and H₂S (0.5 tonnes/day minimum) at rates comparable to 2001 rates (McGee pers. comm., 2007). These data indicate that gas flux has decreased since 1975 and may now be in a steady state.

Surface expressions of the active hydrothermal system beneath Mount Baker include steaming ground, hot springs, and boiling fumaroles in Sherman Crater and the Dorr Fumarole field (Symonds et al., 2003). Sherman Crater gas samples from 1978 and 1991 show elevated helium isotope ratios (³He/⁴He) of 7.61 and 7.70 respectively, indicative of fresh degassing magma at depth (Symonds et al., 2003). At the time, these were the highest helium isotope ratios of any volcano in the Cascade Range (Symonds et al., 2003). The absence of SO₂ from fumarole gas suggests that the system is being scrubbed by groundwater beneath Mount Baker, presenting no dry pathways to the surface (Cynthia Werner, pers. comm., 2007). Additionally, gas-geothermometry equilibrium temperatures of 220-240° C are consistent with active hydrothermal systems at other active volcanoes (Werner et al., 2007).

Gravity

A recently-completed gravity survey has revealed an increase in relative gravity of 1813 ± 361 μgal between 1975 when the first gravity survey was conducted, and 2006 (Hill et al., 2006). A gravity model indicates that the relative gravity increase can be explained by a shallow (< 1 km) sphere or a deeper cylindrical source. However, these data are sparse and much of the gravity change may be related to non-volcanic sources, such as snow mass and ground water variations (Hill, 2007). Like the original gravity survey, the lack of geodetic control precludes isolation of these hypotheses.

Seismicity

Seismic activity around Mt. Baker has been relatively low compared to other Cascade volcanoes (Moran, 2004), suggesting that magma movement, if any, has occurred aseismically. A temporary broadband seismic array deployed on Mount Baker in the summer of 2007 detected several deep long period events (Caplan-Auerbach et al., 2007). Seismic activity of this type is often interpreted as an indicator of magma movement at depth (Power et al., 2005).

1.4 Principles of volcano geodesy

Historically, geodetic studies relied on ground-based surveying techniques, such as leveling lines, dry tilt, and trilateration surveys (Dzurisin, 2003) like those used on Mount Baker in 1981 and 1983 (Chadwick et al., 1985). Over the past decade or so, the advent of space-based geodesy has provided significant advancements in the spatial and temporal resolution of geodetic data on volcanoes. The two most notable examples,

which have been widely employed with success, are global positioning systems (GPS) and interferometric synthetic-aperture radar (InSAR). The integration of ground-based and space-based geodetic techniques have provided scientists with a more complete spatial and temporal picture of what has happened around active and quiescent volcanoes before, during and after eruptions (Dzurisin, 2003).

InSAR geodesy

Interferometric synthetic aperture radar (InSAR) is a satellite-based remote sensing technology that has proven useful for monitoring deformation on a diverse range of active and quiescent volcanoes, including dangerous volcanoes without ground based geodetic monitoring (Lu et al., 2005; Lu et al., 2002b; Pritchard and Simons, 2002).

InSAR is capable of producing a spatially continuous image of ground surface change on the order of about 2-3 cm (Dzurisin, 2003). Thus, by comparing InSAR images over many years, a semi-continuous time series of deformation strength may be determined.

Currently, a significant factor limiting InSAR study is the difficulty to achieve a coherent interferogram in areas of dense vegetation, steep topography, and snow cover variations, a situation common at many volcanoes (Dzurisin, 2007). Advances in processing techniques, e.g. persistent scatterers, and longer wavelength SAR images may eliminate many of these limitations (Hooper et al., 2004). Additionally, InSAR is limited in its ability to measure deformation in only one direction: the component of surface displacement that is line-of-sight to the satellite flight path (Zebker et al., 2000), which has implications for interpreting the deformation source (Dzurisin, 2007). However, this emerging technology may soon be capable of measuring three dimensional deformations (Wright et al., 2004), which will greatly aid interpretations of unrest at active volcanoes.

A SAR interferogram has been produced for Mount Baker spanning the summer of 1997 and 1998 (Michael Poland, unpublished data, 2005). **Figure 1.3** shows a mostly incoherent scene from two ERS-1 images. The cause of incoherence is likely due to thick vegetation, steep slopes, and glaciated terrain on the volcano (Michael Poland, pers. comm. 2006). Unfortunately, InSAR is not currently possible for Mount Baker, necessitating ground based techniques for deformation study.

GPS Geodesy

Since the early 1990s, GPS has become a widely used tool for volcano geodesy because of the relative ease of deployment, low cost and ability to measure in three dimensions (Dzurisin, 2003; Meertens and Smith, 1991). Another benefit of GPS is that the technique is effective in poor weather conditions, although snow accumulation on the GPS antenna can degrade accuracy (Lisowski et al., in press). The following discussion on GPS fundamentals utilized in this thesis is summarized from Dzurisin (2007). GPS point positions are acquired by triangulating a receiver located on Earth using a constellation of ~32 orbiting satellites. At any time, no fewer than 5 of these satellites are visible to a hemisphere, providing the necessary coverage to calculate a position nearly anywhere on the continent. A GPS receiver requires at least four satellite signals to solve a four-variable time-distance equation. Additional satellite signals help improve the position estimate by reducing noise.

A GPS position is determined by calculating the distance between each satellite, which is in a known orbit, and the receiver location, which is unknown. The receiver calculates the time it takes a signal to get from the satellite to the receiver using a time code, known as pseudo random noise, which is transmitted by the satellites.

Uncertainties in the time path are introduced when these signals are refracted in the atmosphere and reflect off nearby objects (“multi-path”) on the ground. However, in recent years much work has been done to identify and eliminate many of these timing errors (Larson et al., 2007). Numerous GPS data processing algorithms (e.g. Bernese, GAMIT, GYPSY-OASIS II) have been developed to conduct error corrections on GPS data that includes atmospheric, multi path and satellite orbit corrections. With processing, GPS positions can be determined to within a few millimeters in the horizontal uncertainty, and a few centimeters in vertical uncertainty. Geodetic GPS enables the capability to measure three-dimensional movements of points on the Earth’s surface on the order of several millimeters per year.

Two styles of GPS geodesy are commonly deployed on volcanoes: continuous GPS and campaign GPS. Continuous GPS requires a permanent monument that is self sufficient with renewable power sources and data telemetry. The additional equipment and labor makes continuous GPS expensive. The benefit of continuous GPS, however, is that a dense time series of data is produced that can detect a change in the rate and direction of surface displacement in near real time. This is a useful capability on active volcanoes where changes often occur abruptly with little precursory warning (Dzurisin, 2003). A campaign style GPS survey is conducted with periodic reoccupations (with intervals of months, years, or decades) of several benchmarks for only brief periods (minutes to hours), and because of this, campaign GPS loses the temporal resolution provided by continuous GPS. The lower cost of campaign surveys means that this method is often employed to monitor a greater number of stations in a broader area than continuous GPS, and therefore provide greater information on the extent and shape of the

deformation source. Because of this, campaign GPS surveys have been used on active and quiescent volcanoes around the world including: Hekla (Iceland), Augustine (Alaska), Medicine Lake (California), South Sister (Oregon), and Etna (Italy), to name a few (Cervelli et al., 2006; Dzurisin et al., 2006; Houlié et al., 2006; Poland et al., 2006b; Sigmundsson et al., 1992). Ideally, continuous and campaign GPS should be used in tandem to provide the benefits of both monitoring strategies (Dzurisin, 2003). At the time of this work, no continuous geodetic monitoring was occurring on Mount Baker. Because of site and cost limitations, continuous GPS monitoring is unlikely in the near future.

1.5 Previous geodetic studies at volcanoes

When magma is intruded or removed from a volcanic system, the resulting change in volume can cause the ground surface around the volcano to deform (e.g., Dzurisin, 2003). With precise geodetic techniques, small surface changes on volcanoes can be characterized. Modeling provides additional insight into the mechanical sources of the observed deformation (Battaglia et al., 2003b; Dzurisin, 2003; Masterlark and Lu, 2004; Moran et al., 2006). Temporal variations in the location and volume of magmatic systems can provide important constraints on the mechanics of volcanic unrest and eruption (Masterlark and Lu, 2004). Therefore, deformation monitoring has become an important component of volcano study on all types of volcanoes (Dzurisin, 2003). With the proliferation of volcano geodesy, every new volcanic event may provide insight into eruption dynamics at a specific volcano, and similar volcanoes by analogy. Ultimately,

geodetic monitoring will provide a better understanding of volcanic processes and allow for more accurate and effective volcano monitoring and emergency response.

What we have learned with geodetic study of stratovolcanoes

Stratovolcanoes commonly experience long periods of quiescence interrupted by brief eruptions (Dzurisin, 2003). Predicting eruptions has been a major focus for volcano scientists, who have had some success in prediction of volcanic activity at stratovolcanoes on a time scale of a few days to a few months (Dzurisin et al., 1983; Swanson et al., 1983). However, predictive capabilities on much longer time scales remain elusive. One reason for this is the lack of long term geodetic datasets. Prior to 1997, only four volcanoes had deformation records longer than several decades, and none of these data were from stratovolcanoes (Dvorak and Dzurisin, 1997).

The use of geodetic techniques has provided important insight into long-term precursors to volcanic eruptions. One important discovery is that some volcanoes undergo a phase of deep, aseismic magma intrusion over periods of years to decades. For example, a geodetic study at South Sister volcano revealed that between 1995 to 2004, surface deformation with a more-or-less constant rate of 3-5 cm/yr had occurred ~5 km west of the summit with no identifiable seismic signal (Dzurisin et al., 2006). The absence of concurrent seismicity in the region around deforming stratovolcanoes suggests that aseismic surface deformation may be an important part of the eruption cycle in a volcanic arc. Aseismic deformation may signal the initial phase of renewed eruptive activity at stratovolcanoes, a phenomenon only detectable with geodetic study (Dzurisin, 2003).

Volcano deformation studies over the years have also provided insight into where a volcano is expected to deform prior and during an eruption. Generally, deformation at stratovolcanoes is greatest centered on the volcanic edifice. For example, prior to the 1980 eruption of Mount St. Helens, a bulge on the flank of the volcano grew at a rate of 1.5-2.5 m/day (Lipman et al., 1981). Although this is an extreme case, it makes sense that the largest deformation should occur around the vent. Additionally, deformation can also occur far from the edifice due to deeper magmatic processes. After the 1980 eruption at Mount St. Helens, deformation was detected as far as 6 km from the edifice, and was interpreted as deflation of a magma chamber due to the removal of magma from beneath the volcano (Dvorak et al., 1981). Occasionally, maximum deformation is not centered on the edifice. At South Sister volcano, maximum surface deformation was detected greater than 5 km from the most recent vent (Dzurisin et al., 2006). Similarly at Lassen Peak, maximum deformation was detected several kilometers south of the edifice (Poland et al., 2004). This fact highlights the need for broad field deformation studies, to avoid missing important deformation signals.

Recent study of deformation has revealed that surface deformation does not always accompany a volcanic eruption. For example Shishaldin Volcano (Alaska), Akutan volcano (Alaska), and Popocatepetl volcano (Mexico), have erupted with very little to no detected deformation (Dzurisin, 2007; Moran et al., 2006). The absence of surface deformation may indicate that deformation is too small to detect, or a complex sequence of inflating and deflating sources may exist (Dzurisin, 2003). These events allude to the complex nature of volcanic systems and the unpredictability that volcanoes exhibit.

Volcano deformation study is one important component of volcano monitoring that commonly includes other geochemical and geophysical data sources (Dzurisin, 2007). The combination of many types of data (e.g., gas, seismic, gravity) has yielded significant insight into the way volcanoes behave during an eruption cycle. Geodetic and gravity measurements are often combined to constrain the change in mass or density beneath a volcano (Williams-Jones and Rymer, 2002) and thus the relative amount of magma that has been introduced or removed from the system. Gravity and geodetic study can provide important information on the eruptive potential of quiescent volcanoes (Gottsmann et al., 2003).

Designing a good GPS network

Large GPS arrays provide the spatial coverage that is necessary to model the shape and depth of a deformation source (Dzurisin, 2003). However, even with few geodetic stations, useful information can be collected. In the case of Grimsvotn volcano (Iceland), seven resurveys of a single mark were successful in recording a period of pre-eruption inflation and subsequent post-eruption subsidence of more than 15 cm over a nine year period (Sturkell et al., 2003). In that study, both horizontal and vertical displacement data were needed to characterize the event, which further highlights the usefulness of three dimensional GPS data sets.

Mount St. Helens is among the most heavily instrumented stratovolcanoes in the world. After the May 18, 1980 eruption the USGS CVO installed an extensive geodetic network of tilt meters, leveling lines, EDM networks and eventually GPS networks (Poland et al., 2006a). Today GPS has replaced much of the ground based geodetic

techniques and currently the volcano has more than 40 campaign GPS benchmarks and continuous GPS stations located around the volcano. Most of these marks are located within 10 km of the volcanic vent but some are located as far as 40 km away (Poland et al, 2006). These far field stations have proven useful for detecting deep intrusions (> 5 km) beneath the volcano (Dzurisin, 2003). However, modeling experiments and experience have shown that a geodetic network that extends radially 20 km on stratovolcanoes is sufficient to detect much of the expected deformation signal (Dzurisin, 2003).

Various modeling experiments using geodetic data from stratovolcanoes have provided some insights into the expected depth and strength of magma chambers (Dzurisin et al., 2006; Lisowski et al., 2007; Masterlark, 2007). Source depth estimates have ranged from 0.5 km to 10 km (Dvorak and Dzurisin, 1997). Detectable source volume changes on the order of 10^5 to 10^7 m³ can be expected in shallow magma chambers without eruptions (Dzurisin, 2007).

According to Dzurisin (2003), the ideal campaign GPS network should include at least one (preferably two), monuments within each 5 km, 10 km, and 20 km quadrant of the volcano, totaling 20 to 24 marks around the edifice. These guidelines are suggested as the minimum; however, more data are always better. Appropriate sites should be adequately dispersed and sufficiently numerous to detect small variable nuances to the deformation signal and be accessible. A number of new GPS benchmarks have been installed at distances of 5 to 10 km around Mount Baker to improve the geodetic coverage for future deformation measurements, and several other locations are suggested

(Figure 1.4). This work benefits future geodetic study by enlarging the aperture of observations for detection of potentially deep deformation sources.

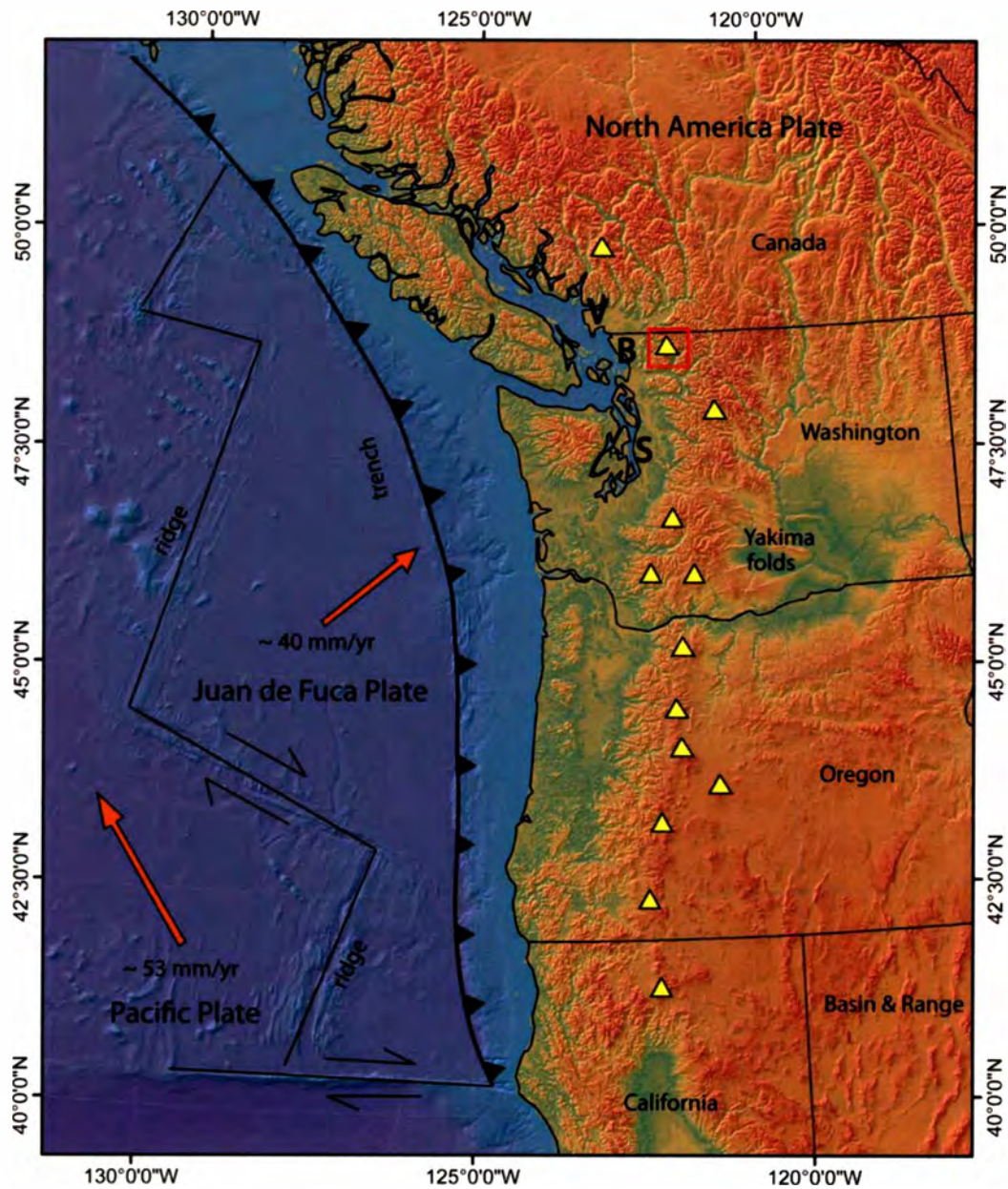


Figure 1.1. Location of Mount Baker (red box) within the Cascade Volcanic Arc (yellow triangles). The Cascadia subduction thrust is indicated by black triangles, along with the oceanic plate velocities relative to North America (Wang et al., 2003). The locations of Bellingham (B), Seattle (S), and Vancouver, B.C. (V) are shown for reference. Topography/bathymetry base map from Haugerud, 2005.

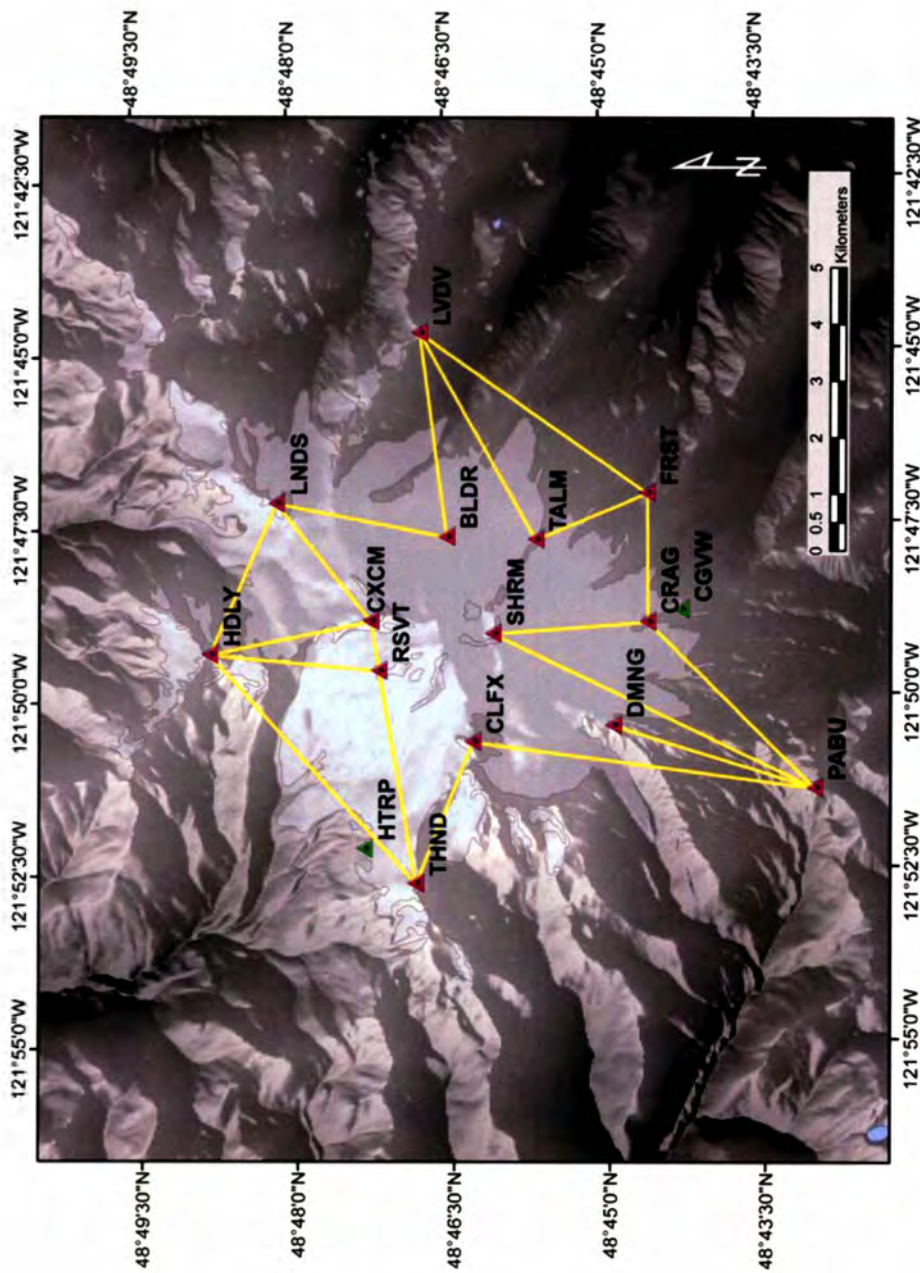


Figure 1.2. The Mount Baker trilateration network consists of fourteen benchmarks (pink triangles) installed by the USGS in 1981. Nineteen slope distance measurements were taken using EDM instruments in 1981 and 1983 (yellow lines). Green triangles are recently installed benchmarks (2004, 2006). Digital elevation base from the National Elevation Dataset (NED), 2006.

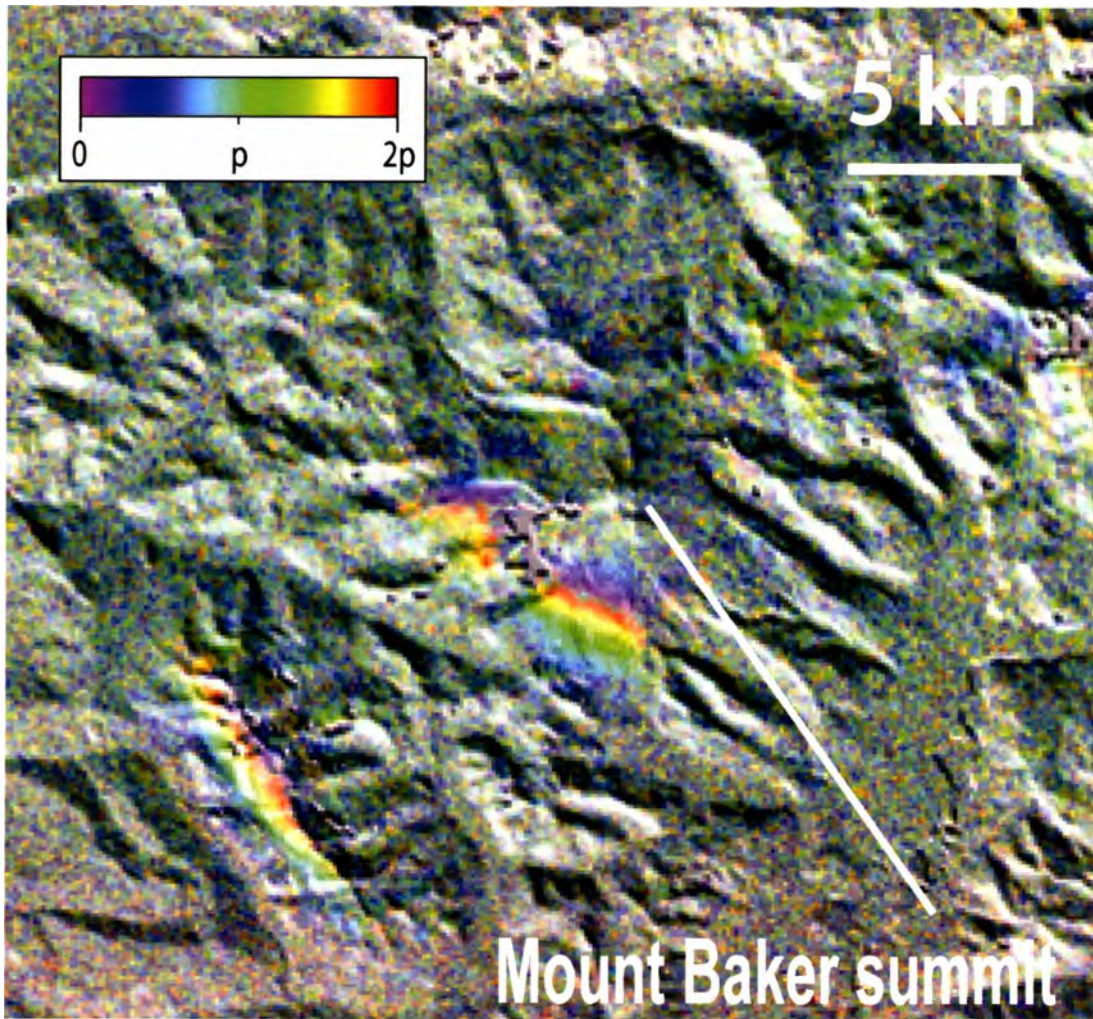


Figure 1.3. Interferometric synthetic aperture radar image generated from ERS-2 images acquired on September 12, 1997 and August 28, 1998. Note incoherence over most of the image as seen by inconsistent pixel gradients. Spatial coherence is not sufficient to determine surface deformation with this image. Figure from Michael Poland (pers. comm. 2006).

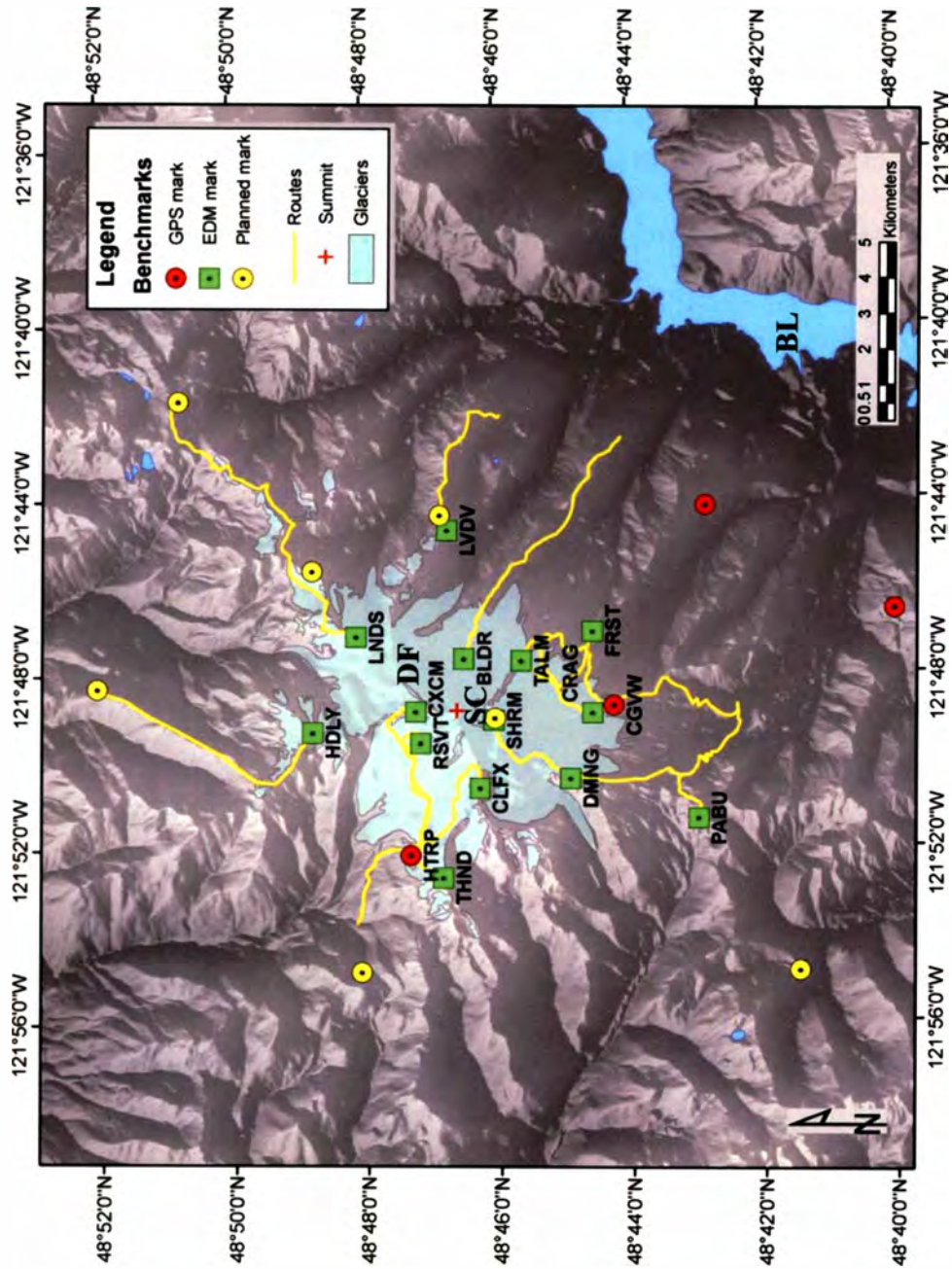


Figure 1.4. Map of benchmarks on Mount Baker. Baker Lake (BL), Sherman Crater (SC) and the Dorr fumaroles (DF) are indicated for reference. Digital topography base map from the NED, 2006.

2.0 Data collection and data reduction

Geodetic data collection on glaciated volcanoes is a challenging yet rewarding endeavor. Access requires long periods of backcountry travel, often in adverse weather conditions. The joys of resurveying a seldom visited mark are well worth the effort. Afterwards one is rewarded by a stunning view and hours of free time to enjoy it while one waits for the GPS receiver to fill itself with satellite positioning information. In this section I outline the site methods used to collect the GPS data and those used to reduce the data for surface deformation study. I include a full discussion of the existing EDM network and uncertainties associated with this data set, as it is important to understand the intricacies of both data types for a meaningful comparison. I provide a comprehensive account of the methods that I use to quantify the GPS data uncertainties and the implications for deformation study on Mount Baker. A field guide for site access is included in **Appendix A**, which provides information on benchmark access and logistics of campaign GPS surveys on Mount Baker.

2.1 The EDM network on Mount Baker

The initial EDM surveys of Mount Baker were conducted by scientists from the US Geological Survey during the summers of 1981 and 1983. The procedures and results of this study are described by Chadwick and colleagues (1985), and summarized here. Initial geodetic surveys used a helicopter to place equipment and personnel at fourteen benchmarks installed on Mount Baker. The survey attempted to place a mark within each 60 degree zone centered on the volcano at both a low and a high elevation in order to

establish a uniform array on all aspects of Mount Baker. However, due to the limited availability of helicopter-accessible outcrops on the glaciated volcano, marks were placed wherever suitable landing sites and outcrops were found. No consideration was made for access to the marks by foot, because foot survey was determined infeasible with EDM equipment.

EDM survey of Mount Baker required a person at each endpoint of a survey line. The EDM instrument was typically placed at a low elevation mark and a distance was determined to the reflector placed higher on the volcano. In addition to a distance measurement, the vertical angle to the sighted mark was recorded to determine approximate station elevations. At each mark the temperature, humidity and barometric pressure were measured and later used to calculate a correction for atmospheric refraction of light, which produces error in the line length estimation. An attempt was made to lessen the atmospheric refraction error by collecting temperature and humidity measurements along the sight line between marks with aircraft to most accurately estimate atmospheric characteristics. These data were determined to not appreciably improve error, and therefore, only endpoint atmospheric measurements were used to calculate EDM uncertainties, which are used in this work. A discussion of EDM error is given in Section 2.4.

2.2 2006 and 2007 campaign GPS resurvey methods

There are two types of monuments installed for geodetic study at Mount Baker reported in this thesis (**Figure 2.1**). Each of the brass benchmarks installed by the USGS in 1981 is referred to as an 'EDM mark'. The remaining marks are stainless steel pins

installed at various times in 2004, 2006, and 2007 and are referenced as ‘GPS marks’. After the EDM marks are measured with a GPS they essentially become GPS marks, however, the distinction remains for clarity.

GPS data were collected using geodetic quality Trimble 5700 dual-frequency GPS receivers. A Trimble Zephyr geodetic antenna was mounted on a portable aluminum tripod typically ~0.5 meters above the mark (**Figure 2.2**). Power was provided by 12 volt sealed lead-acid batteries of various sizes depending on the power requirements for each occupation. Satellite data were logged at 1 Hz using an elevation mask of 5 degrees and a PDOP (percent dilution of precision) mask of 20.

2.2.1 Benchmark reoccupation procedure

EDM Benchmarks on Mount Baker were accessed via backcountry backpacking due to the lack of roads and the prohibition and expense of helicopter transport. The locations of the EDM benchmarks are described in the text and highlighted in black-and-white photographs documented by the original USGS survey (Chadwick et al., 1985). No absolute position, i.e. latitude and longitude, of the marks were provided in the report, which created some uncertainty for locating the benchmarks in the field. The elevations of the marks were provided, however, and were used to estimate the location of each mark. Locating the benchmarks with this limited information was occasionally a challenge for my reoccupation team. However, now that a GPS position has been obtained, any future occupation will be able to locate the mark position efficiently.

I used a standardized procedure to set-up the instrument and begin data collection at each GPS and EDM benchmark. First, the portable tripod was positioned over the mark. This was often frustrating and difficult in the sloping and irregular volcanic rocks that cover the flanks of Mount Baker. However, it is critical that a stable foot placement is found for each of the three tripod legs to prevent any possible movement during data collection from wind disturbance (**Figure 2.2**). Once the tripod was positioned over the mark, I secured the tripod to the outcrop with stones and/or nylon rope to prevent possible disturbance. Next, the tribrach is attached, centered and precisely leveled over the mark on the monument using an optical plumb. At this time the tribrach adapter (“puck”) was carefully fixed to the tribrach. Finally, the brass antenna adapter, with the antenna and cable attached, is secured in the puck with the north axis of the antenna aligned to true north. This is determined by a simple field compass corrected for magnetic declination of the site. Next, I carefully measure the slant height of the antenna with the measuring rod. At least three measurements at different locations on the antenna are recorded. If antenna heights are identical, the set-up was double checked for stability, and for plumb and level of the antenna. When this is verified, GPS data collection was initiated by attaching the antenna cable and power cable to the GPS receiver.

After data collection was terminated, plumb and level are checked. If any movement had occurred, this was noted for inclusion in error estimates. In addition, field notes contained: a list of the equipment used for that occupation, GPS start and stop times, the weather conditions, and detailed information about the condition and stability of the benchmark. This information is later used to produce a rubric for estimating

benchmark instability errors. Photographs also help document the degradation of the benchmarks over time.

Data were collected for as long as possible, but a period of 8-24 hours was typically achieved. In some cases a longer occupation was feasible, and on one occasion (SHRM 2006) only four hours of data were collected due to adverse weather. Ideally, GPS data should be collected for more than eight hours on each of two different GPS days (Michael Poland pers. comm., 2006). A GPS day at Mount Baker begins at 5pm PST, which made data collection for more than 8 hours on the first day inconvenient and therefore this stipulation was rarely achieved. I found that reoccupation times of 18-20 hours were realistic and achievable in most cases (**Table 2.1**). Typically, this was achieved with a start time in the early or late afternoon after a 3-6 hour approach, and a stop time in the late morning the following day.

2.3 GPS data processing

Mount Baker Campaign GPS data were processed at the USGS Cascades Volcano Observatory (CVO) by Dr. Michael Lisowski for both the 2006 and 2007 campaigns. GPS data reduction is a sophisticated, yet routine procedure that is now automated by various proprietary and open source processing programs. GPS data procedures at the USGS have been standardized and automated by the UNIX script package *gp*, which utilizes the GYPSY-OASIS II GPS data processor provided by JPL (Zumberge et al., 1997). Knowledge of UNIX scripting, the GPS data processor and geospatial referencing are necessary to extract meaningful GPS-derived line lengths for comparison to the EDM observations.

2.3.1 Pre-Processing

A pre-processing procedure is required to reformat the raw GPS ephemeris binary data file provided by the receiver, into a universal readable text file (.rnx) for processing. This is accomplished by the TEQC (translation, editing, and quality check) script package provided by UNAVCO (Estey and Marteens, 1999). At this step, a standardized metadata header is updated to include the relevant survey information (equipment used, operator) needed for data processing.

2.3.2 GPS processing

Daily point positions are returned from the automated gp processor in a non-fiducial reference frame, i.e. a position in a non-referenced GPS space. These daily positions are then placed into the current international terrestrial reference frame (ITRF2000) by merging the daily positions to a global network of continuous GPS stations (Altamimi et al., 2002). Because I am interested in positions relative to a fixed location, the network solutions are then placed into a fixed North American reference frame (NOAM ITRF2000) based on an Euler pole by Altamimi and others (2002). Finally, the point solutions are transformed into a local reference frame (north, east, up) defined by five regional continuous GPS stations (DRAO, SEDR, CHWK, BREW, LKCP) surrounding Mount Baker by a 3-dimensional rotation. This step is used to remove common-mode noise and improve accuracy of the position estimate (Michael

Lisowski, pers. comm., 2007). The solutions for each GPS day are merged separately for 2004, 2006 and 2007, because the stations move slowly in the NOAM reference frame.

2.4 Error analysis

The success of any EDM to GPS comparison depends on the accurate and complete accounting of all the associated errors that are inherent in both data types. In addition, set-up and site errors such as benchmark instability must also be accurately determined and included in the final data assessment. While it appears cumbersome at first, diligent attention to error sources during data collection and analysis is achievable and necessary for meaningful results. Each of these error sources has been described and the procedures for identification and correction outlined in the following sections.

2.4.1 EDM line length uncertainty

Electronic distance meter (EDM) surveying techniques have been used since the 1960's for crustal strain measurements across fault zones, e.g. San Andreas Fault (Savage and Prescott, 1973), and surface strain measurements on volcanoes, e.g. Kilauea volcano (Decker et al., 1966). The use of this technology for strain measurement in different environments enables good estimates of the reproducibility of single EDM measurements (Prescott et al., 1979; Savage et al., 1981; Savage and Prescott, 1973; Savage et al., 1987). The precision of a single EDM line length measurement (i) can be estimated at a standard deviation (σ_i) by a function of random (set up errors, benchmark instability), and systematic errors (instrument error). The uncertainty in calculating the correction factor

for error associated with atmospheric refraction (β) is proportional to the length (L) of the line measured. The standard deviation is thus given by (Savage and Prescott, 1973):

$$\sigma_i = \sqrt{\alpha_i^2 + \beta^2 L_i^2} \quad (1)$$

Savage and Prescott (1973) estimated values of alpha (α) and beta (β) from empirical study of trilateration networks in California. They suggest values for $\alpha = 3$ mm, and $\beta = 2 \times 10^{-7}$ and show that these are acceptable values for one standard deviation uncertainties (Savage and Prescott, 1973). By using flight line measurements along the sight path to collect atmospheric data, they were able to minimize the uncertainty related to the correction factor for the atmospheric index of refraction. Therefore, theirs is a lower boundary value for beta (β). These estimates are determined in low relief, arid regions of California from well designed EDM networks and represent the best case scenario for EDM precision.

On stratovolcanoes, greater error in a line length measurement is expected compared to error estimates from ideal conditions described above. Greater error results from measurements over a larger elevation range, which increases the uncertainty due to atmospheric properties along the slant length, and greater presumed benchmark instability in volcanic rock. The overall survey error and expected precision for the 1981-1984 EDM surveys of 142 line length measurements on Cascade volcanoes was estimated at one standard deviation as ± 3.9 ppm (Chadwick et al., 1985). For comparison, precision estimates using the same instrument model at Long Valley (California) produced an error of ± 3 ppm (Chadwick et al., 1985). This error estimate assumes no strain in the networks during the four-year survey period and is considered a 'conservative' estimate by the USGS survey team (Chadwick et al., 1985).

The Mount Baker EDM trilateration surveys contain four types of presumably random error that are associated with a single EDM measurement. Instrument errors are associated with the equipment and given by the instrument manufacturer. The reported error for the Hewlett-Packard 3808A used in the 1981 and 1983 EDM survey was $\pm (5 \text{ mm} + 1 \text{ ppm})$ (Chadwick et al., 1985). Setup errors are caused by improper or imprecise set-up of instruments at the benchmarks. From previous EDM surveys, this random error is assumed to add $\sim 1 \text{ mm}$ to the uncertainty (Savage et al., 1986). Instability from degraded or poorly installed marks adds additional uncertainties. Finally, error results from uncertainty in the atmospheric characteristics between endpoints used to correct for the refraction index. For the Mount Baker EDM surveys, an attempt was made to lessen atmospheric error with repeat flight line measurements of humidity, barometric pressure and temperature with aircraft. This, however, was determined unsuccessful and a standard correction factor is applied to the line length calculation using endpoint measurements of atmospheric properties (Chadwick et al., 1985)

The uncertainty for a single Mount Baker EDM measurement including all random and systematic errors, is estimated (in meters) by:

$$\sigma(\Delta L_i) = \sqrt{(5 \times 10^{-3})^2 + (2 \times 10^{-7} L_i)^2} \quad (2)$$

where ΔL_i is an individual line-length change and L_i is an individual line length. The results of a recent campaign GPS resurvey of the EDM network on South Sister Volcano report a similar error correction (Dzurisin et al., 2006). I use an alpha (α) term of 5 mm and a beta (β) term of 0.2 ppm to maintain consistency with the reported instrument error of 5 mm and with previous workers (Dzurisin et al., 2006). A single line length measurement on Mount Baker (2-6 km) yields one-standard-deviation uncertainty

estimates ranging from 7-14 mm, with longer lines having greater uncertainty (**Table 2.2**).

2.4.2 GPS line length uncertainty

Line lengths from the individual merged GPS solutions are calculated with GYPSY scripts in the gp processing environment. The formal uncertainty in the line lengths derived from GPS is calculated by extracting the covariance for each GPS position solution and propagating the errors. The uncertainty in a static GPS position is a function of atmospheric phase delay, clock bias, satellite orbit uncertainties and multi-path errors. All of these errors, except multi path errors, are eliminated or significantly reduced during processing (Dzurisin, 2007).

The uncertainty in a Mount Baker GPS line length is a function of the formal GPS line-length uncertainty, the uncertainty in the stability of each benchmark, and random set-up errors from each measurement. Line-lengths between GPS positions are determined with scripts run in the gp processing environment (Prescott, 1997). Lengths are reported with a standard error (σ) based on GPS position uncertainties. The standard deviation of these estimated values are likely underestimated by a factor of 2, at least (Michael Lisowski, pers. comm., 2007). To provide the most confidence in a line-length difference calculation, I use 2σ values for static GPS line-length uncertainty estimates. GPS-derived line-length uncertainties range from 4-6 mm at one standard deviation (**Table 2.3**). These estimates are consistent with previous GPS derived line-length studies of trilateration networks, which report a 5mm GPS line length uncertainty (Dzurisin et al., 2006; Savage et al., 1996). GPS uncertainties can be propagated

quadratically with endpoint benchmark instability estimates and setup error to achieve a final GPS-determined line-length uncertainty estimate.

Benchmark stability is estimated by onsite inspection of the monument using visible indicators of degradation or disturbance, e.g. cracks or removal of grout, eroded bedrock, evidence of frost wedging or movement with applied force. Host-rock conditions were also documented and analyzed for evidence of instability. Field notes and site descriptions are included in **Appendix C**. At two sites (LVDV, CRAG), the monument had been vandalized and only a drill hole in bedrock remained. Inspection of other Mount Baker EDM monuments revealed that the measurement mark is placed in the center of the monument and cannot be placed near the monument perimeter where text has been engraved (**Figure 2.1**). Because the brass EDM marks must have fit plumb in the drill core, GPS measurements were taken to the estimated center of the hole. The possibility exists that the drill cores were not geographically plumb and thus there is some uncertainty in the position of the original mark with respect to the center of the drill core. I conservatively approximate the uncertainty in these measurements at 15mm, which includes the uncertainty in the position of the original mark on the monument and the orientation of that monument with respect to the existing drill core. I use this value as an estimate of uncertainty for the position of LVDV, CRAG and LNDS (LNDS had weathered from the bedrock but was repositioned for the survey). Monument BLDR has degraded due to weathering of the surrounding bedrock. I add an uncertainty estimate of 5 mm for slight monument instability. The remaining EDM monuments were found to be in place, unmovable, and showed no visible signs of significant degradation. Assuming

that the host rock is stable, the instability estimate for these monuments is zero.

Benchmark stability estimates are shown in **Table 2.4**.

Set-up errors are difficult to detect. I attempted to identify set-up error by double checking level and plumb before data collection and again after termination of data collection. If any movement was evident, this was measured as a set-up error and included in the benchmark instability estimate as shown in **Table 2.4**.

A repeat survey of mark DMNG spanning a one week period in 2006, allows for GPS resurvey error estimation assuming no displacement has occurred during this period. The resurvey of this mark shows approximately a 2 mm difference in the east component of displacement (**Figure 2.3**). The standard deviation of this comparison would be 1 mm, which can be considered the resurvey error. Although this comparison is not statistically robust, others have estimated a similar value for campaign GPS resurvey error (Mazzotti et al., 2003).

2.5 Uncertainty in the EDM to GPS Comparison

The change in line length (Δ_i) between the 2006/7 GPS and 1981/3 EDM survey on Mount Baker is determined by the difference between the two line lengths measured by each method. The uncertainty in this difference (eq. 3) is the uncertainty in the GPS determined length, and the uncertainty in the EDM determined length added quadratically as given by (Savage et al., 1996):

$$\delta(\Delta_i) = \sqrt{GPS_i^2 + EDM_i^2} \quad (3)$$

Savage and others (1996) determined that EDM line length measurements are systematically longer than GPS line length measurements by 0.283 ± 0.1 ppm. I correct for this systematic bias by increasing GPS derived line lengths by 0.283 ppm, which amounts to <2 mm increase over the longest line length on Mount Baker (PABU-SHRM), or less than 5% of the line length change (**Table 2.3**).

I calculate the uncertainty in line length measurements of the original nineteen trilateration lines on Mount Baker using the mean of the 1981 and 1983 values. The uncertainty in the mean is the uncertainty of a single measurement divided by $\sqrt{2}$. This estimate assumes that errors are random and there are no systematic uncertainties in the two measurements. Given that the same correction procedure and the same instrument were used in both surveys (Chadwick et al., 1985), I consider this assumption reasonable. The values for the line-length change including uncertainties to a standard deviation are given by $\Delta_l \pm \delta_l$ (**Table 2.5**). The uncertainty in the mean 1981-1983 EDM slope distance measurements range from 9-18 mm, which are slightly higher than those estimated for the South Sister EDM to GPS comparison (Dzurisin et al., 2006). These values are used to estimate uncertainties in the surface strain rate calculation in Section 4.

2.6 GPS vector uncertainty

Several benchmarks were measured more than once with campaign GPS during the 2004 (Parker, 2005), 2006, and 2007 summer field seasons. These repeat position measurements provide a displacement vector for each benchmark. The annual rate of movement and the uncertainty in the vector are shown in **Table 2.6**. A linear velocity model is used to estimate the benchmark velocity. In the case when fewer than three

point positions are available (SHRM, HTRP, THND), the velocity model is undetermined and cannot provide meaningful velocity uncertainties. The standard deviation velocity uncertainties (σ_v) are calculated with the gp processor and are based on propagating the formal GPS errors (W) with random noise given by (Prescott, 1997):

$$\sigma_v = \sqrt{W^2 + (0.001\sqrt{T}/T)^2} \quad (4)$$

The last term on the right is a random walk contribution, where T is the time span between observations. **Figures 2.4** and **Figure 2.5** give the best fit linear velocity model to the daily campaign and continuous GPS position data referenced to North America.

Table 2.1. Mount Baker GPS Benchmarks. The date and duration of static GPS measurements used in this thesis are given. Also included are the location of each benchmark in decimal degrees of latitude and longitude and approximate elevation in meters and feet.

#	Station Name	GPS Code	Survey Date	Elapsed time (hours)	Location		Elevation	
					Latitude (°N)	Longitude (°E)	meters	feet
1	Park Butte	PABU	9/25/2004	15	48.7165	-121.8563	1645	5397
			7/8/2006	21	48.7165	-121.8563	1645	5397
			8/15/2007	20	48.7165	-121.8563	1645	5397
2	Deming	DMNG	7/22/2006	20	48.7486	-121.8406	2032	6667
			7/29/2006	11	48.7486	-121.8406	2032	6667
3	Colfax	CLFX	6/23/2006	8	48.7712	-121.8440	2857	9373
4	Cockscomb	CXCM	7/24/2007	17	48.7873	-121.8146	2754	9035
5	Boulder	BLDR	8/19/2006	22	48.7750	-121.7945	2370	7775
6	Talum	TALM	8/29/2007	14	48.7607	-121.7955	2188	7177
7	Sherman Crater	SHRM	7/29/2006	5	48.7677	-121.8181	2971	9747
			7/28/2007	20	48.7677	-121.8181	2971	9747
9	Roosevelt	RSVT	7/25/2006	17	48.7861	-121.8267	2540	8333
11	Thunder	THND	9/4/2004	21	48.7806	-121.8780	2154	7067
			6/28/2006	16	48.7806	-121.8780	2154	7067
12	Crag View	CRAG	9/5/2007	17	48.7411	-121.8150	1966	6450
13	Landes Cleaver	LNDS	9/15/2006	16	48.8022	-121.7858	2049	6722
14	Forest Divide	FRST	8/30/2007	15	48.7427	-121.7846	1566	5139
16	Hadley	HDLY	8/12/2004	12	48.813	-121.8225	2223	7293
17	Lava Divide	LVDV	8/22/2006	19	48.7790	-121.7454	1670	5479
18	Volcano Camp	CGVW	7/8/2006	40	48.7375	-121.8129	1834	6017
19	Heliotrope	HTRP	10/2/2004	20	48.7887	-121.8698	1801	5909
			7/23/2007	19	48.7887	-121.8698	1801	5909

Table 2.2 EDM slope distance measurements from 1981 and 1983 trilateration surveys (Chadwick et al., 1985). Line-length uncertainties are a function of line length and are given at one standard deviation.

Line #	(BM-BM)	EDM length (m)			Mean	sd
		1981	1983	sd		
1	FRST-CRAG	2283.407	2283.403	0.0068	2283.405	0.0073
2	FRST-TALM	2240.844	2240.842	0.0067	2240.843	0.0072
3	FRST-LVDV		4954.203	0.0111	4954.203	0.0136
4	LVDV-TALM	4235.688	4235.682	0.0098	4235.675	0.0119
5	LVDV-BLDR	3702.080	3702.075	0.0089	3702.078	0.0106
6	LNDS-BLDR	3104.315	3104.307	0.0080	3104.311	0.0091
7	LNDS-CXCM		2769.772	0.0075	2769.772	0.0084
8	LNDS-HDLY	2959.836	2959.826	0.0077	2959.831	0.0088
9	HDLY-CXCM	2963.909	2963.905	0.0078	2963.907	0.0088
10	HDLY-RSVT	3022.007	3022.010	0.0078	3022.009	0.0090
11	THND-HDLY	5440.950	5440.950	0.0120	5440.950	0.0148
12	THND-CXCM	4754.880	4754.880	0.0107	4754.880	0.0131
13	THND-RSVT	3842.380	3842.367	0.0092	3842.374	0.0109
14	THND-CLFX	2803.250	2803.253	0.0075	2803.252	0.0085
15	PABU-CLFX	6270.992	6270.990	0.0135	6270.991	0.0169
16	PABU-DMNG	3772.244	3772.236	0.0091	3772.240	0.0107
17	PABU-SHRM	6490.739	6490.733	0.0139	6490.736	0.0175
18	PABU-CRAG	4103.397	4103.389	0.0096	4103.393	0.0115
19	CRAG-SHRM		3128.819	0.0080	3128.819	0.0092

Table 2.3 GPS determined line-lengths from 2004 (Parker, 2005), 2006, and 2007 campaign surveys. Reported uncertainties are the formal one standard deviation errors. Line lengths indicated are corrected for the systematic error from EDM and GPS line-length comparison (Savage et al., 1996). The last column indicates the full error estimate (two standard deviations plus benchmark error) used for subsequent calculations.

Line #	(BM-BM)	GPS line length (m)						Corrected	sd	2*sd	w/BM Error
		2004	sd	2006	sd	2007	sd				
1	FRST-CRAG					2283.439	2283.439	0.002	0.004	0.019	
2	FRST-TALM					2240.842	2240.842	0.003	0.005	0.006	
3	FRST-LVDV					4954.170	4954.171	0.002	0.004	0.019	
4	LVDV-TALM					4235.649	4235.651	0.002	0.003	0.018	
5	LVDV-BLDR			3702.069	0.002		3702.070	0.002	0.004	0.024	
6	LNDS-BLDR			3104.269	0.002		3104.269	0.002	0.004	0.024	
7	LNDS-CXCM					2769.733	2769.734	0.003	0.005	0.020	
8	LNDS-HDLY			2959.788	0.002		2959.789	0.002	0.003	0.018	
9	HDLY-CXCM					2963.865	2963.866	0.003	0.005	0.006	
10	HDLY-RSVT			3021.957	0.002		3021.958	0.002	0.004	0.005	
11	THND-HDLY	5440.908	0.002	5440.905	0.002		5440.907	0.002	0.003	0.004	
12	THND-CXCM					4754.866	4754.868	0.002	0.003	0.004	
13	THND-RSVT			3842.357	0.002		3842.361	0.001	0.003	0.004	
14	THND-CLFX			2803.242	0.003		2803.247	0.003	0.006	0.007	
15	PABU-CLFX			6270.973	0.003		6270.976	0.003	0.006	0.007	
16	PABU-DMNG			3772.250	0.002		3772.253	0.001	0.003	0.005	
17	PABU-SHRM			6490.689	0.003		6490.693	0.003	0.006	0.007	
18	PABU-CRAG					4103.384	4103.385	0.001	0.003	0.019	
19	CRAG-SHRM					3128.708	3128.709	0.004	0.007	0.023	
20	PABU-THND	7330.724	0.002	7330.721	0.002		7330.722	NA	0.001	0.002	
21	PABU-HTRP	8095.433	0.002			8095.433	8095.433	NA	0.001	0.003	
22	THND-HTRP	1136.892	0.002			1136.901	1136.901	NA	0.002	0.004	

Table 2.4 Estimated GPS survey errors for Mount Baker geodetic benchmarks determined for the 2006 and 2007 GPS surveys. Set-up uncertainty includes a standard 1 mm set-up error and any measured survey disturbances. Instability errors are derived from inspection of benchmark conditions as described in the text. Total error estimate is added to the standard deviation uncertainty in the formal GPS slope-distance uncertainties.

BM	Set-up errors (mm)	Instability error (mm)	Total error estimate (mm)
PABU	2	0	2
DMNG	2	0	2
CLFX	1	0	1
CXCM	1	0	1
BLDR	1	5	6
TALM	1	0	1
SHRM	1	0	1
RSVT	1	0	1
THND	1	0	1
LNDS	1	15	16
FRST	1	0	1
HDLY	1	0	1
LVDV	1	15	16
CGVW	1	0	1
HTRP	1	0	1
CRAG	1	15	16

Table 2.5 Line-length changes and strain accumulation rate at Mount Baker from EDM (1981 and 1983) and GPS (2004, 2006 and 2007) measurements (Parker, 2005; this work). The 1981 and 1983 line lengths were averaged to obtain a single baseline dataset. The GPS line-lengths were obtained from 2007 measurements and from 2006 and 2004 measurements when 2007 measurements were unavailable. The strain-rate is the net strain accumulation over 25 years between the surveys. The uncertainties are reported at one standard deviation and extension reckoned positive. Numbers in bold indicate values greater than the reported uncertainty.

Line #	(BM-BM)	Line length		Strain Rate	
		change, ΔL (m)	$\pm \sigma$ (m)	nanostrain/yr	$\pm \sigma$
1	FRST-CRAG	0.034	0.020	603	357
2	FRST-TALM	-0.001	0.010	-12	172
3	FRST-LVDV	-0.032	0.023	-256	186
4	LVDV-TALM	-0.024	0.022	-230	207
5	LVDV-BLDR	-0.007	0.026	-79	279
6	LNDS-BLDR	-0.042	0.025	-535	328
7	LNDS-CXCM	-0.038	0.022	-553	318
8	LNDS-HDLY	-0.042	0.020	-574	276
9	HDLY-CXCM	-0.041	0.011	-556	145
10	HDLY-RSVT	-0.050	0.010	-668	138
11	THND-HDLY	-0.043	0.015	-317	113
12	THND-CXCM	-0.012	0.014	-104	116
13	THND-RSVT	-0.012	0.012	-120	122
14	THND-CLFX	-0.004	0.011	-50	155
15	PABU-CLFX	-0.013	0.018	-82	116
16	PABU-DMNG	0.014	0.012	149	126
17	PABU-SHRM	-0.041	0.019	-254	116
18	PABU-CRAG	-0.008	0.022	-73	213
19	CRAG-SHRM	-0.110	0.025	-1404	319

Table 2.6 Three-component station velocities (V_n, e, u = north, east, up) relative to North America in millimeters with one sigma uncertainties (S_n, e, u). Station codes in bold (last five lines) are part of the Pacific Northwest Geodetic Array, and position data are from USGS crustal deformation program (2007).

Station	Latitude	Longitude	V_n	V_e	S_n	S_e	V_u	S_u
BLDR	48.7750	-121.7945						
CLFX	48.7712	-121.8440						
CXCM	48.7873	-121.8146						
CGVV	48.7375	-121.8129						
CRAG	48.7411	-121.8150						
DMNG	48.7486	-121.8406						
FRST	48.7427	-121.7846						
HDLY	48.8130	-121.8225						
HTRP	48.7887	-121.8698	5.80	4.21	0.60	0.60	-6.59	0.60
LNDS	48.8022	-121.7858						
LVDV	48.7790	-121.7454						
PABU	48.7165	-121.8563	3.53	4.19	1.83	2.10	-15.15	5.58
RSVT	48.7861	-121.8267						
SHRM	48.7677	-121.8181	42.46	4.71	1.0	1.0	-40.27	1.03
TALM	48.7607	-121.7955						
THND	48.7806	-121.8780	2.11	2.30	0.74	0.74	4.38	0.75
BREW	48.1315	-119.6826	1.59	1.17	0.90	0.98	0.79	2.27
CHWK	49.1566	-122.0084	3.18	3.57	1.12	1.13	-1.54	3.08
DRAO	49.3226	-119.6250	1.71	1.32	0.90	0.97	0.31	2.23
SEDR	48.5216	-122.2238	3.44	3.34	0.99	1.03	0.21	2.56
LKCP	47.9444	-121.8309	3.56	3.22	0.97	1.02	-2.58	2.55

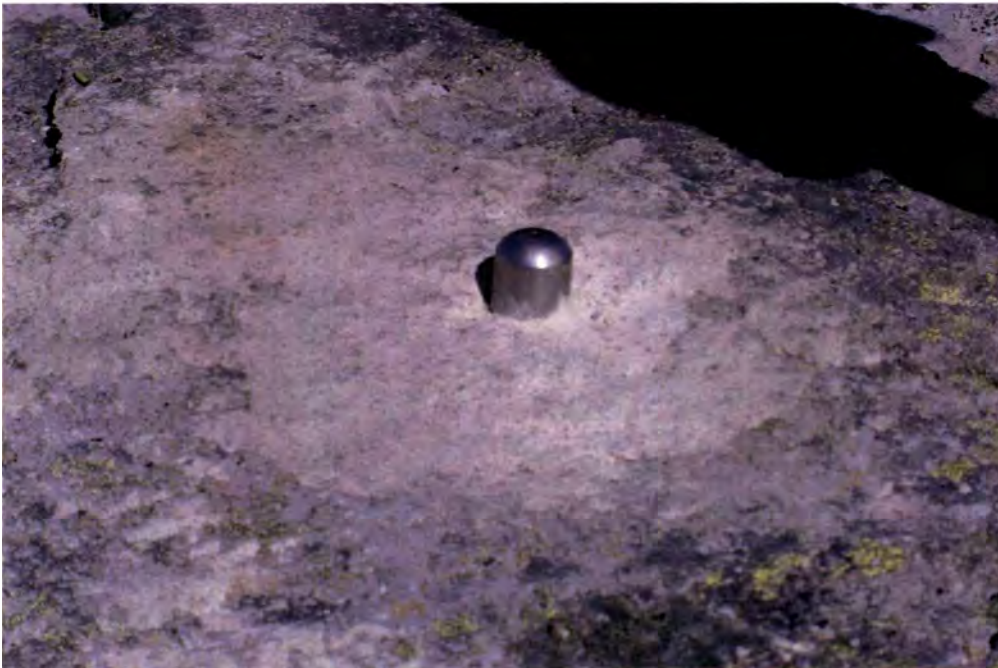


Figure 2.1. Examples of in-situ benchmarks that comprise the Mount Baker geodetic network. **(A)** Measurements on an EDM mark are taken from the dimple located within the box in the center of a brass face plate. **(B)** Measurements of a GPS mark are taken from a dimple on the tip of a stainless steel dowel.



Figure 2.2. View of Mount Baker from the south with campaign GPS survey installation at PABU. The tripod is placed on the outcrop above the benchmark and secured with rocks or rope (1). The tribrach is installed and leveled plumb on the benchmark (2). The antenna with the “puck” adapter and cable is secured (3). The field battery (4) and GPS receiver are connected (5). The location of Colfax Peak (C), Deming (D), Sherman Crater (SC), and Crag View (CV) benchmarks are indicated for reference.

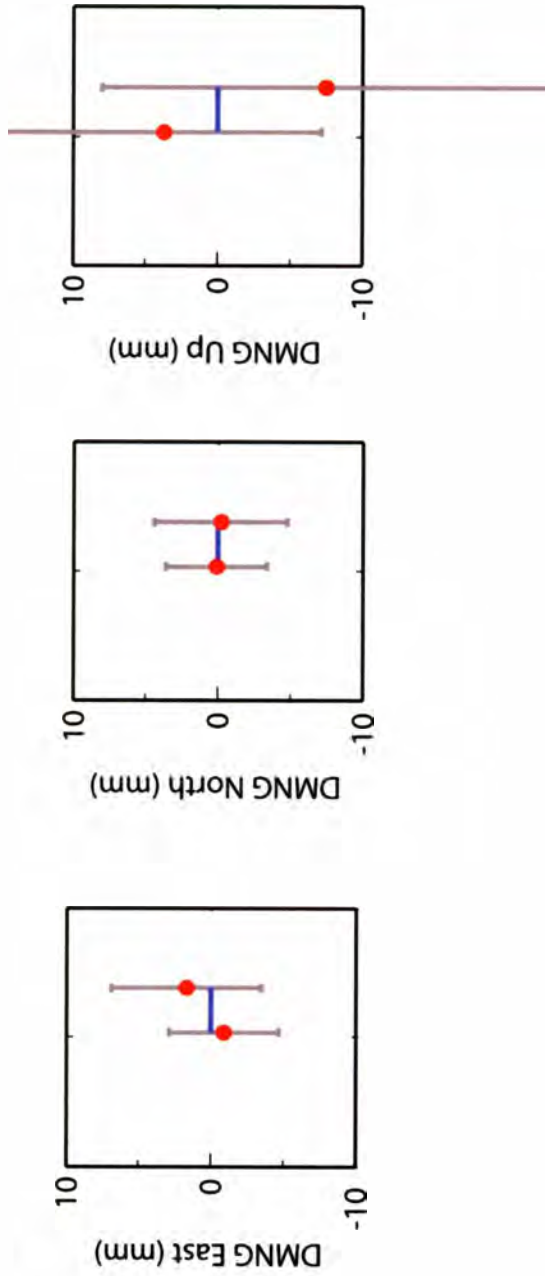


Figure 2.3. Relative position of EDM mark DMNG measured over a one week interval, with respect to an arbitrary origin. In each panel, the first data point corresponds to the measured position on July 22, 2006, and the second point is the measured position of July 29, 2006. Assuming no deformation occurred during this time period, the ~2 mm eastward position difference may be a function of set-up errors and/or noise in the GPS signal.

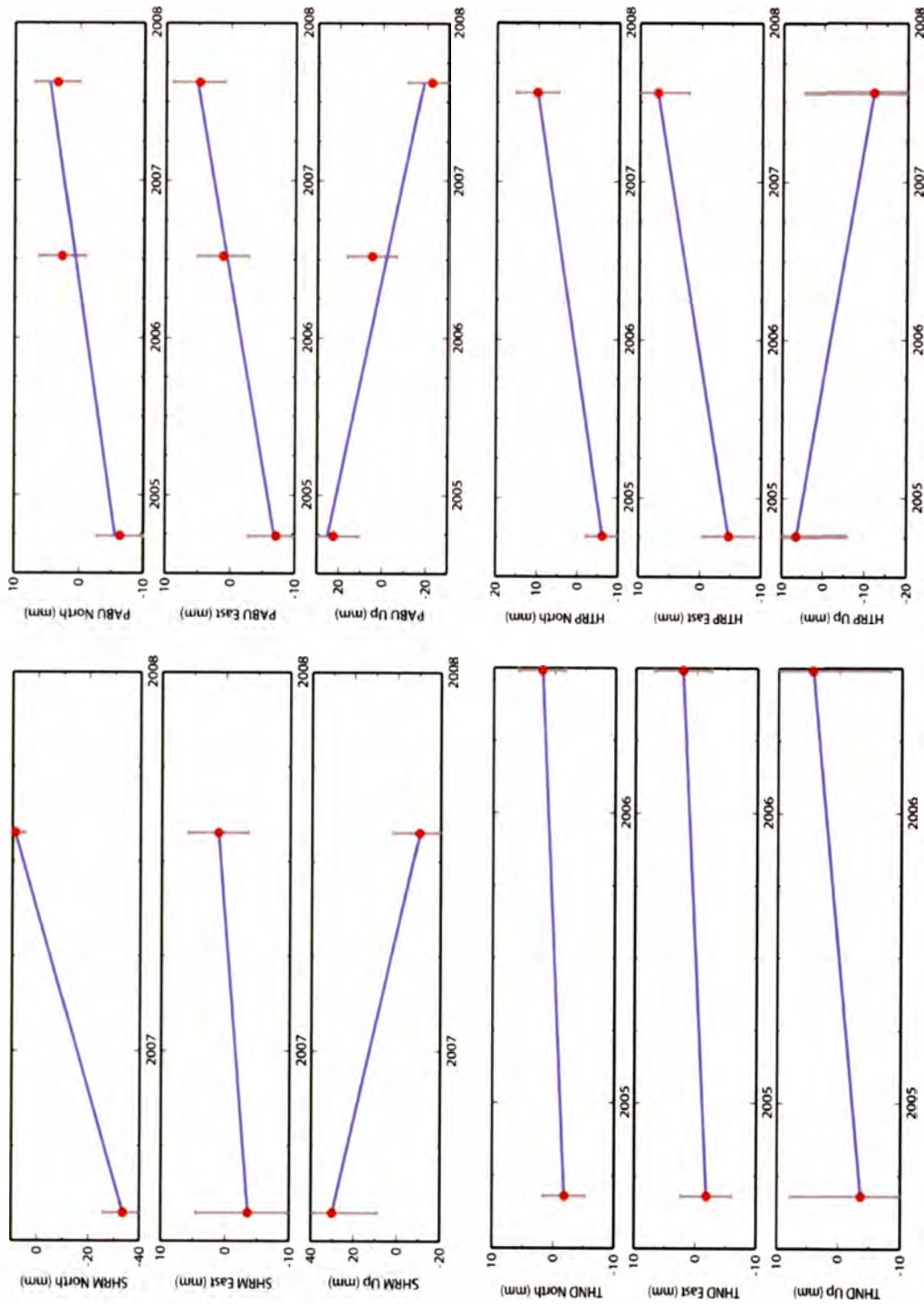


Figure 2.4. Time series plots for repeat campaign GPS positions for sites on Mount Baker. The error bars for individual observations are plus or minus one standard deviation. Linear velocity model (blue line) results are given in Table 2.6. Plots are generated by the USGS Crustal Deformation Archive with data from this work.

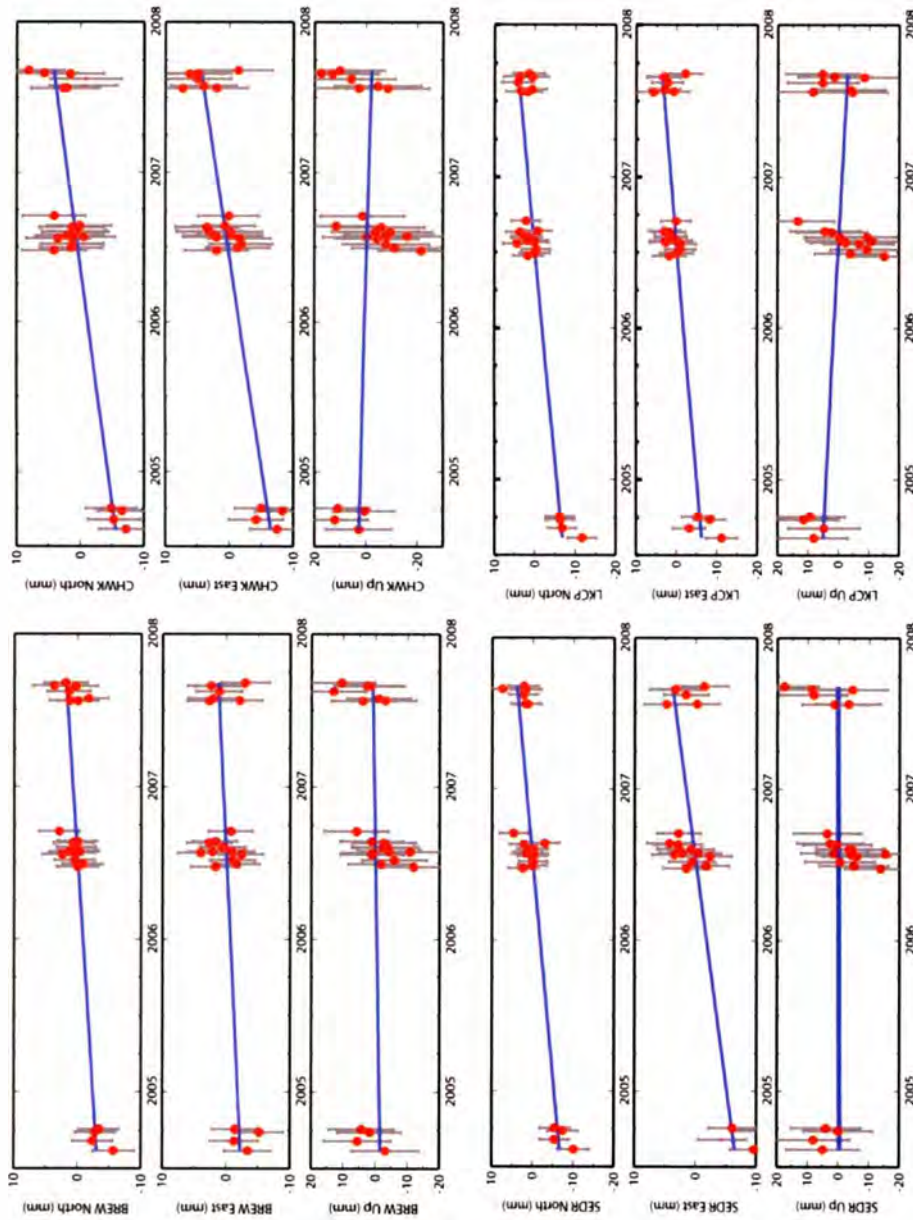


Figure 2.5. Time series plot of continuous GPS station daily solutions used in the local reference for the 2004, 2006, and 2007 campaign GPS daily solutions. The error bars for individual observations are plus or minus one standard deviation. Linear velocity model (blue line) results are given in Table 2.6. Plots are generated by the USGS Crustal Deformation Archive with data from the Pacific Northwest Geodetic Array.

3.0 Results of GPS resurvey

A complete resurvey of the Mount Baker EDM network was conducted over the 2006 and 2007 summer field season. The 2006 summer season recovered ten trilateration lines from GPS positions of nine EDM benchmarks including one 2004 position of EDM mark HDLY (Parker, 2005). Additional surveys in the summer of 2007 successfully recovered the remaining EDM benchmarks to complete the resurvey of the entire trilateration network on Mount Baker. The 2007 survey included new positions on four previously un-surveyed EDM marks (CXCM, TALM, CRAG, FRST) and repeat measurements on two previously surveyed EDM marks (SHRM, PABU) and one GPS mark (HTRP). The slope distance measurements provide strain data that are used to characterize surface deformation on Mount Baker (4.0).

3.1 GPS line lengths

Campaign GPS surveys of 15 EDM benchmarks produced slope distance measurements between each benchmark, which include the 19 trilateration lines established with EDM. The GPS determined line-lengths and the standard deviation uncertainties for each measurement are shown in **Table 2.3**.

3.2 EDM-GPS comparison

Results from the 2006 and 2007 GPS campaigns indicate that 12 of the 19 trilateration lines have slope distance changes greater than the calculated uncertainty

(σ_{Δ}) at one standard deviation. **Figure 3.1** shows the calculated slope distance changes and one sigma uncertainties. Of the 19 lines, 17 have shortened while 2 have extended. With the exception of lines CRAG-FRST and CRAG-SHRM, all lines have length changes within one standard deviation of the mean (-2.5 cm) for the resurvey. The greatest length change occurred on CRAG-SHRM of -11 ± 2.5 cm (-35 ppm), which is nearly three standard deviations outside the mean of the resurvey. The greatest measured extension on CRAG-FRST of 3.5 ± 2 cm (~15 ppm) is over two standard deviations from the mean survey elongation. A single endpoint repeat measurement of line THND-HDLY is consistent with the previous length determined in 2004, which showed ~3 cm of shortening (Parker, 2005). These results show predominant contraction of most lines with an overall greater change per length occurring on the northern flank of the volcano of about -15 ppm. The average change per unit length across the entire trilateration network between 1981 and 2007 is -6.7 ppm with a standard deviation of 10.2 ppm.

3.3 GPS displacement vectors

Horizontal displacement vectors for Mount Baker campaign GPS marks (**Figure 3.2**) relative to North America have been determined. The survey of GPS mark HTRP was conducted to determine if significant displacement occurred at this location between 2004 and 2007. The velocity of HTRP relative to fixed North America is significant at one standard deviation and is consistent in direction and rate with surrounding campaign and continuous GPS displacement vectors. The regional displacements are best fit by a clockwise block rotation model (McCaffrey et al., 2007), which suggests that the Mount Baker campaign GPS network is also influenced by this same upper crustal strain regime.

If the block rotation is removed by subtracting the regional continuous GPS vectors (CHWK, SEDR, BREW, DRAO, LKCP) from the Mount Baker campaign GPS vectors (THND, PABU, HTRP), the resulting displacements would likely be negligible. This would suggest that no significant deformation has occurred between 2004 and 2007 at those sites. Line length changes between PABU-HTRP are within error, also indicating no measurable deformation occurred between 2004 and 2007.

Benchmark SHRM was resurveyed in 2007 because only a short occupation time was achieved in 2006. The 2007 survey determined that the mark has moved (40 ± 10 mm north and 40 ± 30 mm down) indicating significant displacement during one year since the 2006 GPS survey (**Figure 2.5**). Comparison of the PABU-SHRM line length from 2007 indicates extension by ~ 3 cm compared to 2006. A length change of this magnitude is not consistent with the relative line-length changes during the same time period on other lines (PABU-HTRP). I suggest the more likely possibility that the rock hosting the mark is slumping into the crater. The direction of this vector would be consistent with this hypothesis (**Figure 3.2**). This rock, composed of altered breccia, is positioned at the precipice of the crater rim and contains large fractures. Given these indicators, I conclude that I have measured the wasting of the host rock as it falls into the crater.

The slope distance changes detected between Crag View benchmarks (CRAG-SHRM, CRAG-FRST) are inconsistent with the amount and sign of length change in relation to other Baker trilateration lines. The benchmark at CRAG had been vandalized and thus there is already a disproportional amount of uncertainty in the position. However, this uncertainty is exceeded on both lines indicating the position has

significantly moved, either by crustal deformation or mass wasting processes. I have documented the existence of large 'daylight' cracks in the outcrop, which overhangs a shear cliff to the west on the ridgeline. This rock appears very unstable and must be approached with caution. From these observations I conclude that the rock outcrop has shifted by the force of gravity pulling it from the cliff top. Therefore, line-length changes from CRAG endpoints are not recording crustal deformation, but rather the mechanical dismantling of the volcano via gravity.

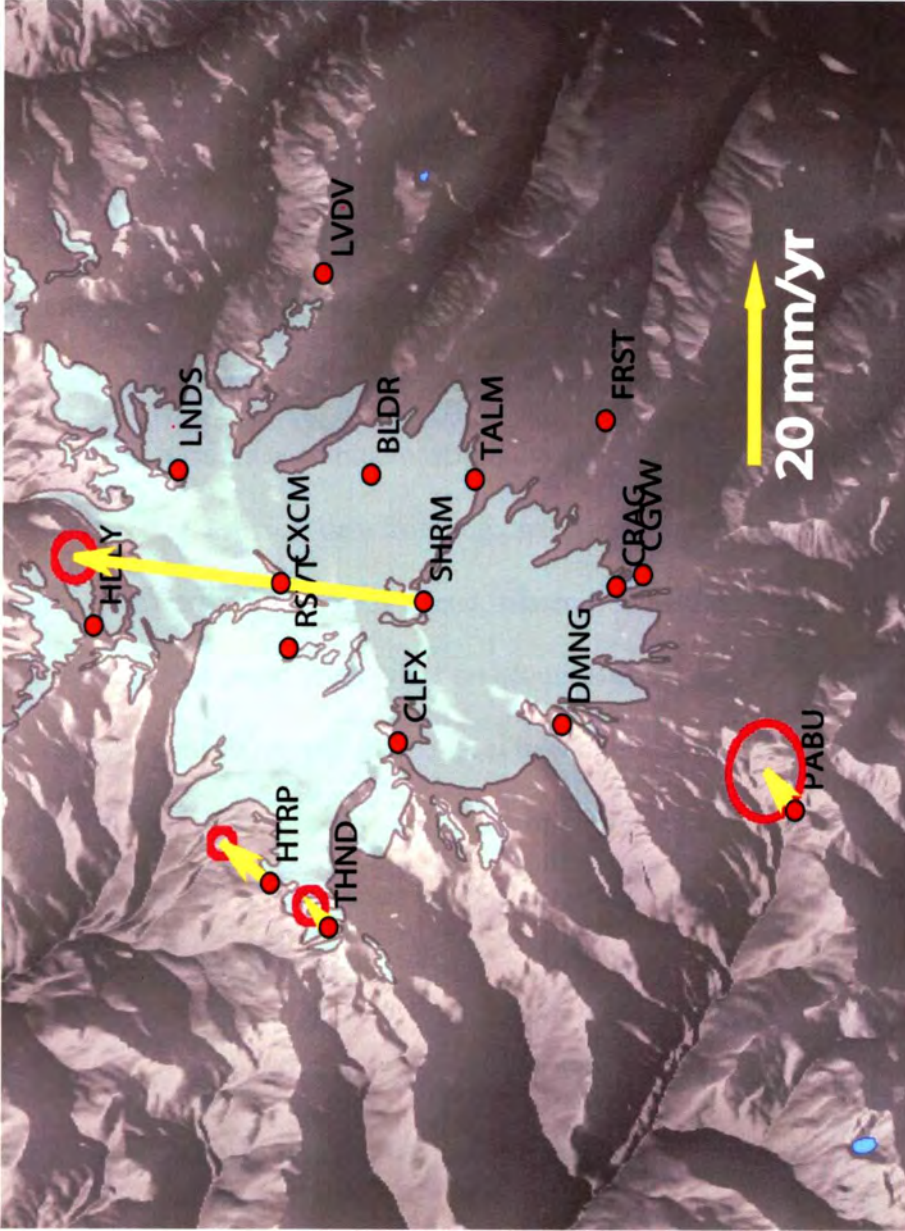


Figure 3.2. Velocity vectors relative to North America and one sigma error ellipses for repeat campaign GPS positions at Mount Baker. See table 2.6 for linear velocity model and text for discussion of uncertainties. Digital elevation base map from the NED, 2006.

4.0 Two-dimensional surface strain analyses

Much of what is known about deformational processes within the crust is by direct observation of strain on the surface (e.g., Dvorak and Dzurisin, 1997; Dzurisin 2003). Surface strain on Mount Baker is measured with changes in slope distances between points on the volcano. This method defines a local reference frame that is not fixed to an external coordinate system. Therefore, strain measurements cannot be directly related to a deformational source, either internal or external to the network. The possibility exists that strain from non-magmatic sources, e.g. subduction loading, and/or block rotation, could accumulate within the locally defined trilateration network. Because of this, I review data from regional surface strain studies that use continuous GPS instruments, campaign GPS, and trilateration methods to characterize the regional elastic strain that could accumulate on Mount Baker. Any remaining deformation beyond the regional contribution would be local to Mount Baker and is most likely volcanic in origin. In the following sections I also provide a discussion on the methods that I used to quantify the strain accumulation and the associated uncertainties on Mount Baker and also a general review of strain.

4.1 Principles of strain and deformation

The following section on the fundamentals of strain is summarized from Means (Means, 1976). Strain is a measure of the amount of deformation and can be determined by measuring the change in position of a point or array of points. Homogeneous strain occurs when a line of undeformed points, if deformed, remain a set of straight and

parallel lines. These lines may have changed in length and/or relative position to each other, and the quantities of this change are classified as normal strain (elongation/contraction), and shear strain, respectively. Elongation (\mathcal{E}) is defined as the ratio between the change in length of the line ($\delta\ell$), and the undeformed length (ℓ).

$$\varepsilon = \frac{\delta \ell}{\ell} \quad (5)$$

Elongation is the component of strain that can be measured by slope distance methods on the Earth's surface, like those on Mount Baker.

Shear strain (γ) is the amount that each particle has moved with respect to another and is measured as an angle from the line that is normal to the elongation direction. This angle is called the angular shear, and is typically measured in radians (ψ), where:

$$\gamma = \tan \psi \quad (6)$$

In the case of a trilateration network, if the set of elongation measurements do not form a closed geometric figure, shear strain cannot be determined (Segall and Matthews, 1988). The Mount Baker trilateration network contains only one closed figure, precluding the possibility of estimating shear strain within the network as the single figure has limited spatial coverage.

Strain can be graphically represented in two dimensions as a strain ellipse with two orthogonal axes that define the orientations of the maximum (ε_1) and minimum (ε_2) principal strain axes. When the incremental strain from a deformation source is so small that the undeformed and deformed strain ellipses are virtually indistinguishable, the angular shear and the shear strain can be considered equal ($\tan \psi \cong \gamma$). By this reasoning, the change in length of a line in the ellipse is very small in relation to the original length ($\delta\ell \cong \ell$) and can be considered infinitesimal. Typically, strain can be

considered infinitesimal if the magnitude ($\delta\ell$) is less than 1% of the measured length (ℓ), or $\delta\ell < 0.01 \ell$. The usefulness of infinitesimal strain is that the relationship in a system of equations between stress and normal and shear strain can be considered linear by ignoring second and higher order terms of the differential equations explaining strain. With this simplification in place, the forces acting deep within the crust can be quantified by direct observation of surface strain.

Often it is useful to quantify the total amount of strain accumulation across the surface of the crust. On volcanoes in particular, where surface deformations are presumed to occur from the inflation or deflation of magma bodies, the expansion or shrinking of the crust is a useful measurement. Areal dilatation is a measure of the change in area per unit area, which is equivalent to the sum of the maximum and minimum principal strain components ($\Delta = \varepsilon_1 + \varepsilon_2$).

4.2 Regional strain accumulation from tectonic sources

Elastic strain in the region around Mount Baker is determined from a network of continuous GPS installed by the Plate Boundary Observatory (PBO), the Pacific Northwest Geodetic Array (PANGA) and the Western Canada Deformation Array (WCDA), and campaign GPS monuments in northwest Washington. McCaffrey and others (2007) use this data to show that the elastic strain field in northwestern Washington best fits a numerical strain model consistent with crustal clockwise rigid block rotation. Much of the Vancouver Island strain field, including the region around Mount Baker, fits this model best, suggesting that the region is moving relative to North America at $\sim 3.3 \pm 0.5 \text{ mm yr}^{-1}$ in the northeastward direction (McCaffrey et al., 2007).

However, it is unclear from their results how much, if any, of this surface velocity may be the result of elastic strain penetrating inland from convergence of the Juan de Fuca plate. Mazzotti and others (2003) show that margin normal GPS velocities decrease exponentially inland from the subduction thrust, and their elastic models predict northeastward velocities of less than 1 mm yr^{-1} 400 km from the plate boundary (Mount Baker is ~ 450 km from the plate boundary). Based on this model (Mazzotti et al., 2003) and other subduction models (McCaffrey et al., 2007; Wang et al., 2003), which predict similar amounts of inland deformation, the amount of margin-normal, subduction-related strain accumulation on Mount Baker is likely to be less than 25 nanostrain/yr.

Geologic and geophysical evidence show that northern Washington (47° to 48° latitude) is undergoing $3\text{-}3.5 \text{ mm yr}^{-1}$ of north-south shortening related to strain accumulation from clockwise rotation of the Oregon forearc into the Puget Sound region (Mazzotti et al., 2002). Velocity models from McCaffrey and others (2007) determined a similar strain accumulation rate of $4.4 \pm 0.3 \text{ mm yr}^{-1}$ relative to Vancouver Island, or a north-south directed (margin parallel) strain accumulation rate of 12.5 nanostrain/yr. Some of this strain accumulation likely penetrates north of 48° lat. as evidence by active contractional structures in northern Whatcom country, WA near Mount Baker (Siedlecki et al., 2007). Based on these results, small amounts of strain accumulation from north-south shortening and/or interseismic subduction loading may be possible on Mount Baker.

4.3 Calculating surface strain-rates from 1981 to 2007

The net strain rate of a Mount Baker trilateration line can be determined by (Savage et al., 1996):

$$\dot{\epsilon} = (dL/dt) / L \quad (7)$$

where dL is the line length change, dt is the elapsed time between reoccupations, and L is the original line length. **Figure 4.1** shows the calculated strain rates of the trilateration lines and the associated uncertainties.

4.3.1 Mount Baker surface strain rate uncertainty estimation

The uncertainties in the measurement of net strain accumulation rates can be quantified using the uncertainties in the slope distance measurement. For each trilateration line (i) the uncertainty in the strain rate ($\delta\dot{\epsilon}$) of a line is (Taylor, 1997):

$$\delta\dot{\epsilon}_i = \sqrt{\left(\frac{\epsilon_i}{\Delta T^2}\right)^2 \delta_T^2 + \left(\frac{1}{T}\right)^2 \delta_\epsilon^2} \quad (8)$$

where T is the elapsed time between observations, ϵ is the elongation on a line, and $\delta_{(T,\epsilon)}$ are the formal standard deviation uncertainties associated with each term. The strain rate is determined from the strain accumulation on each trilateration line over 25 years of elapsed time between surveys as shown in **Table 2.5**.

4.3.2 Calculating the surface strain-rate tensor

The distribution of strain over a two-dimensional surface can be characterized by principal component analysis from line length changes (Prescott et al., 1979; Savage, 1988; Savage et al., 2001; Savage et al., 1981). Because slope distance data, by its nature, does not contain a fixed vertical reference frame, strain in the third dimension cannot be quantified with the EDM to GPS comparison. This is an unfortunate limitation of slope distance data because strain accumulation in the vertical direction can be a significant component of surface deformation from volcanic sources (Dzurisin, 2003). Nonetheless, some constraint on strain accumulation on Mount Baker can be achieved with this approach, even though it is limited to horizontal dimensions. By assuming that strain accumulates uniformly within the network, I map the strain rates on each of the trilateration lines as a function of the orientation of the trilateration lines (θ) measured in degrees from north. I use a least-squares nonlinear regression to determine the best-fit strain model for the data. The strain model is derived from the relationship between elongation and infinitesimal strain expressed as (Jaeger and Cook, 1976):

$$\dot{\epsilon}_1 \cos(0.01745(\theta - \varphi))^2 + \dot{\epsilon}_2 \sin(0.01745(\theta - \varphi))^2 \quad (9)$$

which is a sinusoid that describes the components of the two-dimensional strain-rate tensor. The regression solves for the magnitude of the maximum ($\dot{\epsilon}_1$) and minimum ($\dot{\epsilon}_2$) principal strain-rates and the orientation (φ) of the maximum principal strain-rate axis.

The magnitude of the standard deviation uncertainties in the extension rate of each trilateration line varies with each line. Because the errors are not the same across the network, a weighted estimator will fit the strain model to data with lesser uncertainty best. I weight the data by the inverse variance (σ^2) of the strain rate for each line. The

regression is run and 68% confidence intervals are calculated for each solvable model parameter (maximum principal strain-rate, minimum principal strain-rate and orientation).

4.4 Results of surface strain model

The average rate of surface strain accumulation that best approximate line length changes on Mount Baker between 1981 and 2007 is shown in **Table 4.1**. Uncertainties are reported at one standard deviation. The best fit sinusoid is shown in **Figure 4.2**. Data are plotted with 2σ error bars and 68% confidence intervals for the model fit. Both the weighted and the non-weighted data are plotted for comparison.

The weighted and unweighted models show a similar orientation of major axis contraction in the north-south direction with the un-weighted model showing lesser uncertainty in the orientation of the principal component axes. The un-weighted sinusoid shows greater uniaxial contraction in the north-south direction and lesser amounts of east-west contraction, or even possibly some east-west extension. The weighted data produces less eccentricity of the sinusoid than the un-weighted model, indicating that this model predicts a nearly biaxial surface strain distribution. My weight scheme has muted the amplitude of the sinusoid producing a more axisymmetric strain tensor that predicts shortening on both principal axes at one standard deviation.

The four lines with SHRM and CRAG endpoints are suspected to contain significant movements from processes unrelated to surface deformation. To investigate how these data affect the strain model results, I have removed these data from the regression by down weighting their influence to zero. The result is a slight decrease in the

magnitude of the maximum principal component by 26 nanostrain yr^{-1} , and an increase in the magnitude of the minimum principal component by 37 nanostrain yr^{-1} . The revised model maintains a similar orientation of the principal axes. The uncertainties in the strain rate decreased by 20% while the uncertainty in the orientation of the axes increased by 40%. The weighted SHRM-and-CRAG-omitted model is nearly identical to the original with a 4% difference in areal dilatation. This model is preferred based on the unreliability of the CRAG and SHRM lines. The results indicate that between 1981 and 2007 areal dilatation accumulated at a rate of -417 ± 141 nanostrain yr^{-1} .

4.5 Discussion of surface strain model

Deformation of the local reference frame is not expected from simple block rotation. In order for strain to accumulate on Mount Baker, a strain differential must exist across the aperture of the trilateration network. In the absence of a numerical model, I estimate the possible contribution of tectonic strain accumulation within the Mount Baker trilateration network by comparing the surrounding continuous GPS and campaign GPS velocities (**Table 2.6**). These velocities have components of both interseismic and secular strain and represent the current time-variable surface displacement relative to North America. The continuous GPS stations with well-determined velocities (SEDR, CHWK, LKCP) show predominant North-East motion at approximately 3 mm yr^{-1} . These vectors are consistent with those predicted by the block rotation hypothesis of McCaffrey and others (2007), indicating that most of this displacement is likely due to rigid block rotation. In comparison, Baker campaign GPS sites PABU, HTRP, and THND have similar velocities to the surrounding continuous

GPS stations and are also consistent with the regional strain observations and the block rotation model. A small differential between the north and east velocity components (0.2 mm yr^{-1} and -0.3 mm yr^{-1} respectively) at SEDR and CHWK is possible; however, these values are within uncertainty. Assuming this regional strain gradient is real and has been constant since 1981, a small amount of uniaxial north-south contraction of approximately $-3 \text{ nanostrain yr}^{-1}$ would accumulate within the Mount Baker trilateration network. The amount of strain accumulation predicted by a comparison of regional continuous GPS velocities is less, by two orders of magnitude, than the rate of strain accumulation measured on Mount Baker during the past quarter century.

Surface strain studies in Western Washington and Southern British Columbia (**Figure 4.3**) have determined areal dilatation rates by trilateration and GPS over the past several decades. Dilatation rates estimated with EDM in Seattle, WA by Savage and colleagues (1991) show accumulations of $-38 \pm 24 \text{ nanostrain yr}^{-1}$, comparable to GPS estimated rates of $-30 \pm 0.5 \text{ nanostrain yr}^{-1}$ (McCaffrey et al., 2007). Likewise, areal dilatation rates in southwest British Columbia are estimated at approximately $-20 \text{ nanostrain yr}^{-1}$ (Mazzotti et al., 2003). These estimates are from locations closer to the subduction zone, west of the volcanic arc, and are likely upper bounds values for strain within the arc, because strain from subduction sources is expected to decrease inland. For comparison, areal dilatation rates from tectonic sources at Mount St. Helens were calculated at $-15 \pm 3 \text{ nanostrain yr}^{-1}$ (Lisowski et al., in press). A robust estimate of the amount of interseismic elastic strain accumulation related to either locked subduction loading or north-south directed forearc contraction within the North Cascades volcanic arc has not been produced (McCaffrey et al., 2007). However, even if similar rates of

tectonic strain accumulation exist on Mount Baker, these would account for at most ten percent of the total measured areal dilatation rate of -420 ± 140 nanostrain yr^{-1} . These results suggests that surface deformation on Mount Baker over the past quarter century has not accumulated entirely from regional interseismic elastic strain, but from some other source, such as depressurization of a magmatic or hydrothermal system beneath Mount Baker.

Table 4.1 Results of surface strain-rate tensor model fit to line length data, assuming uniform strain accumulation. Reported uncertainties are plus or minus one standard deviation, with azimuth measured from north to maximum principal axis and extension reckoned positive. The preferred model is indicated in bold.

Model	ϵ_1 , nanostrain/yr	ϵ_2 , nanostrain/yr	Azimuth ϵ_2, degrees clockwise from North	Aereal Dilatation (Δ), nanostrain/yr				
Weighed all data	-322	± 128	-111	± 115	-9.2	± 33.5	-433	± 172
Un-weighted all data	-516	± 166	-035	± 150	-8.2	± 18.4	-551	± 224
Weighted (no: SHRM, CRAG)	-269	± 100	-148	± 100	-4.3	± 52.9	-417	± 141

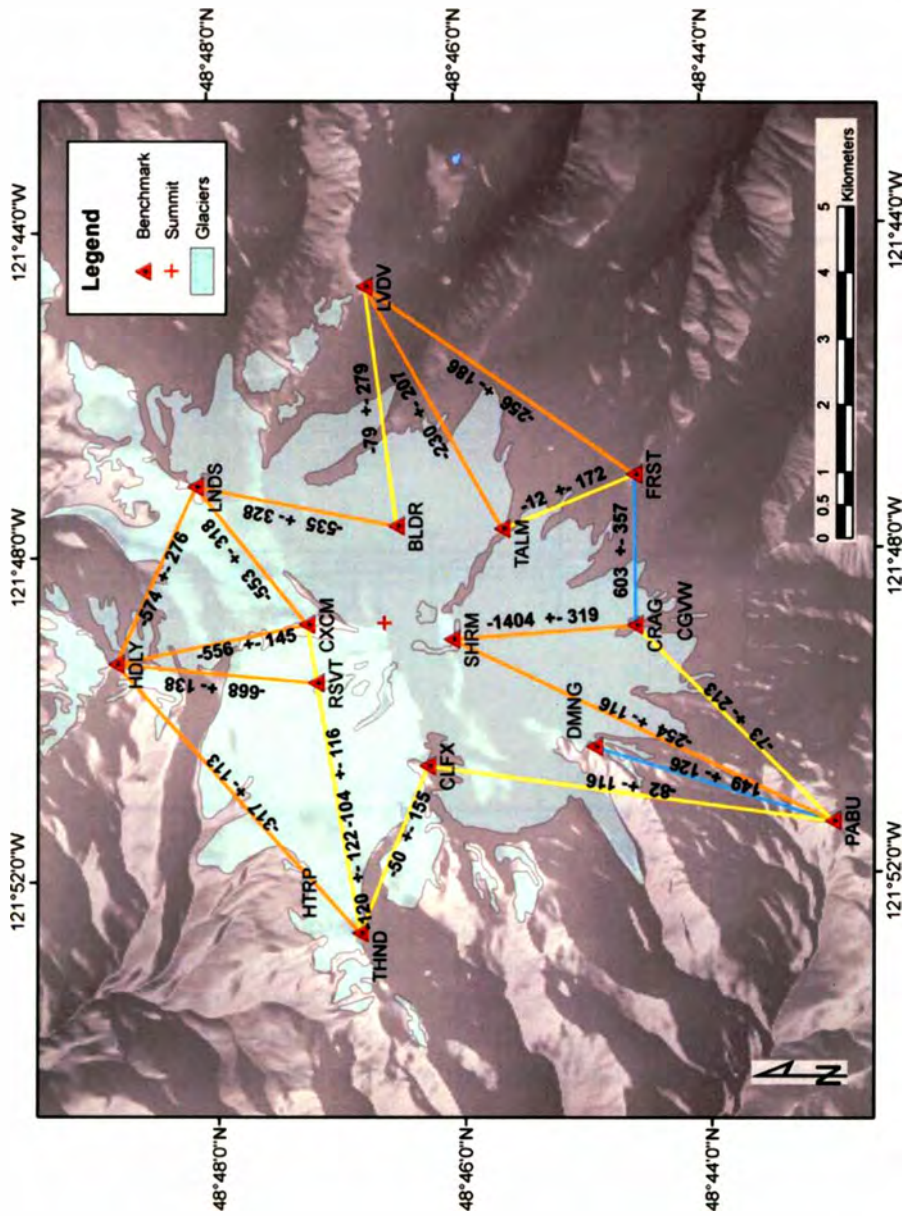


Figure 4.1. Strain accumulation (nanostrain yr⁻¹) between 1981/1983 and 2006/2007 for the 19 trilateration lines on Mount Baker. Reported uncertainties are one standard deviation and extension is reckoned positive. Benchmarks that comprise the Mount Baker trilateration network are indicated by red triangles. Strain-rates greater than uncertainty are indicated by orange lines. Digital elevation base map from the NED, 2006.

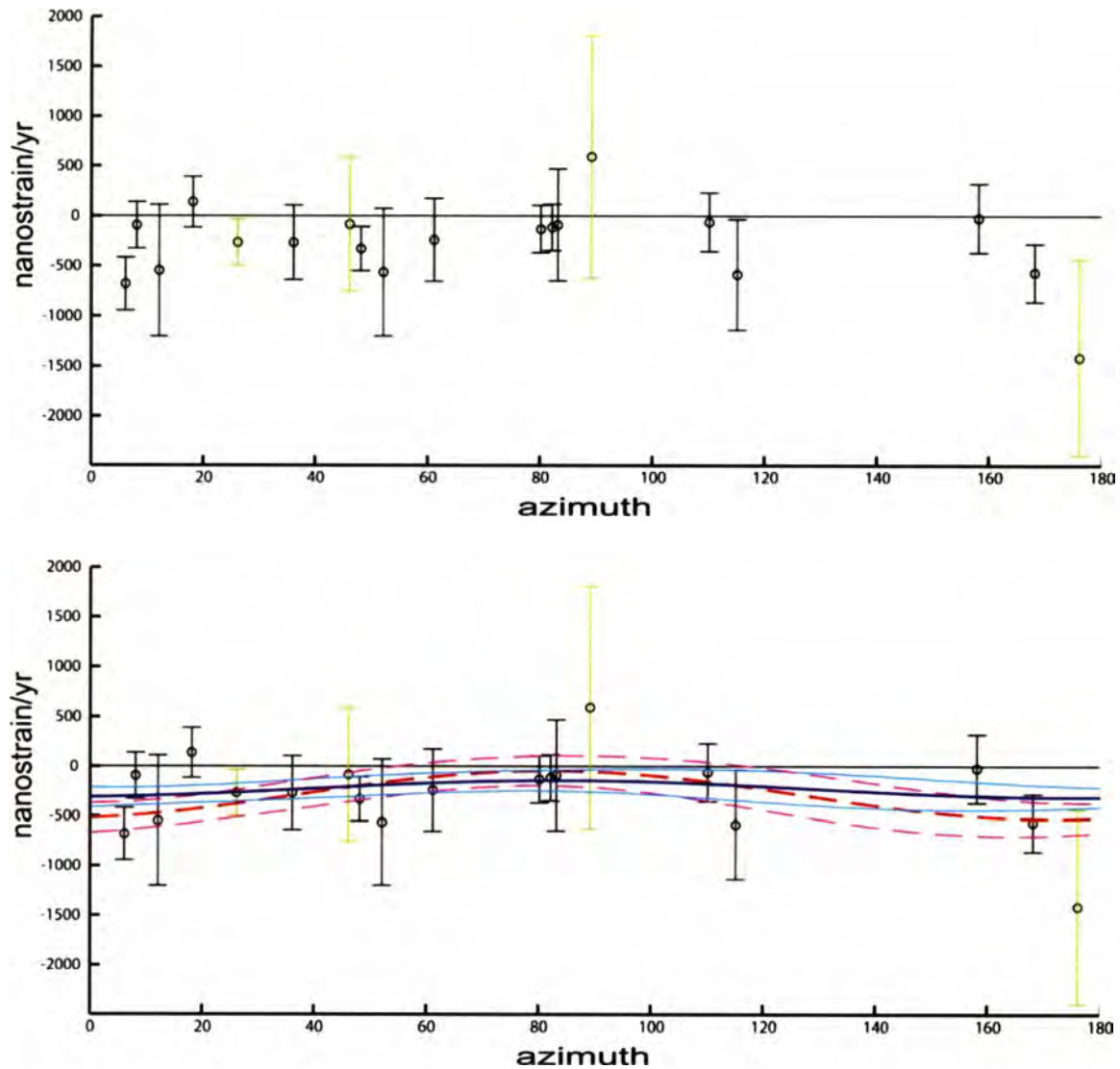


Figure 4.2. Strain accumulation rate (nanostrain/yr) for each trilateration line plotted as a function of azimuth (degrees) measured from north. Error bars are plus or minus two standard deviations. Data in green are lines which include SHRM or CRAG endpoints. The top plot shows data without model fits. The bottom plot shows the best fit sinusoids for each of the surface strain tensor models. The model is weighted (solid blue lines) by the uncertainties in the strain-rate to best fit the model to the data with lesser uncertainty. The red dashed line is the unweighted model for comparison. The light blue (solid) and red (dashed) lines above and below the darker sinusoids represent the 68% confidence intervals for each model. The preferred model for data excluding SHRM and CRAG is nearly identical to the weighted model (solid blue line), and is omitted for clarity.

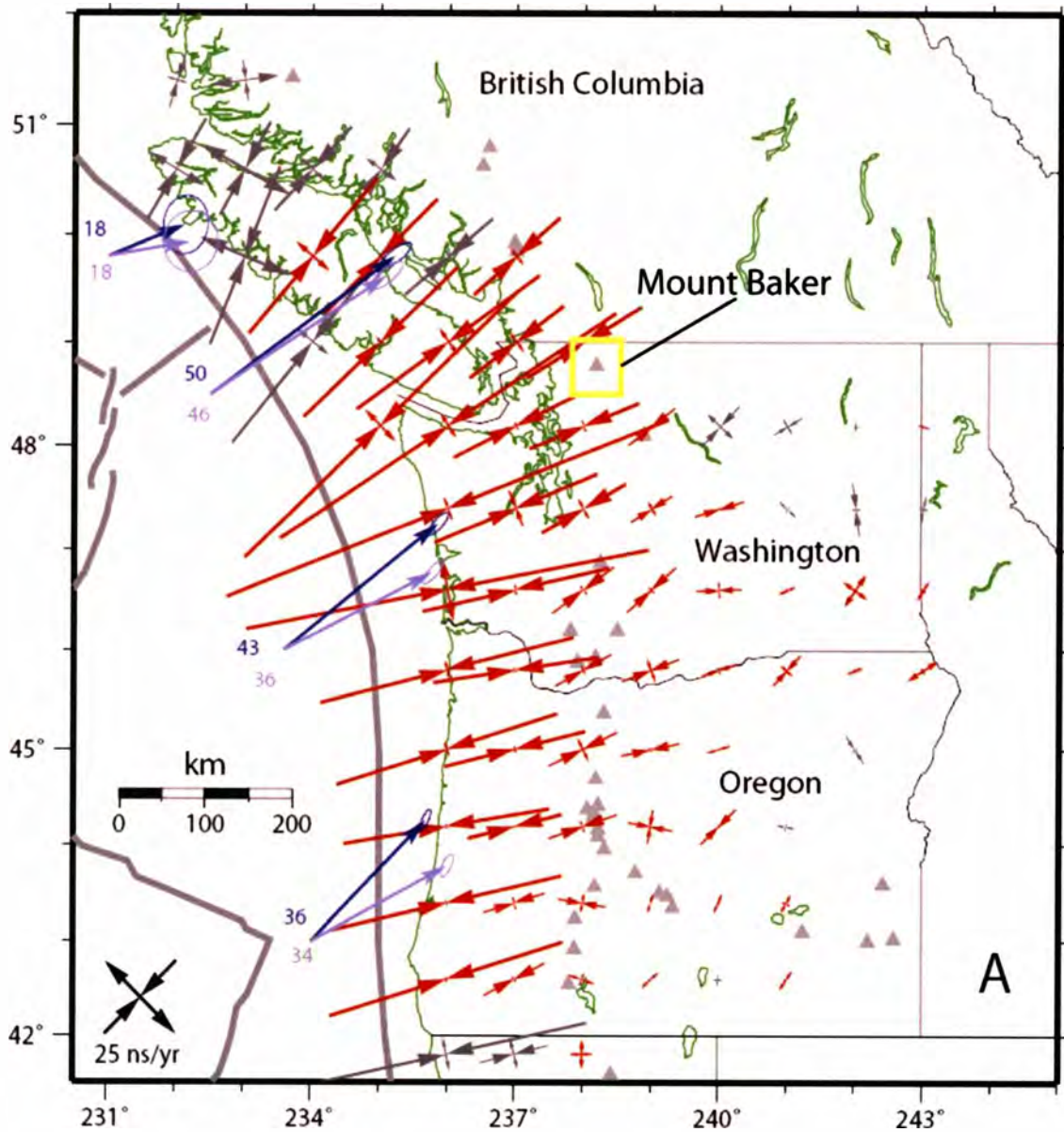


Figure 4.3. Surface strain-rates for the Cascade Forearc. Blue arrows indicate the plate convergence vectors (mm/yr) relative to North America (dark blue) and the Cascadia Forearc (light blue). Red arrows indicate the GPS derived surface strain-rate orientation (nanostrain/yr). Major volcanic centers are shown with grey triangles and the location of Mount Baker is indicated by yellow box. Figure from McCaffrey et al. (2007). Note that surface strain accumulation near Mount Baker is approximately -25 nanostrain/yr.

5.0 Modeling the source of deformation

At volcanoes, surface strain can result from changes to the magmatic or hydrothermal system. For example, inflation of a magma chamber by intrusion of new magma causes a change in volume and/or pressure within the chamber (Johnson et al., 2000). General conclusions on the evolution of a magmatic system can be deduced by simple characterization of surface deformation, i.e. whether the volcano is inflating or deflating, however, more complex physical relationships can be inferred using geomechanical models. Elastic dislocation (ED) models are commonly used to obtain important information about the mechanics of active magmatic systems (Dzurisin, 2007; Masterlark, 2007). ED models use the theory of continuum mechanics to describe the mechanical properties of the crust and implement constitutive equations to predict the resulting deformation of the Earth's surface (Mogi, 1958; Okada, 1985). These fundamental equations allow us to relate surface strain measurements to magmatic processes occurring deep within the crust where direct observations are impossible (Delaney and McTigue, 1994).

The goal of the elastic dislocation modeling experiments presented here is to obtain additional information on the depth and strength of the deformation source. This information may help evaluate competing hypotheses about the quiescent state at Mount Baker, including relationships between ongoing gas emissions (Werner et al., 2007), microgravity increase (Hill, 2007), and the fundamental question of whether the deformation source at Mount Baker is hydrothermally or magmatically related.

5.1 Analytical elastic dislocation solutions

Analytical models have been used to interpret surface deformation on volcanoes since Mogi (1958) proposed a point source dislocation as an idealized representation of an inflating or deflating magma chamber. The point source model (commonly known as a Mogi source) has been widely used to fit surface deformation data at volcanoes, such as Kilauea (Yang et al., 1992), Mt. Etna (Bonaccorso et al., 1994), South Sister (Dzurisin et al., in press) and many others. Other source geometries (e.g. ellipsoids, sills, dikes, cylinders) also have been used to fit geodetic data. However, sufficient geodetic data are required in order to distinguish between these more complex shapes and the most simple deformation geometry of a point source. Dieterich and Decker (1975) show that a unique solution to uniform surface deformation produced by different source shapes cannot be achieved without vertical and horizontal deformation data. Modeling may also rely on other geological and geophysical evidence to help distinguish between source model geometry (Dzurisin, 2003). In the absence of either deformation component, the simple point source model is most appropriate unless additional geophysical or geologic data suggests otherwise.

EDM data from Mount Baker are not defined in a fixed reference frame, which prohibits distinguishing absolute horizontal and vertical displacements from line length changes. Any strain detected by an EDM line is relative to other lines that may record variable components of both vertical and horizontal deformation. Because source geometry becomes ambiguous in the absence of either deformation component, a simple point source model is the most appropriate geometry for modeling Mount Baker

deformation data. This approach minimizes the assumptions of the deformational source, providing the greatest potential for meaningful interpretations.

5.1.1 The point source model and reference system

Surface displacements produced by an inflating or deflating point source (Mogi, 1958) referenced in a Cartesian coordinate system (x,y,z) are given by (Lisowski, 2007):

$$\begin{pmatrix} u \\ v \\ w \end{pmatrix} = \alpha^3 \Delta P \frac{(1-\nu)}{G} \begin{pmatrix} \frac{x}{(x^2 + y^2 + d^2)^{3/2}} \\ \frac{y}{(x^2 + y^2 + d^2)^{3/2}} \\ \frac{d}{(x^2 + y^2 + d^2)^{3/2}} \end{pmatrix} \quad (10)$$

where u , v , w are displacements at the free surface of the half-space in the x , y (horizontal) and, z (vertical) directions respectively. **Figure 5.1** shows the reference system used to compute surface deformation resulting from a point source. The point source dislocation is centered at a depth (d), and deformation is determined by the radial distance from the center of the cavity (0, 0, d) to a point on the free surface. Deformation relative to the origin (0, 0, 0) can be defined by replacing the last term on the right with:

$$\begin{pmatrix} u, v \\ w \end{pmatrix} = \begin{pmatrix} \frac{\sqrt{x^2 + y^2}}{(z^2 + x^2 + y^2)^{3/2}} \\ \frac{d}{(z^2 + x^2 + y^2)^{3/2}} \end{pmatrix} \quad (11)$$

The pressure change ΔP , the radius of the sphere α , and the material constants shear modulus G , and Poisson's ratio ν , are inseparable scaling terms that define the strength of

the deformation. Because these terms are inseparable, a small pressure change in a large cavity will produce the same deformation as a large pressure change in a small cavity. The change in volume (ΔV) of the pressurized cavity can be approximated by (McTigue, 1987):

$$\Delta V_{cavity} = \pi\alpha^3 \frac{\Delta P}{G} \quad (12)$$

where α is the assumed radius of the spherical cavity. For all the models, I assume typical values for effective shear modulus (G) and Poisson's ratio (ν) of 30 GPa and 0.25 respectively, and a reasonable estimate of chamber radius of 1000m (Lisowski, 2007; Turcotte and Schubert, 1982). This model is valid where the depth is much greater than the radius of the source and the pressure distribution in the sphere is symmetrical (McTigue, 1987).

Figure 5.2 shows the predicted horizontal and vertical displacement profiles normalized to the depth of the source. Deformation is axisymmetric and the greatest vertical displacement occurs directly above the source. The greatest amount of horizontal displacement occurs at a radial distance (r) approximately 70% of the source depth from the center and decreases with distance from the source. The horizontal component of displacement exceeds the vertical at greater than one source depth (d) from the center of deformation ($r > d$).

5.1.2 Topographic correction for analytical models

The effects of topography on modeled deformation can significantly distort the predicted surface deformation and influence interpretation of the deformation data

(Williams and Wadge, 1998). Most analytical models assume a flat Earth by using an elastic half-space solution. This assumption is particularly unrealistic in volcano deformation studies and therefore a number of methods (Williams and Wadge, 1998; Williams and Wadge, 2000) have been developed to more realistically model surface deformation in the high relief areas around volcanoes. The effects of topography on surface displacements are greatest above the center of the deformation source, (assuming an axisymmetric source) and decrease quickly as the radial distance approaches the depth of the source (McTigue and Segall, 1988). Because the amount of displacement is scaled by the depth of the source, the effects of topography are magnified with increasingly shallow source depths. Therefore, topographic corrections to deformation models become important on volcanoes with potentially shallow magma systems.

Topography has the effect of masking the strength of horizontal and vertical displacements thereby mimicking a greater source depth than predicted by a topographically accurate model. Williams and Wadge (1998) show for the case of Etna volcano, surface displacements predicted by a magma chamber at 4 km depth would overestimate vertical displacements by 240% and radial displacements by 300%, if the effects topography were not included. Cayol and Cornet (1998) investigated the effect of topography on the deformation field. They calculate displacements using a numerical boundary element model and then invert those results to produce depth and strength estimates using an analytical Mogi model. Their results show that for average slope angles from 10° to 30° , the modeled strength of the source is overestimated by 10% to 50%, with the greater disparity produced by steeper volcanoes (Cayol and Cornet, 1998). Their inversion also showed that on volcanoes with similar average slope angles to Etna

(15°), the source depth fit best when measured from a reference elevation at the summit of the volcano (Cayol and Cornett, 1998). For inversion of volcano deformation data using a point source, neglecting topographic effects would significantly overestimate source depth and/or underestimate source strength (volume/pressure). For high relief volcanoes, such as Mount Baker (average slope angle of 24°), topographic corrections are an important step to produce more meaningful results from the inversion model.

The appropriate topographic correction model can depend on a number of factors, including the slope of the volcano, the location and type of deformation data, and the inferred depth of the source (Williams and Wadge, 2000). A reference elevation correction is the simplest method, and has been used to correct topographic effects on Etna (Bonaccorso et al., 1996). Williams and Wadge (1998) show that an optimized reference elevation method is most appropriate for correcting horizontal deformation data. However, optimizing the reference elevation method becomes difficult without prior knowledge of the likely depth of the primary magma chamber or guidance from a numerical model. In the absence of prior source knowledge or a numerical model, Williams and Wadge (2000) suggest selecting a reference elevation between the average and maximum relief and decrease this value with increasing source depth. As an alternative, Williams and Wadge (1998) propose a variable depth model, which computes the analytical solution at each point on the surface by varying the depth to the source based on the topography at the point. They find that this method is superior when correcting vertical displacement data and tilts, but the reference elevation method is more appropriate for horizontal deformation correction. One additional option is the topographically corrected model (TC) produced by Williams and Wadge (2000). The TC

method uses higher order corrections to the analytical solution for topographic perturbation on surface displacement in three dimensions, which is computationally complex. While this method has been shown to more accurately account for topographic effects, the slight improvement over simpler methods (e.g., reference elevation method) provides little value considering the assumptions of the chosen model and the quality of the current Mount Baker dataset.

5.2 Model inversion

Geophysical inverse methods provide the framework by which the relationship of a given physical model to the supplied observational data may be quantified. Not only are the best fit source parameters identified, but the appropriateness of a model can be quantified using statistical methods. Inverse methods provide the most robust approach for defining the fitness of a given model and the degree of the model validity. The utility of any inversion, however, is dependent on the model assumptions and therefore, any statistical tests on the validity of the model are also dependent upon these assumptions (Cervelli et al., 2001).

5.2.1 Introduction to inverse models

Inverse modeling is a mathematical approach used to determine best-fit model parameters to geodetic data. A forward model is solved iteratively by systematically replacing the model parameters (location and strength) and calculating the goodness-of-fit of the data to the model. The relationship between the geodetic data and the

parameters in the forward model is nonlinear and is expressed by the matrix equation (Cervelli et al., 2001):

$$\mathbf{D}_{//} = \mathbf{G}(\mathbf{m}) + \varepsilon \quad (13)$$

where $\mathbf{D}_{//}$ is the observed deformation vector, \mathbf{m} is the vector of model parameters, and \mathbf{G} is the function that describing the forward model. The parameter ε represents observation errors arising from noise in the data and errors in the chosen source model, which in this case ignores inhomogeneous and anisotropic properties of the crust.

The Mount Baker problem is simple, with only 19 data and a four-parameter point source model. Because of this, the entire parameter space can be searched for the best fit solution to the data. Therefore, the need for optimization techniques and the possibility of finding a local minimum in misfit space are eliminated. This approach insures that the global minimum is found, which represents the best fit model to the data.

5.2.2 Inversion methods for Mount Baker data

The Mount Baker slope-distance-change inverse problem is defined as a function of the chosen point source model (\mathbf{G}) to the observational data ($\mathbf{D}_{//}$). The “optimal” model parameters (\mathbf{m}) are returned when the combination of free parameters minimizes the function in a least-squares sense. The model fitness is quantified in vector terms by the squared residual norm estimator (L_2 norm) given by (Cervelli et al., 2001):

$$L_2 = \sqrt{\sum_{i=1}^N | r_i^T r_i |} \quad (14)$$

where \mathbf{r} is the residual vector between the data and the model and N is the number of data. This value is similar to the root mean square error (RMSE) estimator.

I correct my model experiments for a topographically induced scale error in the displacement calculation by using the reference elevation method (Williams and Wage, 1998). I select a reference elevation of 2000 meters based on the median elevation of Mount Baker. The same reference elevation was determined to be the most appropriate choice at Mt. Etna with a magma chamber depth of 4 km (Williams and Wage, 1998). This method effectively places the displacement vectors near the free surface of the half-space, which is assumed to coincide with mean sea level. Depths to source estimates are calculated from the reference elevation.

The Mount Baker deformation data are transformed from a geographic coordinate system (latitude, longitude) into a local Cartesian reference frame (northing, easting) in order to calculate relative surface displacements within the elastic half-space. Slope-distance changes are estimated from the forward model by differencing the displacement vectors between known benchmark locations and their predicted (modeled) location. The line-length changes from the model are compared to the data. A derivative-based algorithm (Levenberg-Marguardt) is used to find a combination of input parameters that minimizes the model residuals identified by equation 14. With each iteration of the algorithm, new initial parameters are determined based on the “down hill” least-squares solution until the functions’ derivative converges to zero, which defines a minimum misfit of the data to the model. Any derivative-based algorithm is sensitive to the initial parameter estimate and may become trapped in local minima within misfit space (e.g. Lisowski, 2007; Cervelli et al., 2001). No *a priori* information exists to indicate the possible position of a magma chamber beneath Mount Baker. Therefore, a search

method must be implemented to locate the model input parameters that produce the best fit by locating the global minimum within misfit space.

I systematically searched for a global minimum by establishing a grid in geographic space and calculating the local minimum within each grid cell. Minima for each cell were tallied and evaluated to determine the cell with the lowest misfit; the global minimum. The interval and extent of the grid spacing is somewhat arbitrary, but limited by the expected extent of detectable volcanic deformation sources (Dzurisin, 2003). I chose a geographic search extent of 20 km by 20 km in surface centered on the summit of Mount Baker. I selected a search interval that seems appropriate for the spatial relationships of the model (usually 100-meter cells). It is important to select a sufficiently dense grid to locate all the significant local minima.

First, I invert for the optimal combination of depth and strength by constraining the location of the point source to be directly beneath the summit. Based on the surface strain model results, I used a deflationary point source. For every 100 meter grid increment of depth the misfit is computed for a 10^5 volume increment (from -10^6 to -10^8 m^3), to produce a 1,000 by 1,000 matrix of misfit values. **Figure 5.3** is an example of the three dimensional topology of misfit space derived from the initial input parameter matrix. The first inversion experiment produced an optimal depth around 6000 m with a volume change of -14×10^6 m^3 . This method gives an initial estimate for the unconstrained inversion problem, which solves for all four parameters (northing, easting, depth, volume change). This model is then run over several iterations in the vicinity of the median optimal fit values which typically range from 4000 m to 6000 m in depth and -6 to -13×10^6 m^3 in volume change. In each model run, the best fit horizontal location

of the point source is well constrained with optimal parameter returns in the vicinity of the global optimized easting and northing at 285 m and 1360 m, respectively. A model with these source location estimates is once more inverted for optimal values. **Figure 5.4** shows the population distribution for the optimal location- (northing, easting) constrained inversion and the estimated 95% confidence intervals for each parameter (**Table 5.1**). A commonly used indicator of model fitness is the Chi square statistic, which provides a measure of error in fitting the observational data to the predicted data (Battaglia and Segall, 2004). The weighted Chi square (χ_w^2) value, normalized by the degrees of freedom in the model (number of data minus number of free parameters) is given by (Newman et al., 2006):

$$\chi_w^2 = \frac{1}{(N - M)} \sum_{i=1}^n \left(\frac{r_i}{\sigma_i} \right)^2 \quad (15)$$

Where r is the individual residual line-length and σ is the individual line-length uncertainty. The reduced Chi square estimator is plotted as a function of depth and volume changes for a model with the optimal horizontal location (**Figure 5.5**). A model that more accurately predicts the data with correctly assessed uncertainties produces a reduced Chi square value near one. There is only a 1.7% chance that a valid model parameter may fall outside a reduced Chi square value of two (Taylor, 1997). The lowest Chi square value indicates a model located at 5.4 km depth with a volume change of $-11 \times 10^6 \text{ m}^3$.

Confidence intervals for model parameter estimates are difficult to define due to the non-linear nature of the problem. The data likely contain correlated noise, which further complicates statistical reasoning and produces a sample set of returned optimal

parameters with an unknown population distribution. Therefore, standard Gaussian statistics cannot be used to determine confidence intervals for the returned optimal source parameters. I assess confidence intervals for the model parameters using probability plots built into the Matlab working environment (Mathworks) by assuming a non-parametric probability distribution fit to the data. Optimal point source confidence intervals are estimated and shown in **Figure 5.4**. Parameter correlation and distributions can be qualitatively examined by scatter plots similar to Cervelli and others (2001). The covariance plots (**Figure 5.6**) show a strong correlation between depth and volume change as is expected by the analytical equation. In comparison the correlation between northing and easting is lower, as indicated by the elliptical cluster.

5.3 Inversion model results

The optimal point source is 1360 meters north and 285 meters east of the summit, beneath the Dorr fumaroles, at a depth of 5.4 km (3.4 km MSL) with an estimated volume change of $-11 \times 10^6 \text{ m}^3$. **Figure 5.7** shows the location of the point source with the predicted displacement vectors from the forward model. The modeled line-length changes are shown with the observed line-length changes for each line, except those with SHRM and CRAG endpoints, which were removed from the analysis to avoid biasing the results with the unreliable data. Overall the model appears to fit the data quite well. The magnitude and style of the predicted extensions (i.e. elongation or contraction) are consistent within the expected errors and magnitude of change, with the exception of line PABU-CLFX. This inconsistency may indicate instability of the CLFX benchmark, an un-modeled property of the volcano, or errors in the model. The model appears to fit the

lines on the northern flank of the volcano best, with the exception of THND-CXCM. Other important features are also captured well by the model. For example, near-zero extension detected on line TALM-FRST, which has relatively little observational error, is closely predicted by the model. The elongation of PABU-DMNG is also explained by the model. The deformation on the south side of the volcano, however, is loosely constrained due to the lack of reliable slope distance measurements from SHRM and CRAG marks.

Figure 5.8 shows the data uncertainties plotted versus the model residuals. In the event when the model predicts a value beyond the uncertainty for the observed value, this would plot above the diagonal line. For the best fit model, all the observations with the exception of lines PABU-CLFX and THND-CXCM can be explained to within one standard deviation of the data uncertainties. If the model is correct, the unpredictability of these lines suggests unmodeled properties of the volcano, errors in the model or perhaps underestimated uncertainties in the location of the marks. The proportion of the variability in the data predicted by the source model is quantitatively determined by the unit quotient of the modeled residuals and the predicted data, which is known as the R^2 value (Battaglia et al., 2003a). A R^2 value of 1 indicates that the model can fully explain the variability in the data, while a R^2 value of 0 indicates that the model is not able to explain any of the data. The best fitting point source model at Mount Baker produces an R^2 value of 0.91, indicating a majority of the data are explained by the model.

The model can account for much of the deformation detected, indicating that a point source model is appropriate, at least to a first order, for modeling physical changes to the magmatic or hydrothermal system at Mount Baker. It is important to note that this

result does not represent a unique solution to the problem. In fact, there are likely many other shapes and strengths that may produce similar results. The large uncertainties (1-2.5 cm) in the GPS to EDM comparison owe to rather noisy data. Combined with the relatively small deformation signal, the signal/noise ratio yields rather large uncertainties in the model parameters. Because of this, it is possible to fit the model reasonably well within a range of parameter estimates. In addition, this data type does not permit distinguishing different model geometries. Therefore any volume changes are also loosely constrained because volumetric changes are variable for different sources shapes (Johnson et al., 2000). Microgravity studies (Hill, 2007), and gas data (Werner et al., 2007) give us only relative proxies on the physical parameters of the magmatic or hydrothermal system. We have no seismic data to constrain the potential location of a magma chamber. Therefore any statistical approach used for identifying a more appropriate inversion model would likely fail from lack of a superior *a priori* forward model.

Table 5.1 Optimal parameters and upper and lower 95% confidence intervals for each of the four point source model parameters.

Optimized Model	Optimal Value	Confidence Interval	
		-95%	+95%
Depth (m)	5400	2970	6620
Volume Change (10^6 m^3)	-11	-1.7	-16.4
Easting (m)	285	-10	646
Northing (m)	1360	970	2350

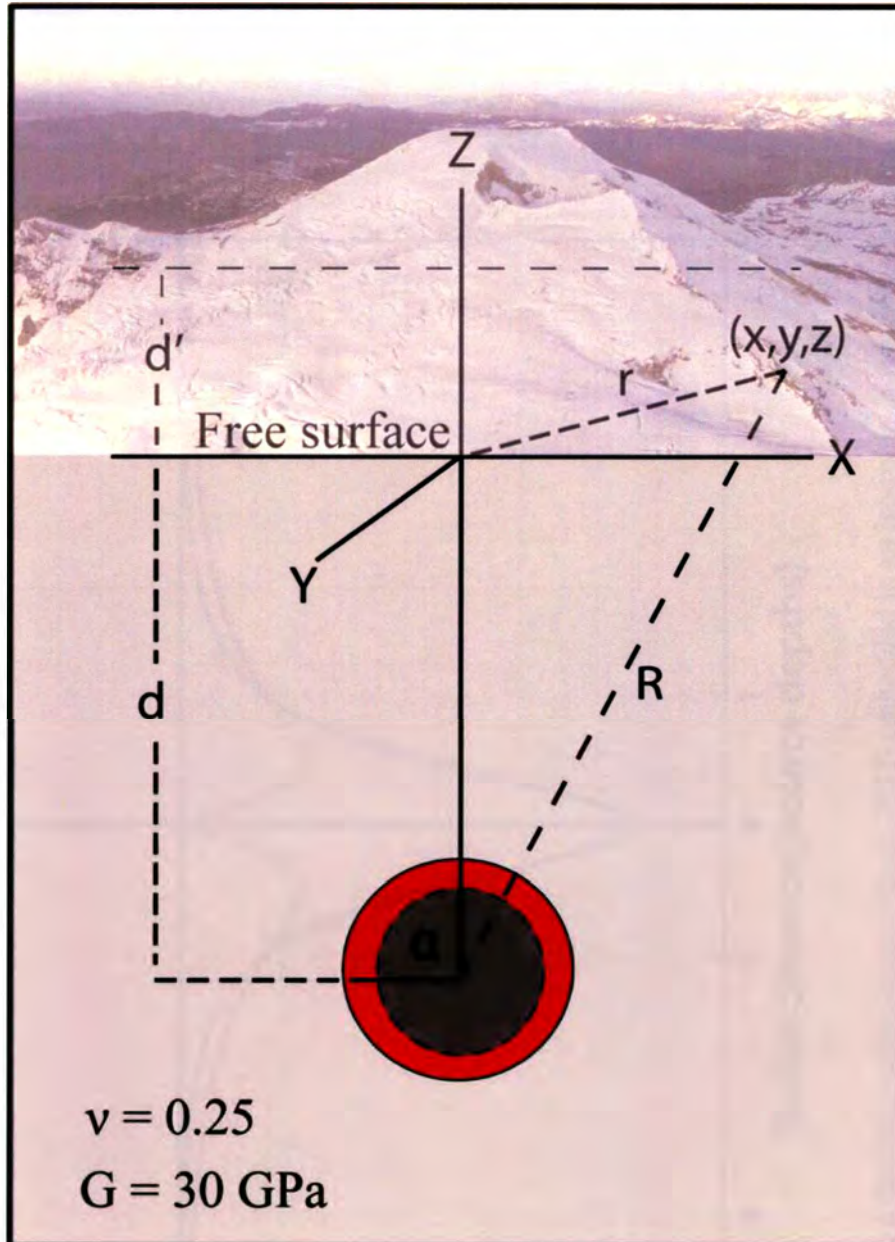


Figure 5.1. Schematic of coordinate system used to calculate surface displacements using an elastic dislocation model. The point source (Mogi source) is embedded in a homogeneous, linear elastic, isotropic half space at a depth (d). R is the distance from the center of the point source to the location of deformation (x, y, z) on the surface. The radial distance (r) is measured from the point on the free surface directly above the source. A reference elevation is used to correct for topography (d') (Williams and Wadge, 1998). The material properties of Poisson's ratio (ν) and elastic shear modulus (G) are assumed constants used in modeling experiments. A magma chamber radius (α) of 1000 m is assumed for volume calculations. Background photo by John Scurlock, 2005.

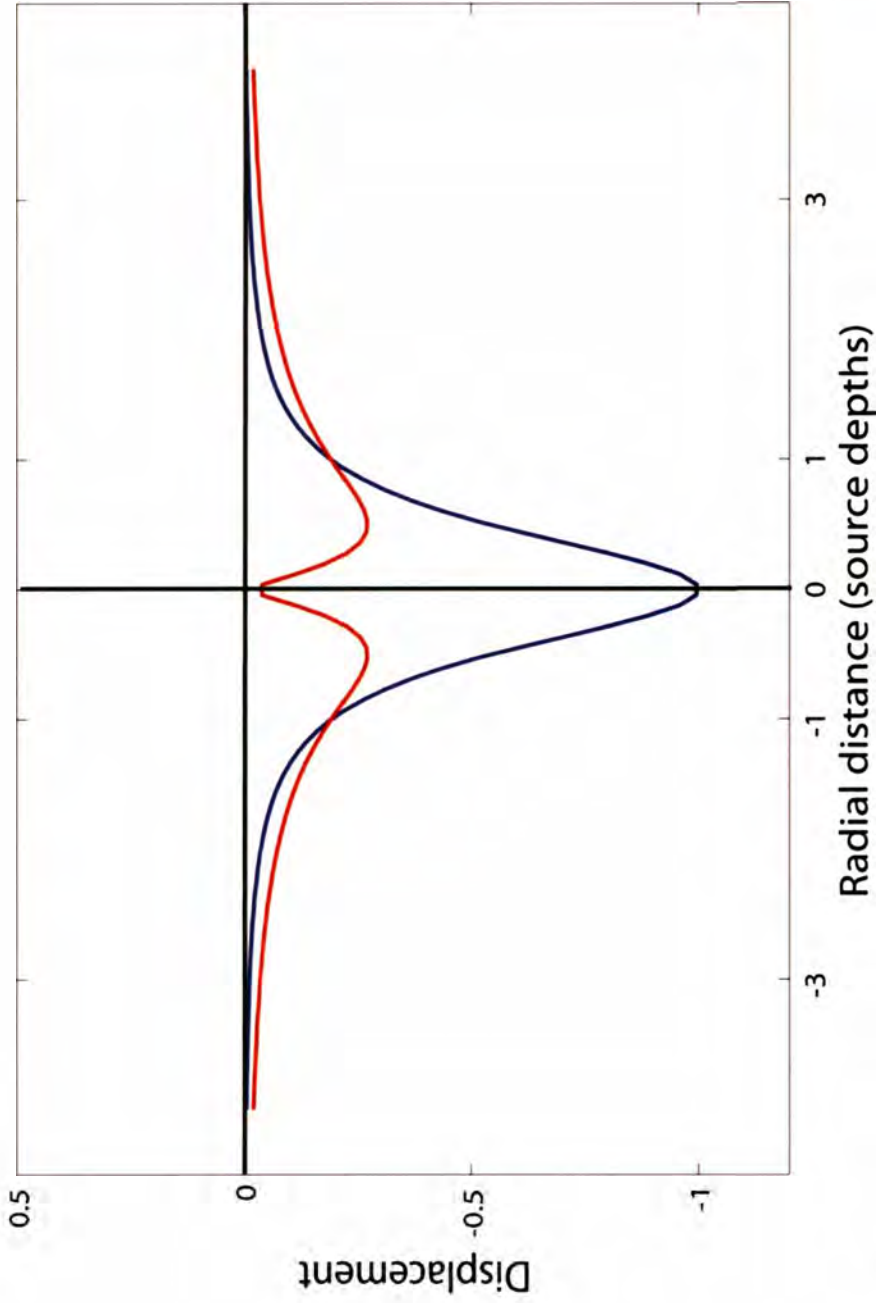


Figure 5.2. The analytical solution to a deflating point source (Mogi, 1958) embedded in an isotropic, homogeneous, semi-infinite elastic half-space. The vertical (blue) and radial (red) displacements are normalized to source depth and maximum vertical displacement, which occurs directly above the source. Note that the absolute magnitudes of radial and vertical displacement are equal at $r = d$, and the magnitude of the horizontal component of displacement is greater at $r = \pm 1d$.

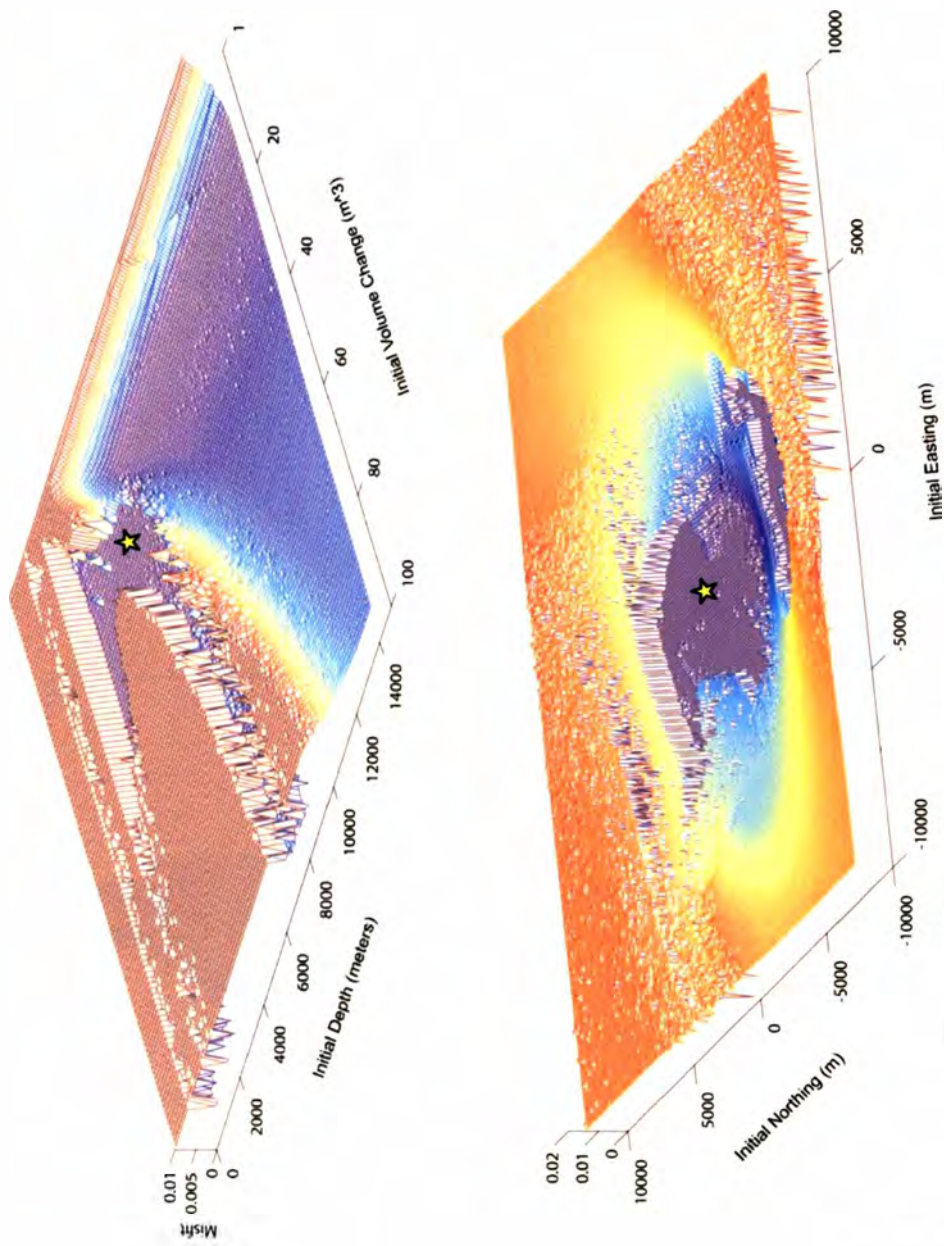


Figure 5.3. Example of model misfit plotted as a function of initial input parameters. In the top plot, the source location was held constant and only the depth and pressure was varied for optimal fitness. In the bottom plot, the model is left unconstrained and the location and strength of a point source were inverted for best fitness. The global minimum for each model is indicated with a yellow star.

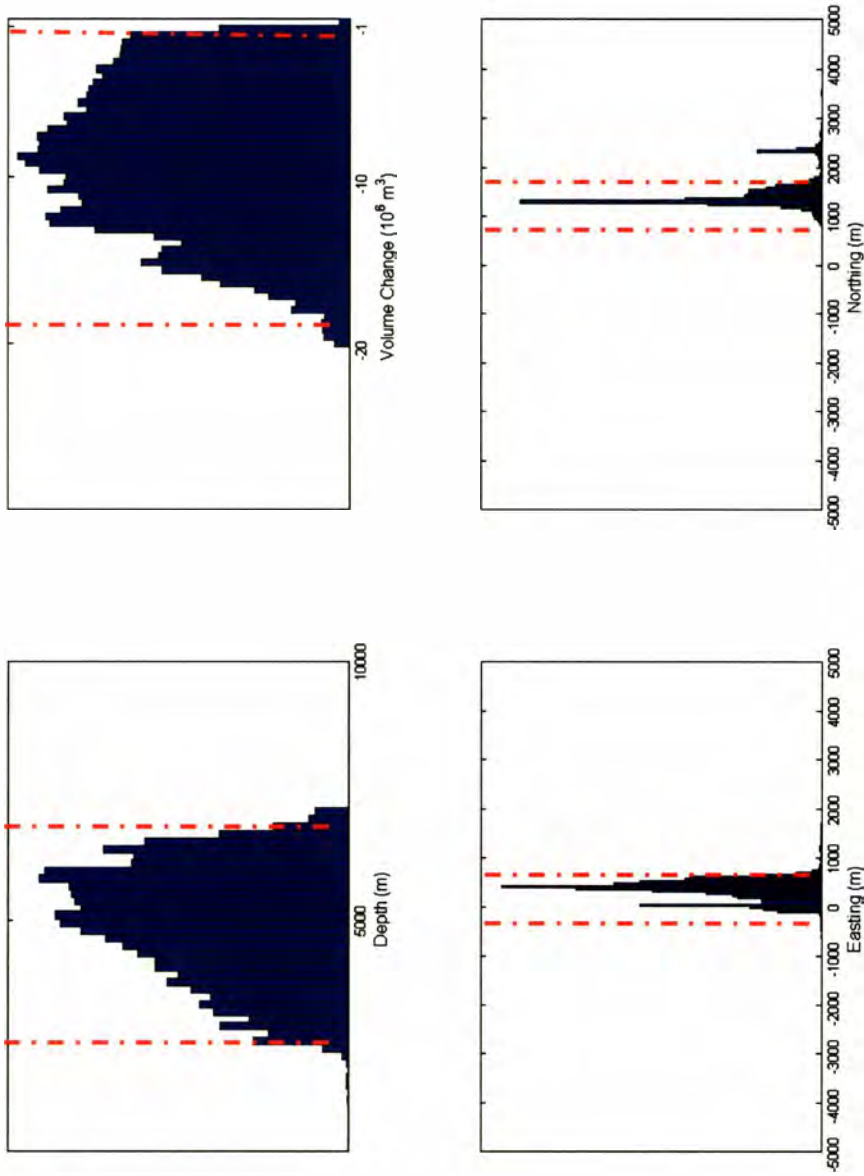


Figure 5.4. Histograms of the distribution of source parameters for the optimal point source model. Red vertical lines indicate the 95% probability values from the median of the sample. The reference origin for easting and northing is centered on Mount Bakers' summit.

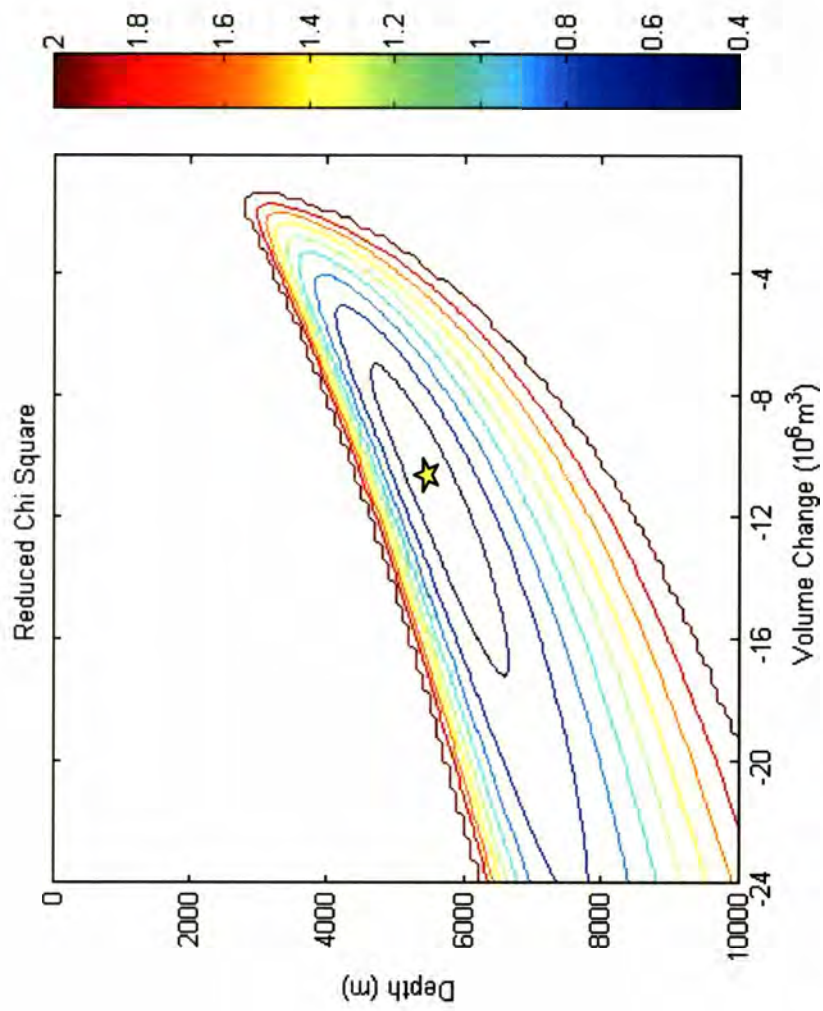


Figure 5.5. Reduced Chi Squared estimator for model 'fitness' as a function of depth and volume change for Mount Baker line-length changes. The lowest Chi square value indicates the relative best fit point source model parameters of a location constrained (northing, easting) to be 1.5 km north-northeast of the summit of Mount Baker. Yellow star indicates the location of the best fit model.

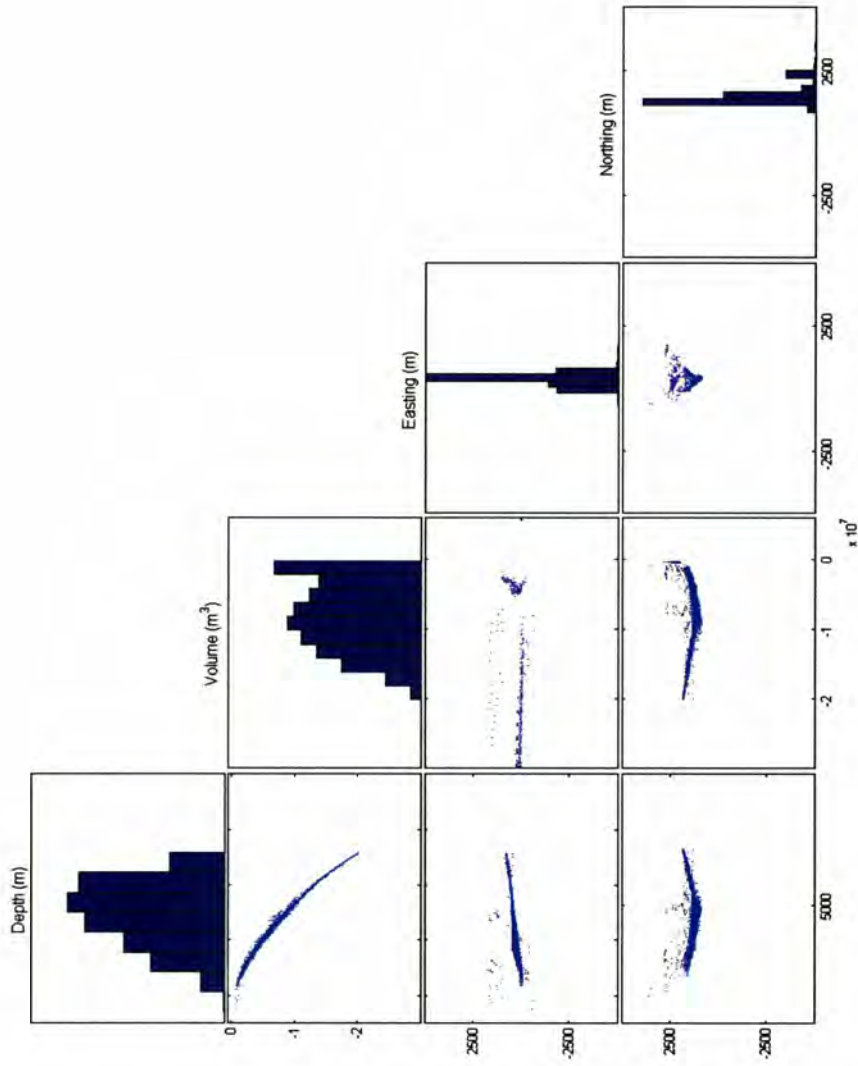


Figure 5.6. Covariance plot for best fit point source model of Mount Baker deformation. Scatter plots show the correlations between parameter pairs indicated by column heading. The histograms represent the distribution of the model parameters. Note strong correlations between depth and volume change. The horizontal location of the source is less correlated.

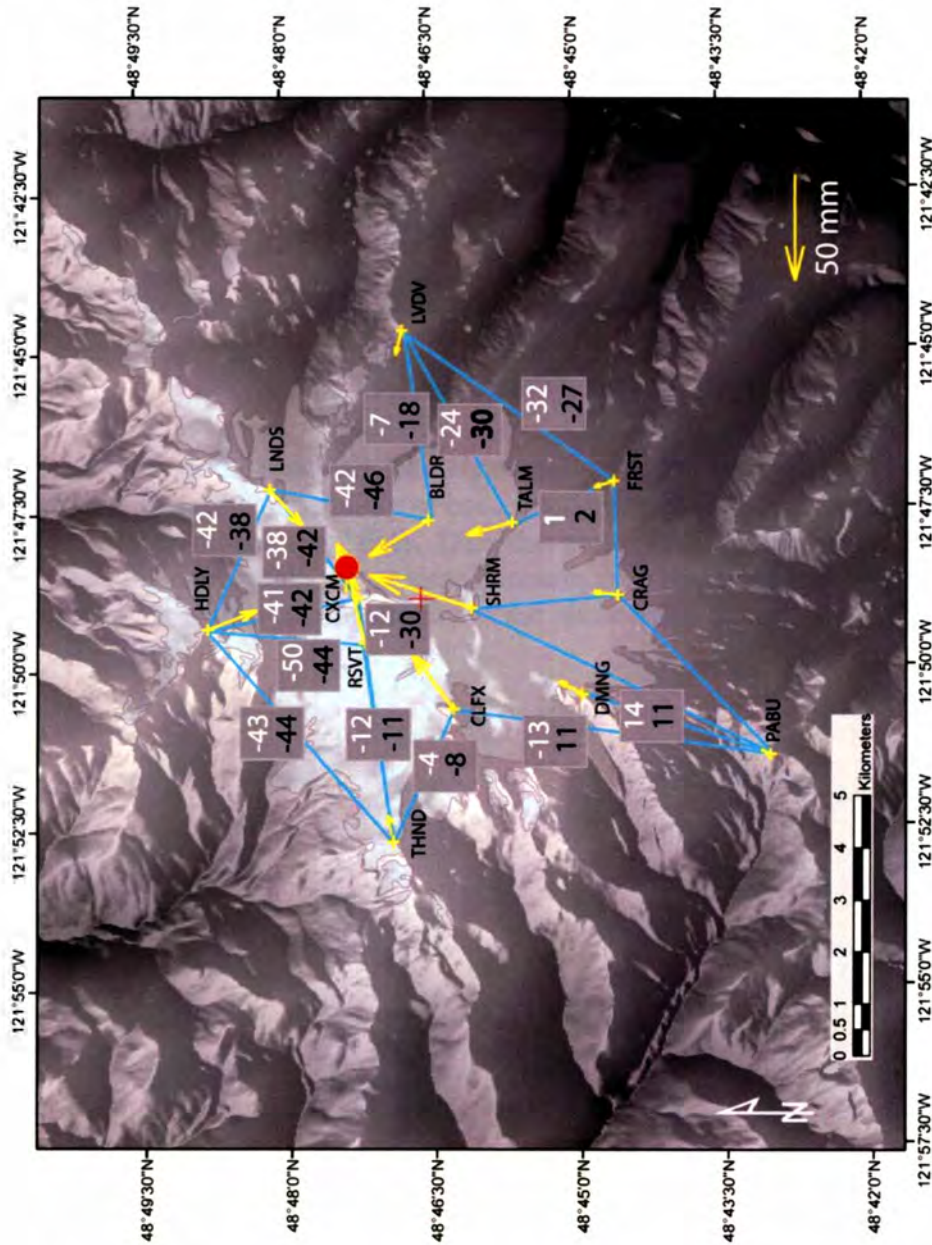


Figure 5.7. Comparison of point source model and observations at Mount Baker. Observed (white numbers) line-length changes in millimeters at Mount Baker from GPS and EDM comparison and predicted (black numbers) values are from the best-fit point source model base on inversion of slope-distance changes. The red dot is the surface location of the best fit point source at a depth of 5.4 kilometers. The yellow arrows are the predicted horizontal displacement vectors from the point source model. The red cross indicates the summit of Mount Baker. Digital elevation base map from NED, 2006.

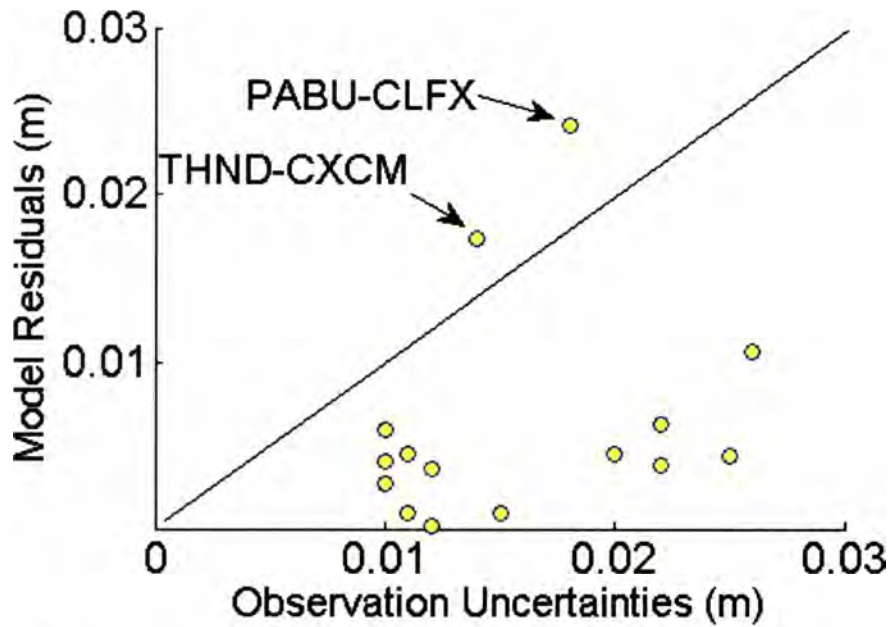


Figure 5.8. Model residuals for the optimal point source model. The calculated one-standard-deviation uncertainty of each line-length change is plotted versus the residuals of the best fit model to the data. Data that plot below the line indicate that the model predicts the data within the expected uncertainty. Note that nearly every model prediction is within the uncertainty of the observation except lines THND-CXCM and PABU-CLFX.

6.0 Interpretation and discussion

Edifice contraction of Mount Baker implies depressurization or volume loss of a source at depth. In a volcanic system like Mount Baker, this could result from either a depressurized hydrothermal system, deflation of the magma chamber, or a combination of these. Persistent degassing of magmatic gasses from fumaroles strongly suggests the presence of a magma body beneath Mount Baker (Werner et al., 2007). A magmatic heat source would be necessary to produce the 1975 thermal event which preceded the geophysical changes observed on the volcano since then (Hill 2007; this work). Likewise, much of the upper edifice and Sherman Crater is formed from acidically altered breccia deposits and lava flow (Warren et al., 2006), suggestive of a long lived hydrothermal system beneath Baker. Both of these sources are plausible and likely related causes of deformation at Mount Baker.

The model results predict nearly 10 cm of maximum subsidence over the 25 years between measurements (~4 mm/yr). Comparable subsidence rates are observed at other quiescent volcanoes in the Cascades. For example, Lassen Peak has been subsiding for nearly two decades at a maximum rate of 10 mm/yr (Poland et al., 2004). Similarly, Medicine Lake volcano has subsided at a maximum rate of 8.6 mm/yr since 1954 (Dzurisin et al., 2002). If deformation is still occurring, it is likely very slight as the several repeat GPS surveys since 2004 show no significant ongoing deformation beyond background signal (Parker, 2005; this work). Based on declining gas emission rates since the 1975 event (Werner et al, 2007), it seems most likely that the deformation rates on Mount Baker were most likely highest during the 1980's, assuming that the two phenomena are related. The data does not preclude the possibility that episodic periods

of edifice inflation and deflation have resulted in a net edifice deflation since 1981. However, due to lack of significant seismicity during this time (Steve Malone pers. comm., 2007) or other supporting evidence, the idea of a single (perhaps long-lived) subsidence event seems most likely.

Hydrothermally-produced surface subsidence at volcanoes can occur from poroelastic and thermalelastic contraction in shallow source regions (Masterlark et al., 2004). For example, InSAR studies at Kiska volcano, Alaska, indicate surface subsidence detected during steam venting has resulted from a decrease of pore fluid pressure in a shallow (< 1 km deep) hydrothermal system (Lu et al., 2002a). Because of the active hydrothermal system at Mount Baker, the possibility of hydrothermal driven deformation warrants consideration. The best fit source depth at Mount Baker was found to be relatively deep (3-7 km), inconsistent with the shallow source regions (<1 km) inferred to produce deformation from poroelastic processes (Masterlark and Lu, 2004; Mossop and Segall, 1999). Modeling results suggest that near-surface poroelastic deformation sources would not contribute much to the edifice-wide deformation because the model does not fit the data well at depths of 0-2 km. However, these results cannot rule out the possibility of deformation driven by depressurization of a deep hydrothermal system.

A potential hydrothermal source of deformation could involve breaching of a self-sealed confining layer that can develop near the brittle-ductile transition zone (3-4 km) above a crystallizing magma chamber (Fournier, 2007). This type of confined hydrothermal system would develop under lithostatic pressure trapping magmatic brine and steam that accumulates from volatile exsolution. The sealed layer may be breached

by over pressurization of the confined hydrothermal system or seismic activity, thereby releasing a surge of magmatic fluids upwards into the hydrostatic sub-volcanic hydrothermal system (Fournier, 1999). This compelling hypothesis is consistent with the abrupt increase in thermal and gas emissions at Mount Baker during 1975 (Frank et al., 1977) and may also explain subsequent contraction of the edifice (this work) via depressurization of a deep hydrothermal system. However, there was no recorded seismic activity to indicate a trigger (Frank et al., 1977). Other workers have used surface water chloride concentrations to infer a magmatically driven hydrothermal system at South Sister, Oregon (Wicks Jr. et al., 2002). Chloride concentrations in samples from Sherman Crater rose from 0.9 – 1.6 mg/L in 1974 to 28 mg/L in 1975 and then decreased to 8.8 – 13 mg/L in 1976 and 1978 (Frank and Krimmel, 1980). For comparison, spring samples at South Sister found anomalous dissolved chloride concentrations of up to 18.6 mg/L beyond background values during the deformation event (Wicks et al., 2002). The spike in chloride concentrations detected during and after the 1975 thermal event at Mount Baker indicates a pulse of magmatically derived fluids, consistent with a breached confined hydrothermal system.

Depressurization of the hydrothermal and magmatic system may act in concert to produce the edifice contraction seen on Mount Baker. The depth of the best fit deformation source at Mount Baker is coincident with a brittle-ductile transition zone inferred at other aseismically deforming volcanoes in the Cascades (Dzurisin et al., 2006). Gradual intrusion of new volatile-rich magma prior to 1975 may have provided the trigger to breach a lithostatically pressurized hydrothermal cap. Subsequent steady depressurization may drive exsolution of the volatile phase in the intruded magma

resulting in persistent degassing and subsequent edifice deflation from cooling and pressure/volume loss. A pulse of new volatile-rich magma intruding beneath Mount Baker prior to 1975 is consistent with the abrupt increase in gas and heat flux observed in 1975 (Frank et al., 1977). Aseismic magma intrusion (i.e., edifice inflation) has been inferred at other quiescent stratovolcanoes (e.g. South Sister, OR; Peulik, AK) at source depths similar to that inferred at Mount Baker (Dzurisin et al., in press; Lu et al., 2002b). A decrease in the rate of persistent degassing since 1975 (Werner et al., 2007) would suggest ongoing depletion of the initial volatile source, thereby depressurizing the magmatic system. However, continued degassing may also indicate recharge of volatile saturated magma, perhaps from convection within the magma reservoir (Cynthia Werner, pers. comm., 2007). Because no geodetic monitoring occurred prior to the 1975 thermal event, an episode of edifice inflation would have gone undetected. This scenario cannot be eliminated as a potential trigger mechanism for deflation of Mount Baker given the geodetic data alone. Thus, we must rely on gas and gravity data to help differentiate potential deformation mechanisms.

Gas emission data suggest either a continued supply of volatile rich magma or steady exsolution of a single magma pulse (perhaps via convection) that intruded prior to deformation measurements. I favor the latter, as steady flux of new magma into the shallow magma chamber should produce inflation, not deflation of the volcano. Using the gas emission rate of McGee and colleagues (2001), I estimate the volume of undegassed magma assuming the addition of no new magma. The time series of degassing at Mount Baker is not well known and therefore, not well constrained. An average CO₂ degassing rate of 150 tonnes/day as seen in 2007 produces a cumulative CO₂ mass flux of

1.7×10^9 kg. This gas flux rate is probably a lower bound considering that flux rates were greater during the 1975 thermal event (Frank et al., 1977). Given the partial specific density of CO_2 in liquid phase (1400 kg/m^3), and neglecting chamber pressure changes from a decrease in shear properties and compressibility of the magma, the magma volume change by removal of 1.7×10^9 kg of dissolved CO_2 is thus $1.2 \times 10^6 \text{ m}^3$ (Spera, 2000). By this calculation a minimum of 10-20% of the net volume change ($-11 \times 10^6 \text{ m}^3$) may be the result of carbonate loss. By these estimates, CO_2 degassing alone is likely not sufficient to produce the entire volumetric deformation signal detected at Mount Baker. The amount of dissolved H_2O in andesite magma can be a significant portion (35-90%) of the total volatiles by weight in andesite magma. Decreasing the density of the magma by exsolution of 3% by weight H_2O would increase the magma density by $\sim 5\%$, and therefore, decrease the volume of the magma chamber (Wallace, 2000). Thus, magmatic water loss could provide an additional mechanism to deflate the magma chamber beneath Mount Baker, either via steam in the vapor phase or by hydrothermal advection in liquid phase.

Thermal contraction of a magma body may provide an additional mechanism for deformation at Mount Baker. Calculations following the work of Masterlark and Lu (2004) indicate that a spherical magma chamber with a radius of 1000 m would require a temperature decrease of 100 to 250°C to explain the deformation, depending on the volume change of the source. Heat from a magma chamber at 5 km depth could be removed via conduction through the crust or advection in a hydrothermal system.

Subsidence of a volcano would produce a gravity increase, all else being equal. The theoretical free air gradient correction (Williams-Jones and Rymer, 2002) for the

predicted downward vertical surface displacement of 10 cm at Sherman Crater is 30 μgal . However, a relative microgravity increase of $1564 \pm 33 \mu\text{gal}$ was observed at SHRM between September 1980 and July 2005 (Hill, 2007). Nearly 5 meters of vertical displacement is required to completely account for the gravity increase at Sherman Crater as a function of elevation change alone. Therefore, the remaining change must be a function of additional mass beneath the volcano and/or a redistribution of mass closer to the surface near the gravity station.

I use the result of the point source inversion to compute the expected gravity change at SHRM (site near the gravity measurement) as purely a function of mass change within a magma chamber (Johnson, 1995). Approximately $3 \times 10^9 \text{ m}^3$ of new andesitic magma would be required to produce the gravity increase at SHRM. A volume increase of this magnitude should produce inflation of the volcano. Similarly, a point source model is used to determine a density change required to purely explain the gravity increase. A 1000 m radius chamber at 6 km depth would have to experience a density change of 3.00 g/cm^3 to explain these observations. However, expected density variations in a subsurface magmatic system are at least 1 to 2 orders of magnitude less (Spera, 2000). Mass redistribution from intrusion of magma nearer to the surface seems unlikely during a period of very little seismicity (Steve Malone, pers. comm., 2007). Therefore, I infer that changes to the magmatic system alone cannot account for the gravity changes detected at Sherman Crater given the assumptions of the point source model.

Mount Baker has been persistently degassing since 1981, thereby removing mass from somewhere beneath the volcano. A gravity decrease would be expected from

degassing (mass loss). The net decrease in relative gravity since 1975 at the intermediate site (Crag View) (Hill, 2007), is consistent with the idea of mass loss and densification, which is supported by the deformation results. The fact that relative gravity has increased by ~ 400 μgals since 1981 at the intermediate site (Crag View) indicates that a switch in the gravity mass/density trend has occurred (also seen in the gravity trend at SHRM). Perhaps the volcano is experiencing a period of inflation and is recovering some of the net contraction that was recorded during the past 25 years. However, the deformation data suggest that little deformation is currently occurring on Mount Baker.

Hill (2007) detected gravity changes of several hundred microgals between 2005 and 2006 at locations on the flanks of Mount Baker. At some stations, a relative decrease in gravity was detected. Hill (2007) concluded that seasonal variations in snow cover and groundwater fluctuation can account for several hundred microgals of change (Hill, 2007). The Sherman Crater station that detected the large (~ 1500 μgal) increase from 1980 to 2006 may also be affected by intermittent snow cover and groundwater variations and would be sensitive to near surface variations of mass and density related to hydrothermal activity in Sherman Crater. A gravity increase could accumulate from groundwater recharge or precipitation of new minerals from solution in the shallow hydrothermal system near the gravity station during the past quarter century.

The large Sherman Crater gravity signal is inconsistent with the expected gravity trend observed at the Crag View station, which suggests that much of the mechanism for gravity increase at SHRM is local to that site. A deep source of mass or density change should also produce a significant gravity increases ($\sim \frac{1}{2}$ as much) at Crag View as well as Sherman Crater. The combined effects of seasonal snow and ice variations in Sherman

Crater and the effects of mass redistribution and density variation from mineralization in the shallow sub-crater hydrothermal system might provide the mechanism for the Sherman Crater gravity anomaly without similar scale variations at the intermediate flank sites. However, due to the sparse density of the gravity data and large variability in the data from large non-volcanic sources, few physical constraints can be placed on the magmatic system beneath Mount Baker from gravity inversion.

7.0 Conclusions

GPS resurvey of the Mount Baker trilateration network in 2006 and 2007 reveals that line-lengths have predominantly shortened over the past quarter century. The rate of shortening on any line is 2 mm/yr or less. Much of the deformation is centered on the northern flank of Mount Baker where the greatest line-length change (HDLY-RSVT) occurred at -17 ± 4 ppm. The greater uncertainties of EDM line lengths (1-2 cm) and instability of several benchmarks produces significant uncertainty for detecting strain accumulation on the southern flank of Mount Baker.

Strain accumulation across the aperture of the geodetic network indicates a net edifice contraction at a rate of -417 ± 141 nanostrain/yr. This rate of areal dilatation is distinctly different, by an order of magnitude, than the maximum expected strain accumulation from regional tectonic sources. Thus the deformation source must be local to Mount Baker. Edifice contraction implies depressurization/deflation of a source region beneath the volcano and persistent heat and gas flux from Mount Baker suggest that the deformation is driven by a magmatic or hydrothermal mechanism.

Elastic dislocation models indicate that the observed deformation can be adequately described using a point source located 1.5 km northeast of the summit at a depth of 4 to 6 km, consistent with volcanic sources of deformation detected at similar volcanoes. The point source model predicts a volume change of -2×10^6 to -16×10^6 m³ depending on the depth of the source. Whether the source mechanism is purely magmatic or hydrothermal cannot be determined with the available data; however, the deformation is likely a result to physical changes to both of these active systems inferred beneath Mount Baker. The modeling results indicate that the surface subsidence at

Mount Baker is related to a volume decrease resulting from some combination of density increase, thermal contraction, and mass loss in a shallow magma chamber and/or depressurization of a deep hydrothermal system. Observed gravity changes may partially result from a deep source but are also likely the result of near surface changes in the hydrothermal system and variations to the ice and groundwater mass in Sherman Crater.

These results have important implications for the eruptive evolution of Mount Baker and other similar volcanoes. Aseismic deformation seems to be an important component of unrest at quiescent stratovolcanoes. In the case of Mount Baker, deflation indicates the volcano is in a relaxed state, suggesting an eruption is not imminent. However, sudden inflation could indicate the addition of new magma and increase the potential for an eruption. With campaign GPS, periodic surveys of just a few benchmarks could detect this precursory event. An additional benefit of this study is an improvement in the resolution and precision of the geodetic monitoring capabilities at Mount Baker. These three-dimensional GPS data provide a new baseline to detect even smaller changes to the surface around the volcano, thus providing improved constraints on the deformation mechanism.

7.1 Future monitoring and geodetic study of Mount Baker

The surface deformation detected at Mount Baker indicates that physical changes have occurred since 1981 and that these changes are likely the result of volcanic processes. Due to the proximity of Mount Baker to population centers (**Figure 2.1**), monitoring of this volcano should be a priority (Ewert et al., 2005). The most significant

hazards from Mount Baker during the Holocene have been from flank collapse debris flows, landslides, and lahars (Scott et al., 2003b). These deposits have been identified in the surrounding low-land areas with some flows reaching as far as the Skagit River and Fraser River valleys (Scott et al., 2001). The potential for flank collapse debris flows or glacier melting from phreatomagmatic eruptions is a realistic possibility. Like the 1975 thermal event that melted much of the Sherman Crater glacier (Frank et al., 1977), renewed thermal activity could initiate a disastrous result.

The lack of significant seismic activity during the deformation period indicates that seismic monitoring alone may be insufficient to alert scientists to further changes beneath the volcano. Continued geodetic monitoring should be a part of ongoing study at Mount Baker. Due to the axisymmetric shape of common deformational sources at volcanoes (Dzurisin, 2003), the repeat occupation of only two marks on opposite sides of the edifice can provide useful deformation information by indicating either inflation or deflation of the edifice. I suggest periodic GPS measurements of GPS marks HTRP and CGVW. These marks are both installed in solid bedrock in proximity to established hiking and camping areas on Mount Baker, facilitating easy access without any glacier travel. A line between the marks (HTRP in the north, CGVW in the south) bisects much of the edifice and should provide unambiguous information on the style of deformation that may occur. Additionally, both of these marks are within 4 km of the summit, providing the greatest sensitivity to horizontal deformation (the component of deformation GPS can most accurately measure) from sources at 5-6 km depth (see **Figure 5.2**). If ongoing deformation is detected by these means, than a complete

reoccupation of the geodetic network with campaign GPS may be warranted to further characterize the deformation.

Given that GPS measurements between 2004 and 2007 (PABU, HTRP) suggest that any deformation at Mount Baker is within a velocity error of 2-3 mm/yr, I suggest that periodic occupations of HTRP and CGVW should occur at a minimum of every 5 years, unless seismic or thermal observations indicate renewed activity at Mount Baker. If the net deformation rate measured since 1981 is ongoing, a change in length between CGVW-HTRP should be detectable beyond error (~ 5 mm/yr) in 8 years from now (2015), based on the model.

Resurvey of the dry tilt sites (Frank et al., 1977; Daneil Dzurisin, pers. comm., 2006) may provide independent confirmation of the GPS to EDM survey results. To test if the observed deformation may be detectable with dry tilt, I have modeled the cumulative radial tilt from the best fit point source at the three dry tilt sites (Frank et al., 1977) located on Mount Baker. A point source model predicts ~ 8 μ rad of tilt at the proximal sites. This amount of tilt should be detectable with dry-tilt survey equipment (Frank et al., 1977).

In anticipation of renewed activity at Mount Baker, a broader geodetic network is suggested. A number of new benchmarks were installed during this study (**Figure 1.4**), but were not surveyed with GPS. To complete the broader network, I suggest additional marks at the locations indicated in Figure 1.4. These locations are selected near roads within 20 km of the summit of Mount Baker. Experience has shown that displacement measurements at these distances are important for characterizing the shape of deep (4 to 7 km) deformation sources (Dzurisin, 2003). A deformation source of similar depth

beneath Mount Baker is inferred from the results of this study, suggesting that broad field deformation study will improve the capability to characterize the source of ongoing unrest at Mount Baker.

8.0 References

- Altamimi, Z., Sillard, P. and Boucher, C., 2002. ITRF2000; a new release of the international terrestrial reference frame for earth science applications. *Journal of Geophysical Research*, 107: no.B10.
- Battaglia, M. and Segall, P., 2004. The interpretation of gravity changes and crustal deformation in active volcanic areas. *Pure and Applied Geophysics*, 161(7): 1453-1467.
- Battaglia, M., Segall, P., Murray, J.B., Cervelli, P. and Langbein, J., 2003a. The mechanics of unrest at Long Valley caldera, California. 1. Modeling the geometry of the source using GPS, leveling and 2-color EDM data. *Journal of Volcanology and Geothermal Research*, 127(3-4): 195-217.
- Battaglia, M., Segall, P. and Roberts, C., 2003b. The mechanics of unrest at Long Valley caldera, California. 2. Constraining the nature of the source using geodetic and micro-gravity data. *Journal of Volcanology and Geothermal Research*, 127(3-4): 219-245.
- Bonaccorso, A., Ferrucci, F., Patané, D. and Villari, L., 1996. Fast deformation processes and eruptive activity at Mt. Etna (Italy). *Journal of Geophysical Research*, 101(B8): 17,467-17,480.
- Bonaccorso, A., Velardita, R. and Villari, L., 1994. Ground deformation modeling of geodynamic activity associated with the 1991-1993 Etna eruption. *Acta Vulcanologica*, 4: 87-96.
- Bortleson, G.C., Wilson, R.T. and Foxworthy, B.L., 1977. Water-Quality Effects on Baker Lake of Recent Volcanic Activity at Mount Baker, Washington. *U.S. Geol. Surv. Prof. Paper 1022-B*, (29 pp.).
- Caplan-Auerbach, J., Park, M. and Hadley, S., 2007. Preliminary Results From a Temporary Seismic Network at Mt. Baker, Washington, *Eos Trans. AGU*, 88(52).
- Cayol, V. and Cornet, F.H., 1998. Effects of topography on the interpretation of the deformation field of prominent volcanoes; application to Etna. *Geophysical Research Letters*, 25(11): 1979-1982.
- Cervelli, P., Murray, M.H., Segall, P., Aoki, Y. and Kato, T., 2001. Estimating source parameters from deformation data, with an application to the March 1997 earthquake swarm off the Izu Peninsula, Japan. *Journal of Geophysical Research*, 106(B6): 11,217,11,237.

- Cervelli, P.F., Fournier, T., Freymueller, J. and Power, J.A., 2006. Ground deformation associated with the precursory unrest and early phases of the January 2006 eruption of Augustine Volcano, Alaska. *Geophysical Research Letters*, 33(18): L18304, doi:10.1029/2006GL027219.
- Chadwick, W.W., Iwatsubo, E.Y., Swanson, D.A. and Ewert, J.W., 1985. Measurements of slope distances and vertical angles at Mount Baker and Mount Rainier, Washington, Mount Hood and Crater Lake, Oregon, and Mount Shasta and Lassen Peak, California, 1980-1984. U.S. Geol. Surv. Open-File Rep. 85-205, (98 pp.).
- Decker, R.W., Hill, D.P. and Wright, T.L., 1966. Deformation measurements on Kilauea Volcano, Hawaii. *Bulletin of Volcanology*, 29: 721-731.
- Delaney, P.T. and McTigue, D.F., 1994. Volume of magma accumulation or withdrawal estimated from surface uplift or subsidence, with application to the 1960 collapse of Kilauea Volcano. *Bulletin of Volcanology*, 56(6-7): 417-424.
- Dieterich, J.H. and Decker, R.W., 1975. Finite element modeling of surface deformation associated with volcanism. *Journal of Geophysical Research*, 80(29): 4094-4102.
- Dvorak, J., Okamura, A.T., Mortensen, C. and Johnston, M.J.S., 1981. Summary of electronic tilt studies at Mount St. Helens. In: P.W. Lipman and D.R. Mullineaux (Editors), *The 1980 Eruptions of Mount St. Helens, Washington*, U.S. Geol. Surv. Prof. Paper, 1250, (844 pp.).
- Dvorak, J.J. and Dzurisin, D., 1997. Volcano geodesy; the search for magma reservoirs and the formation of eruptive vents. *Reviews of Geophysics*, 35(3): 343-384.
- Dzurisin, D., 2003. A comprehensive approach to monitoring volcano deformation as a window on the eruption cycle. *Reviews of Geophysics*, 41(1): 1001, doi:10.1029/2001RG000107.
- Dzurisin, D., 2007. *Volcano Deformation: Geodetic Monitoring Techniques*. Praxis, Chichester, UK, 441 pp.
- Dzurisin, D., Lisowski, M. and Wicks, C., in press. Continuing inflation at Three Sisters volcanic center, central Oregon Cascade Range, USA, from GPS, InSAR, and leveling observations.
- Dzurisin, D., Lisowski, M., Wicks Jr., C.W., Poland, M.P. and Endo, E.T., 2006. Geodetic observations and modeling of ongoing inflation at the Three Sisters volcanic center, central Oregon Cascade Range, USA. *Journal of Volcanology and Geothermal Research*, 150: 35-54.

- Dzurisin, D., Poland, M.P. and Bürgmann, R., 2002. Steady subsidence of Medicine Lake Volcano, Northern California, revealed by repeated leveling surveys. *Journal of Geophysical Research*, 107(B12): 2372, doi:10.1029/2001JB000893.
- Dzurisin, D., Westphal, J.A. and Johnson, D.J., 1983. Eruption prediction aided by electronic tiltmeter data at Mount St. Helens. *Science*, 221(4618): 1381-1383.
- Estey, L.H. and Martens, C.M., 1999. TEQC: The multi-purpose toolkit for GPS/GLONASS data. *GPS Solutions*, 3(1): 42-49.
- Ewert, J.W., Guffanti, M. and Murray, T.L., 2005. An assessment of volcanic threat monitoring capabilities in the United States: framework for a National Volcano Early Warning System. U.S. Geol. Surv. Open File Rep. 2005-1164, (62 pp.).
- Fournier, R.O., 1999. Hydrothermal processes related to movement of fluid from plastic into brittle rock in the magmatic-epithermal environment. *Economic Geology*, 94: 1193-1212.
- Fournier, R.O., 2007. Hydrothermal systems and volcano geochemistry. In: D. Dzurisin (Editor), *Volcano deformation: geodetic monitoring techniques*. Praxis, Chichester, UK. pp. 321-341.
- Frank, D. and Krimmel, R.M., 1980. Progress report on chemical monitoring of the subglacial stream draining Sherman Crater, Mount Baker, Washington. *EOS*, 61(6): pp 69.
- Frank, D., Meier, M.F. and Swanson, D.A., 1977. Assessment of increased thermal activity at Mount Baker, Washington, March 1975-March 1976. U.S. Geol. Surv. Prof. Paper 1022-A, (49 pp.).
- Gardner, C.A., Cynthia A., Scott, K. M., Miller, C. D., Myers, B. M., Hildreth, W., and Pringle, P. T. 1995. Potential volcanic hazards from future activity of Mount Baker, Washington. U.S. Geol. Surv. Open-File Rep. 95-0498, (16 pp.).
- Gottsmann, J., Berrino, G., Rymer, H. and Williams-Jones, G., 2003. Hazard assessment during caldera unrest at the Campi Flegri Italy: a contribution from gravity-height gradients. *Earth and Planetary Science Letters*, 211(3-4): 295-305.
- Haugerud, 2005. Digital elevation model (DEM) of Cascadia, latitude 39N-53N, longitude 116W-133W, U.S. Geol. Surv. Open-File Rep. 99-369, see <http://geopubs.wr.usgs.gov/open-file/of99-369>.
- Hildreth, W., 1996. Kulshan caldera: A Quaternary subglacial caldera in the North Cascades, Washington. *Geological Society of America Bulletin*, 108(7): 786-793.

- Hildreth, W., Fierstein, J. and Lanphere, M., 2003. Eruptive history and geochronology of the Mount Baker volcanic field, Washington. *Geological Society of America Bulletin*, 115(6): 729-764.
- Hill, K.S., 2007. Microgravity survey of Mount Baker, Washington. Masters Thesis, Western Washington University, Bellingham, WA. 128 pp.
- Hill, K.S., Crider, J.G., Williams-Jones, G., 2006. Significant gravity change detected at Mount Baker, Washington, 1975-2005. *Abstracts with Programs - Geological Society of America*, 38(5): 76.
- Hooper, A., Zebker, H., Segall, P. and Kampes, B., 2004. A new method for measuring deformation on volcanoes and other natural terrains using InSAR persistent scatterers. *Geophysical Research Letters*, 31: doi:10.1029/2004GL021737.
- Houlié, N., Briole, P., Bonforte, A. and Puglisi, G., 2006. Large scale ground deformation of Etna observed by GPS between 1994 and 2001. *Geophysical Research Letters*, 33(2): doi:10.1029/2005GL024414.
- Hyde, J.H. and Crandell, D.R., 1978. Postglacial volcanic deposits at Mount Baker, Washington, and potential hazards from future eruptions, U.S. Geol. Surv. Prof. Paper 1022-C, (17 pp.).
- Jaeger, J.C. and Cook, N.G.W., 1976. *Fundamentals of rock mechanics*. Halsted Press, London, UK, 488 pp.
- Johnson, D.J., 1995. Gravity changes on Mauna Loa Volcano. In: J.M. Rhodes and J.P. Lockwood (Editors), *Mauna Loa Revealed: structure, composition, history and hazards*. Geophysical Monograph. AGU, Washington, D.C, pp. 127-144.
- Johnson, D.J., Sigmundsson, F. and Delaney, P.T., 2000. Comment on "Volume of magma accumulation or withdrawal estimated from surface uplift or subsidence with application to the 1960 collapse of Kilauea volcano" by P.T. Delaney and D. F. McTigue. *Bulletin of Volcanology*, 61(7): 491-493.
- Larson, K.M., Bilich, A. and Axelrad, P., 2007. Improving the precision of high-rate GPS. *Journal of Geophysical Research*, 112(5): doi:10.1029/2006JB004367.
- Lipman, P.W., Moore, J.G. and Swanson, D.A., 1981. Bulging of the north flank before the May 18 eruption - Geodetic data. In: P.W. Lipman and D.R. Mullineaux (Editors), *The 1980 Eruptions of Mount St. Helens, Washington*, U.S. Geol. Surv. Prof. Paper pp. 1250, pp.143-155.
- Lisowski, M., 2007. Analytical volcano deformation source models. In: D. Dzurisin (Editor), *Geodetic Monitoring Techniques*. Praxis, Chichester, UK, pp. 279-304.

- Lisowski, M., Dzurisin, D., Denlinger, R.P. and Iwatsubo, E.Y., in press. GPS-measured deformation associated with the 2004-2006 dome-building eruption of Mount St. Helens, Washington, U.S. Geol. Surv. Prof. Paper.
- Lu, Z., Masterlark, T. and Dzurisin, D., 2005. Interferometric Synthetic Aperture Radar (InSAR) Study of Okmok Volcano, Alaska, 1992-2003: Magma Supply Dynamics and Post-emplacment Lava Flow Deformation. *Journal of Geophysical Research*, 110(B2): B02403, doi:10.1029/2004JB003148.
- Lu, Z., Masterlark, T., Power, J.A., Dzurisin, D. and Wicks, C., 2002a. Subsidence at Kiska Volcano, Western Aleutians, detected by satellite radar interferometry. *Geophysical Research Letters*, 29(18): 1855, doi:10.1029/2002GL014948.
- Lu, Z. et al., 2002b. Magmatic inflation at a dormant stratovolcano: 1996-1998 activity at Mount Peulik volcano, Alaska, revealed by satellite radar interferometry. *Journal of Geophysical Research*, 107(B7): 2134, doi:10.1029/2001JB000471.
- Malone, S.D., 1979. Gravity changes accompanying increased heat emission at Mount Baker, Washington. *Journal of Volcanology and Geothermal Research*, 6(3-4): 241-256.
- Malone, S.D. and Frank, D., 1976. Monitoring Mount Baker volcano. *Earthquake Information Bulletin*, 8(2): 21-25.
- Masterlark, T., 2007. Magma intrusion and deformation predictions: Sensitivities to the Mogi assumptions. *Journal of Geophysical Research*, 112(B6): doi:10.1029/2006JB004860.
- Masterlark, T. and Lu, Z., 2004. Transient volcano deformation sources imaged with interferometric synthetic aperture radar: Application to Seguam Island, Alaska. *Journal of Geophysical Research*, 109(B01401): doi:10.1029/2003JB002568.
- Mathworks, inc., Matlab software v.7.0, see: <http://www.mathworks.com/>.
- Mazzotti, S. et al., 2003. Current tectonics of northern Cascadia from a decade of GPS measurements. *Journal of Geophysical Research*, 108(B12): 2554, doi:10.1029/2003JB002653.
- Mazzotti, S., Dragert, H., Hyndman, R.D., Miller, M.M. and Henton, J.A., 2002. GPS deformation in a region of high crustal seismicity; N. Cascadia forearc. *Earth and Planetary Science Letters*, 198(1-2): 41-48.
- McCaffrey, R. et al., 2007. Fault locking, block rotation and crustal deformation in the Pacific Northwest. *Geophysical Journal International*, 169(3): 1315-1340.

- McGee, K.A., Doukas, M.P. and Gerlach, T.M., 2001. Quiescent hydrogen sulfide and carbon dioxide degassing from Mount Baker, Washington. *Geophysical Research Letters*, 28(23): 4479-4482.
- McTigue, D.F., 1987. Elastic stress and deformation near a finite spherical magma body: resolution of the point source paradox. *Journal of Geophysical Research*, 92(B12): 12,931-12,940.
- McTigue, D.F. and Segall, P., 1988. Displacements and tilts from dip-slip faults and magma chambers beneath irregular surface topography. *Geophysical Research Letters*, 15(6): 601-604.
- Means, W.D., 1976. *Stress and strain: Basic concepts of continuum mechanics for geologists*. Springer, London, UK, 339 pp.
- Meertens, C.M. and Smith, R.B., 1991. Crustal deformation of the Yellowstone caldera from first GPS measurements: 1987-1989. *Geophysical Research Letters*, 18(9): 1763-1766.
- Mogi, K., 1958. Relations between the eruptions of various volcanoes and the deformations of the ground surfaces around them. *Bulletin of the Earthquake Research Institute*, 36(2): 99-134.
- Moran, S.C., 2004. Seismic monitoring at Cascade volcanic centers, 2004 - Status and recommendations. U.S. Geol. Surv. Sci. Inv. Rep. 2004-5211, (28 pp.).
- Moran, S.C., Kwoun, O., Masterlark, T. and Lu, Z., 2006. On the absence of InSAR-detected volcano deformation spanning the 1995–1996 and 1999 eruptions of Shishaldin Volcano, Alaska. *Journal of Volcanology and Geothermal Research*, 150: 119-131.
- Mossop, A. and Segall, P., 1999. Volume strain within The Geysers geothermal field. *Journal of Geophysical Research*, 104(B12): 29,113-29,131.
- National elevation dataset, 2006. U.S. Geol. Surv. Fact Sheet 148-99. see: <http://ned.usgs.gov/>.
- Newman, A.V., Dixon, T.H. and Gourmelen, N., 2006. A four-dimensional viscoelastic deformation model for Long Valley caldera, California, between 1995 and 2000. *Journal of Volcanology and Geothermal Research*, 150: 244-269.
- Okada, Y., 1985. Surface deformation due to shear and tensile faults in a half-space. *Bulletin of the Seismological Society of America*, 75(4): 1135-1154.
- Pacific Northwest Geodetic Array Station data (Table 2.6), see: <http://www.geodesy.cwu.edu/>.

- Parker, K.W., 2005. The Mount Baker Project: Geology, Geodesy, and global positioning system survey in Mount Baker Wilderness, Washington, Undergraduate thesis, Western Washington University, Bellingham, WA, 74 pp.
- Poland, M., Bawden, G., Lisowski, M., Dzurisin, D., 2004. Newly discovered subsidence at Lassen Peak, southern Cascade Range, California, from InSAR and GPS. *EOS Trans. AGU* 85 (47).
- Poland, M., Hamburger, M. and Newman, A., 2006a. The changing shapes of active volcanoes: History, evolution, and future challenges for volcano geodesy. *Journal of Volcanology and Geothermal Research*, 150: 1-13.
- Poland, M.P., Bürgmann, R., Dzurisin, D., Lisowski, M., Masterlark, T., Owen, S., Fink, J., 2006b. Constraints on the mechanism of long-term, steady subsidence at Medicine Lake volcano, northern California, from GPS, leveling, and InSAR. *Journal of Volcanology and Geothermal Research*, 150: 55-78.
- Power, J.A., Stuihler, S.D., White, R.A. and Moran, S.C., 2005. Observations of deep long-period (DLP) seismic events beneath Aleutian arc volcanoes: 1989-2002. *Journal of Volcanology and Geothermal Research*, 138(3-4): 243-266.
- Prescott, W.H., 1997. GPS Processing Manual. U.S. Geol. Surv. see: <http://quake.usgs.gov/research/deformation/gps/gpmanual/index.html/>.
- Prescott, W.H., Savage, J.C. and Kinoshita, W.T., 1979. Strain accumulation rates in the western United States between 1970 and 1978. *Journal of Geophysical Research*, 84(B10): 5423-5435.
- Pritchard, M.E. and Simons, M., 2002. A satellite geodetic survey of large-scale deformation of volcanic centres in the central Andes. *Nature*, 418: 167-171.
- Radke, L.F., Hobbs, P.V. and Stith, J.L., 1976. Airborne measurements of gases and aerosols from volcanic vents on Mt. Baker. *Geophysical Research Letters*, 3(2): 93-96.
- Savage, J.C., 1988. Principal component analysis of geodetically measured deformation in Long Valley caldera, eastern California, 1983-1987. *Journal of Geophysical Research*, 93(B11): 13,297-13,305.
- Savage, J.C., Gan, W. and Svarc, J.L., 2001. Strain accumulation and rotation in the Eastern California Shear Zone. *Journal of Geophysical Research*, 106(B10): 21,995-22,007.
- Savage, J.C., Lisowski, M. and Prescott, W.H., 1981. Geodetic strain measurements in Washington. *Journal of Geophysical Research*, 86(B6): 4929-4940.

- Savage, J.C., Lisowski, M. and Prescott, W.H., 1991. Strain Accumulation in Western Washington. *Journal of Geophysical Research*, 96(B9): 14493-14507.
- Savage, J.C., Lisowski, M. and Prescott, W.H., 1996. Observed discrepancy between Geodolite and GPS distance measurements. *Journal of Geophysical Research*, 101(B11): 25,547-25,552.
- Savage, J.C. and Prescott, W.H., 1973. Precision of geodolite distance measurements for determining fault movements, *Journal of Geophysical Research*, 78 (26), pp. 6001-6008.
- Savage, J.C., Prescott, W.H. and Lisowski, M., 1987. Deformation along the San Andreas Fault 1982-1986 as indicated by frequent Geodolite measurements. *Journal of Geophysical Research*, 92(B6): 4785-4797.
- Scott, K.M., Macias, J.L., Naranjo, J.A., Rodríguez, S. and McGeehin, J.P., 2001. Catastrophic debris flows transformed from landslides in volcanic terrains: Mobility, hazard assessment, and mitigation strategies. *U.S. Geol. Surv. Prof. Paper 1630*, (59 pp.).
- Scott, K.M. and Tucker, D.S., 2003. The Sherman Crater eruptive period at Mount Baker, north Cascades; A.D. 1843 to present; implications for reservoirs at the base of the volcano. *Abstracts with Programs - Geological Society of America*, 35(6): 321.
- Scott, K.M., Tucker, D.S. and McGeehin, J.P., 2003. Holocene history of Mount Baker volcano, North Cascades. *Congress of the International Union for Quaternary Research*, 16: 162.
- Segall, P. and Matthews, M.V., 1988. Displacement calculations from geodetic data and the testing of geophysical deformation models. *Journal of Geophysical Research*, 93(B12): 14954-14966.
- Siedlecki, E.M., Schermer, E.R., 2007. Paleoseismology of the Boulder Creek Fault, Kendall, WA. *Abstracts with Programs - Geological Society of America*, 39(4): 26.
- Sigmundsson, F., Einarsson, P. and Bilham, R., 1992. Magma chamber deflation recorded by the global positioning system: the Hekla 1991 eruption. *Geophysical Research Letters*, 19(14): 1483-1486.
- Spera, F., 2000. Physical properties of magma. In: H. Sigurdsson (Editor), *Encyclopedia of volcanoes*. Academic Press, London, UK. pp. 171-190.

- Sturkell, E., Einarsson, P., Sigmundsson, F., Hreinsdottir, S. and Geirsson, H., 2003. Deformation of Grimsvotn volcano, Iceland: 1998 eruption and subsequent inflation. *Geophysical Research Letters*, 30(4): 1182,doi:10.1029/2002GL016460.
- Swanson, D.A., Casadevall, T., Dzurisin, D., Malone, S., Newhall, C., Weaver, C., 1983. Predicting eruptions at Mount St. Helens, June 1980 through December 1982. *Science*, 221(4618): 1369-1376.
- Symonds, R.B., Janik, C.J., Evans, W.C., Ritchie, B.E., Counce, D., Poreda, R.J., and Iven, M., 2003. Scrubbing masks magmatic degassing during repose at Cascade-Range and Aleutian-Arc volcanoes. U.S. Geol. Surv. Open-File Rep. 03-435, (21 pp.).
- Tabor, R.W., Haugerud, R.A., Hildreth, W. and Brown, E.H., 2003. Geologic map of the Mount Baker 30- by 60-minute quadrangle, Washington. U.S. Geol. Surv. Data Series. 205.
- Taylor, J.R., 1997. *An Introduction to Error Analysis: The study of uncertainties in physical measurements*. University Science Books, Sausalito, CA, 327 pp.
- Tucker, D., Hildreth, W., Ullrich, T. and Friedman, R., 2007. Geology and complex collapse mechanisms of the 3.72 Ma Hannegan caldera, North Cascades, Washington, USA. *Geological Society of America Bulletin*, 119(3/4): 329–342.
- Tucker, D.S. and Scott, K.M., 2006. A magmatic component in 19th century Mount Baker eruptions? Abstracts with Programs - Geological Society of America, 38(5): 75.
- Turcotte, D.L. and Schubert, G., 1982. *Geodynamics: Applications of Continuum Physics to Geological Problems*. John Wiley and Sons, New York, 450 pp.
- U.S. Geological Survey Crustal Deformation Archive, 2007. see: <http://quake.usgs.gov/research/deformation/gps/auto/MtBaker/>.
- Wallace, P., 2000. Volatiles in magmas. In: H. Sigurdsson (Editor), *Encyclopedia of volcanoes*. Academic Press, London, UK, pp. 149-170.
- Wang, K., Wells, R., Mazzotti, S., Hyndman, R.D. and Sagiya, T., 2003. A revised dislocation model of interseismic deformation of the Cascadia subduction zone. *Journal of Geophysical Research*, 108(B1): doi:10.1029/2001JB001227.
- Warren, S.N., Watters, R.J. and Tucker, D.S., 2006. Future Edifice Collapse as a Result of Active Hydrothermal Alteration and Geologic Structure at Mt. Baker, Washington: *Eos Trans. AGU*, 87(52), Fall Meet. Suppl., Abstract V53A-1746.

- Werner, C., Evans, W.C., McGee, K.A., Doukas, M.P., Tucker, D.S., Bergfeld, D., Poland, M.P. and Crider, J.G., 2007. Quiescent degassing of Mt. Baker Volcano, Washington, USA. Abstracts with Programs - Geological Society of America, 39(4): 65.
- Wicks Jr., C.W., Dzurisin, D., Ingebritsen, S., Thatcher, W., Lu, Z., Iverson, J., 2002. Magmatic activity beneath the quiescent Three Sisters volcanic center, central Oregon Cascade Range, USA. *Geophysical Research Letters*, 29(7): 10.1029/2001GL014205.
- Williams-Jones, G. and Rymer, H., 2002. Detecting volcanic eruption precursors: a new method using gravity and deformation measurements. *Journal of Volcanology and Geothermal Research*, 113: 379-389.
- Williams, C.A. and Wadge, G., 1998. The effects of topography on magma chamber deformation models: Application to Mt. Etna and radar interferometry. *Geophysical Research Letters*, 25(10): 1549-1552.
- Williams, C.A. and Wadge, G., 2000. An accurate and efficient method for including the effects of topography in three-dimensional elastic models of ground deformation with applications to radar interferometry. *Journal of Geophysical Research*, 105(B4): 8103-8120.
- Wright, T.J., Parsons, B.E. and Lu, Z., 2004. Toward mapping surface deformation in three dimensions using InSAR. *Geophysical Research Letters*, 31: L01607, doi:10.1029/2003GL018827.
- Yang, X.-M., Davis, P.M., Delaney, P.T. and Okamura, A.T., 1992. Geodetic analysis of dike intrusion and motion of the magma reservoir beneath the summit of Kilauea Volcano, Hawaii; 1970-1985. *Journal of Geophysical Research*, 97(B3): 3305-3324.
- Zebker, H.A., Amelung, F. and Jonsson, S., 2000. Remote sensing of volcano surface and internal processes using radar interferometry. In: P.J. Mouginiis-Mark, J.A. Crisp and J.H. Fink (Editors), *Remote Sensing of Active Volcanism*. Geophysical Monograph. American Geophysical Union, Washington DC, pp. 179-205.
- Zumberge, J.F., Heflin, M.B., Jefferson, D.C., Watkins, M.M. and Webb, F.H., 1997. Precise point positioning for the efficient and robust analysis of GPS data from large networks. *Journal of Geophysical Research*, 102(B3): 5005-5017.

9.0 Appendices

A. Mount Baker campaign GPS field guide

March 2008

Mount Baker GPS Field Guide



Brendan Hodge

Mount Baker GPS Campaign Field Guide

Introduction

Geodetic surveys on active volcanoes, such as Mount Baker, can provide important insights into magmatic processes beneath the volcano. The fact that surface deformation often precedes eruptions makes geodetic study a valuable monitoring tool. Mount Baker hosts a network of geodetic benchmarks installed on all aspects of the volcano. These benchmarks were first surveyed with EDM in 1981 and 1983. Campaign GPS surveys in 2004, 2006 and 2007 have resurveyed the original EDM benchmarks and new GPS marks have been installed to expand the coverage and monitoring capabilities of the geodetic network on Mount Baker. The field methods for campaign style GPS surveys on Mount Baker are outlined in this field guide. Route descriptions are given for efficient access to benchmarks around Mount Baker. Benchmark locations in latitude and longitude are given for locating the marks easily with handheld GPS.



Photo: View of Sherman Peak (upper right) and the Roman Wall looking east from the summit of Colfax Peak. Benchmark (CLFX) is seen in foreground.

How to use this Guide:

- Decide on the survey objective. Once you know what mark(s) will be surveyed, plan the approach and route to the location while considering route conditions and weather forecasts. This guide can help estimate travel times and logistics for the survey using the provided maps and route descriptions.
- Gather the appropriate survey, camping and safety gear needed for the trip. Gear recommendations are included in this guide.
- Need more information? Additional references and useful tips are also provided in this guide.

Approach

Mount Baker is accessed from the north via highway 542 or from the south via highway 20. With the exception of HDLY, LNDS, LVDV and BLDR all the remaining marks are best accessed from either the Heliotrope Ridge trailhead on the north or from the Schriebers Meadow trailhead (a.k.a. Mount Baker NRA trailhead) on the south. Travel times are from the geology building at Western Washington University. The National Forest Service (FS) publishes a nice rip resistant map of Mount Baker with FS roads and some major trails included.



Heliotrope Ridge Trailhead

Take state highway 542 from Bellingham to Glacier. Just past the Glacier Forest Service station turn right onto route 39. This road follows Glacier Creek to the Heliotrope Ridge trailhead. Approximate travel time 100 minutes.

Schriebers Meadow Trailhead

Take Interstate 5 south from Bellingham and take the Cook Rd. exit east to Sedro-Woolley. Take state highway 20 until you reach and obscure turn onto route 11 just past Birdsvie. Exit off route 11 onto route 12 and then route 13 will take you to the trailhead. The access roads to LVDV and BLDR are found off of route 11. Drive time to Schriebers Meadow is approximately 120 minutes.

Route Description Introduction

The route descriptions in this guide give general route paths that the author used to access the benchmark sites. Use the route map provided as an approximate route keeping in mind that glaciers and snow conditions change and many variations to a route may exist. Place names and landmarks may be obscure at first. Reference USGS topographic maps and the Cascades Alpine Guide by Fred Beckey for additional information on places and routes. Conditions are variable throughout the year and may influence travel times and safety on the route. Always use your best judgement and not that of this guide. Be safe and have fun!



Key to Hazards-

Steep slopes: ice axes need for self arrest, snow/ice/rock protection and crampons may be useful.

Rock fall: potential exposure to rockfall. Wearing a helmet would be a good idea.

Exposure: the benchmark or route is exposed to a potentially fatal fall from cliff.

Mosquitoes: bugs may exist at camp and will drive you insane. Bring spray!

Cravasses: potential to cross crevasses. Bring rope and rescue gear.

Bears: we saw one!

Disclaimer.....

Any reference is not a substitute for experience. Gain the appropriate skills, knowledge and experience needed to safely travel on Mount Baker. The author is not liable for any decision made by the use of this guide.

Route Descriptions

1. Landes Cleaver (LNDS) – 6 to 8 hours from car

From the Artist Point parking lot, hike Ptarmigan Ridge trail past Camp Kiser and join the glacier to traverse below the cliffs to the south. Traverse low on steep snow to gain the summit of the west Portal. Climb down to rock outcrop and ascend steep snow and ice to broad low angle col at south end of west Portal. Climb ridge and steep snow to gain passage along the bottom of ridge between exposed cliffs. Mark is located near the edge of the ridge leading toward the south-west. This mark has weathered from the outcrop and only a hole remains. I suggest installation of a mark in the west Portal to facilitate easier access. Hazards: Steep snow/ice, rock fall, crevasses.

2. Lava Divide (LVDV) – 2 to 3 hours from car

Follow faint trail through forest and meandering meadows to the base of a steep grass covered slope. Climb slope on right of cliffs and gain ridge leading toward the mark location. The mark was vandalized and only a hole remains. A new mark should be installed in bedrock on the flat clearing before the last steep step approaching the old mark location. This is also the site of an excellent camp site and water source. Hazards: mosquitoes.

3. Crag View (CGVW) – 2 to 3 hours from car

Follow Scott Paul trail to a clearing and overlook one hour from the car. Find faint trail up steep grassy slopes and follow to the mark. Mark located on top of rounded outcrop near the end of the trail. Camp sites are abundant.

4. Boulder (BLDR) – 9 to 11 hours from car

This mark is approached via one very long strenuous day or two days with a camp below the glacier (recommended). Follow a seldom traveled trail through forest until trail opens to moraines and heather. Climb moraines to base of a columnar andesite cliff requiring fifth class climbing to gain top of ridge. A fixed rope existed in 2007 to facilitate the 'scramble'. Climb steep trail through trees to gain ridge and find a flat camp near the start of the snow field. Access glacier on right side of rocky ridge and begin the slog up to the benchmark aiming for the base of the rocky cleaver bisecting the Boulder Glacier and the Talum Glacier. Stay right and follow the rocky ridge up steep snow slopes. At the last rocky outcrop find the mark on the eastern end of the ridge by walking toward Shuksan. If you can't see Shuksan, what are you doing up there?! Good bivey sites are found on the low angle bench near the mark. Hazards: Bears, rock fall, crevasses, steep slopes, exposure.

Route Descriptions

5. Colfax (CLFX) – 7 to 9 hours from car

Access to this bench mark is easiest via the standard Coleman Glacier climbers' route from the Heliotrope Ridge trailhead. Begin at the trailhead and hike 2.5 miles to the climber's camp at 6000 feet. If conditions and time allow, continue up the route and establish camp at 9,000 feet in a col between the Roman Wall and the eastern aspects of Colfax Peak. Time from TH to high camp is ~6 hours. Pay attention to snow conditions and be aware of crevasse danger along the route. From this camp the summit of Colfax peak and the bench mark is gained by crossing a broad snowfield that begins to angle up and left toward a rocky ridgeline. A burgschrund guards passage to the upper snow slopes and in favorable conditions a snow bridge may exist to permit passage. Climb up steep slopes (45) and cross the burgschrund. If the burgschrund is exposed, and passage is not possible, a variation can be climbed by accessing steep snow slopes on the southern aspect of the ridgeline down and to the left of the burgschrund. Traverse 30 meters upward to gain a set of narrow vertical chimneys. Climb the 5 meter chimney and proceed on snow by traversing above the burgschrund up to the right. Follow snow slopes to the summit of the sub peak. At the summit, descend to the south along a short rocky buttress to a moderate angle snow slope and traverse this slope to the flat col connecting the two peaks. Climb two short snow ramps to a pinnacle that appears to be the summit, this is not the summit. Walk along the snow ridge to the next and slightly higher rock pinnacle to the west and rejoice to have located the BM and Summit! The BM is located on the rock outcrop next to a vertical precipice. Hazards: crevasses, rock fall, steep slopes, exposure.

6. Thunder (THND) – 1 to 2 hours from climber's camp.

From camp ascend a rising traverse on lower angle slopes to gain the broad bowl shaped amphitheater. The mark is located near the top of the steep snow slope in an obvious pointed outcrop on the ridge crest. Good camp sites exist near the mark on flat ground. Hazards: steep snow, crevasses.

Route Descriptions

7. Roosevelt (RSVT) – 4 to 5 hours from climber's camp

From climber's camp make a long upward traverse above the rock band and head toward the low angle compression zone of the Coleman Glacier where it accumulates debris from the North Face of Mount Baker. This route has many large crevasses and requires clear weather to efficiently navigate the maze. Traverse the Coleman Glacier gaining elevation when possible. The Benchmark is at the northern tip of the lower angle end of the north ridge on Mount Baker. Gain the north ridge by either climbing the 'Hourglass Couloir' or circle around to the Roosevelt Glacier and climb steep snow bridges spanning the burschgrund along the north ridge. Either way is technical and the choice depends on conditions and preference for your cup of objective hazards. A small bivey site is possible near the mark. Hazards: Rock fall, crevasses, steep snow, exposure.

8. Heliotrope Ridge (HTRP) a.k.a, climber's camp – 2 hours from car

Follow the well traveled trail from the Heliotrope Ridge trail head to the broad bench below the start of the glacier. This site has abundant camping and a water source.

9. Deming (DMNG) – 4 to 5 hours from car

To access the Deming mark, hike the Railroad Grade trail from the Schriebers Meadow trailhead and continue up the moraine to snow slopes west of the Easton Glacier. Locate the tall, craggy outcrop and gain the top by ascending a steep snow slope right below the start of glacier ice on the Easton Glacier climbing route. A short hike over rock and snow will lead you to the mark location at an obvious location near the southern tip of the broad plateau. Excellent bivey sites are nearby. Hazards: steep snow.

10. Park Butte (PABU) – 3 to 4 hours from car.

This mark is easily accessible by the Schriebers Meadow trail to the Scott Paul trail (west), through Morotsovich Meadow and finally up the Park Butte Lookout trail (approximately 3 miles from trail head). Mark is found along the short rocky ridge, ~20 meters south of the lookout, on a small bench next to a steep cliff. If the lookout is occupied, bivey sites are found down slope where the trail meets a clear, flat area, next to the horse hitch. Hazards: exposed outcrop.

Route Descriptions

11. Sherman Crater (SHRM) – 4 to 5 hours from High Camp

Follow the well established climber route up the Easton Glacier until the base of Pooch Peak at ca. 9500 ft. Climb glacier up and right toward the saddle between Sherman Peak and Pooch Peak. Mark is in small boulder on edge of Sherman Crater (or was). A good camp is found on the crater glacier if conditions permit passage over the crevasse between the glacier and the crater rim. Hazards: Crevasses, steep slopes, rock fall.

12. Cockscomb (CXCM) – 6 to 7 hours from climber's camp

Cross the Coleman Glacier as for Roosevelt but continue staying high close to the north ridge and find a line past large crevasses on the Roosevelt Glacier. Ascend the first snow field above the start of the Cockscomb cleaver. Climb up steep snow past a loose rock band and head for a lone boulder on the second snow field. From here, traverse up and to the left to gain ridge overlooking the Mazamas Glacier and the Dorr Fumarole field. There is a large burschrund guarding the access to the top of the ridge. If possible, climb up the ridge and cross the snow bridge on the right (north side) of the burschrund. Otherwise, traverse left on steep snow below the burschrund to try to gain the ridge. A nice flat and sheltered snow platform is found near the mark which is located on the ridge crest. Fix a rope to prevent a slip from ridge to the glacier below. Hazards: crevasses, rock fall, steep slopes, exposure.

13/17. Forest (FRST) – 2 to 3 hours from CGVW

Traverse snow slopes by crossing rocky ridges below Crag View while making a descent toward the Squak Glacier. Cross the glacier and descend toward a small passage between the Squak and a rocky ridge. Find a path through moraines to a steep grassy slope below the last bunch of trees on the ridge crest. Gain the ridge crest and descend down while keeping to the left until you reach the edge of the ridge overlooking the Talum Glacier. Follow the ridge to a sandy knoll and find the mark in a small rock near a bush on the southern edge of the knoll. Alternatively, hike Crag View and traverse high on the Squak Glacier to gain the passage at the end of Forest Divide and descend the ridge to the mark. The route to FRST from TALM requires some clever route finding through the complex terrain below the Talum Glacier. Exit the Boulder Glacier at the bottom of the Talum cleaver and either descend and navigate through the debris or ascend higher to traverse on the Talum glacier and gain Forest Divide. The lower route may require some technical climbing to pass intermittent cliff bands, while the high route is longer. We took the lower way, it was more interesting but maybe not much quicker. Hazards: rock fall, crevasses, steep slopes, mosquitoes.

Route Descriptions

14. Crag View (CRAG) – 30 minutes from CGVW

Climb talus or snow to the ridge crest and follow to find mark in sketchy rock overhanging the west side of Crag View. A new GPS mark is installed in hole from vandalized EDM mark. The mark is believed to be moving from gravity and therefore a resurvey would not benefit deformation study. Follow ridge by down-climbing an exposed traverse to gain the Squak Glacier to access Talm, Forest or Sherman sites. Hazards: exposure.

15/16. Talum (TALM) – 3 to 7 hours from CGVW depending on route

Approaching this mark presents several options. The choice of option depends on your skill/risk level and if you are also going to survey FRST in the same trip. I found it made the most logistical sense to survey TALM the first day. Move the survey to FRST the second and then hike out on the third. Make sure to carry adequate battery power for such a long survey time. 10 Ah of power should do it. Approach times to Talum depend on the acceptable risk level of the team. After crossing the Talum Glacier you are faced with two options. (1) Climb (remember you have a heavy pack) up a steep talus slope with many loose rocks and tenuous foot and hand holds aiming for the notch north of the pinnacle on the Talum Cleaver. Each member must be comfortable with fifth class climbing and serious exposure. Two hours of difficult (yet safer) glacier travel is avoided. A Red Socks hat was lost here in 2007. (2) Descend Talum glacier to the base of the ridge where a passage is possible onto the Boulder Glacier. Climb the Boulder Glacier following the ridge to a flat bivey site near the large notch in the ridge. The bench mark is on the ridge and may require a few rock moves depending on the snow level at the time. Talum is a difficult survey. Bring good help. Hazards: steep slopes, crevasses, rock fall, exposure.

18. Hadley (HDLY) – 6 to 10 hours.

Hadley is the only mark I did not survey in 2006 or 2007. Suggested route is from the Wells Creek road up Cougar Divide to Chowder Ridge via a steep traverse on the west face of Hadley Peak.

Benchmark Locations

#	Station Name	GPS Code	Survey Date	Elapsed time (hours)	Location		Elevation	
					Latitude (°N)	Longitude (°E)	meters	feet
1	Park Butte	PABU	9/25/2004	15	48.7165	-121.8563	1645	5397
			7/8/2006	21	48.7165	-121.8563	1645	5397
			8/15/2007	20	48.7165	-121.8563	1645	5397
2	Deming	DMNG	7/22/2006	20	48.7486	-121.8406	2032	6667
			7/29/2006	11	48.7486	-121.8406	2032	6667
3	Colfax	CLFX	6/23/2006	8	48.7712	-121.844	2857	9373
4	Cockscomb	CXCM	7/24/2007	17	48.7873	-121.8146	2754	9035
5	Boulder	BLDR	8/19/2006	22	48.775	-121.7945	2370	7775
6	Talum	TALM	8/29/2007	14	48.7607	-121.7955	2188	7177
7	Sherman Crater	SHRM	7/29/2006	5	48.7677	-121.8181	2971	9747
			7/28/2007	20	48.7677	-121.8181	2971	9747
9	Roosevelt	RSVT	7/25/2006	17	48.7861	-121.8267	2540	8333
11	Thunder	THND	9/4/2004	21	48.7806	-121.878	2154	7067
			6/28/2006	16	48.7806	-121.878	2154	7067
12	Crag View	CRAG	9/5/2007	17	48.7411	-121.815	1966	6450
13	Landes Cleaver Forest	LNDS	9/15/2006	16	48.8022	-121.7858	2049	6722
			8/30/2007	15	48.7427	-121.7846	1566	5139
16	Hadley	HDLY	8/12/2004	12	48.813	-121.8225	2223	7293
17	Lava Divide	LVDV	8/22/2006	19	48.779	-121.7454	1670	5479

The table above gives the name, location in latitude/longitude, and elevation for each benchmark on Mount Baker. Also shown is the date of first GPS survey and the elapsed time of data collection.

Equipment

Static campaign GPS survey equipment checklist

Backcountry configuration

- 1.) Trimble 5700 unit
- 2.) Geodetic antennae
- 3.) Tribrach
- 4.) Optical plummet (optional)
- 5.) Puck w/adapter
- 6.) Measuring pole
- 7.) Antennae cable
- 8.) Tripod
- 9.) Compass

Power Supply

- 1.) Battery(s)
- 2.) Battery cable
- 3.) Solar Panel/with converter (if necessary)

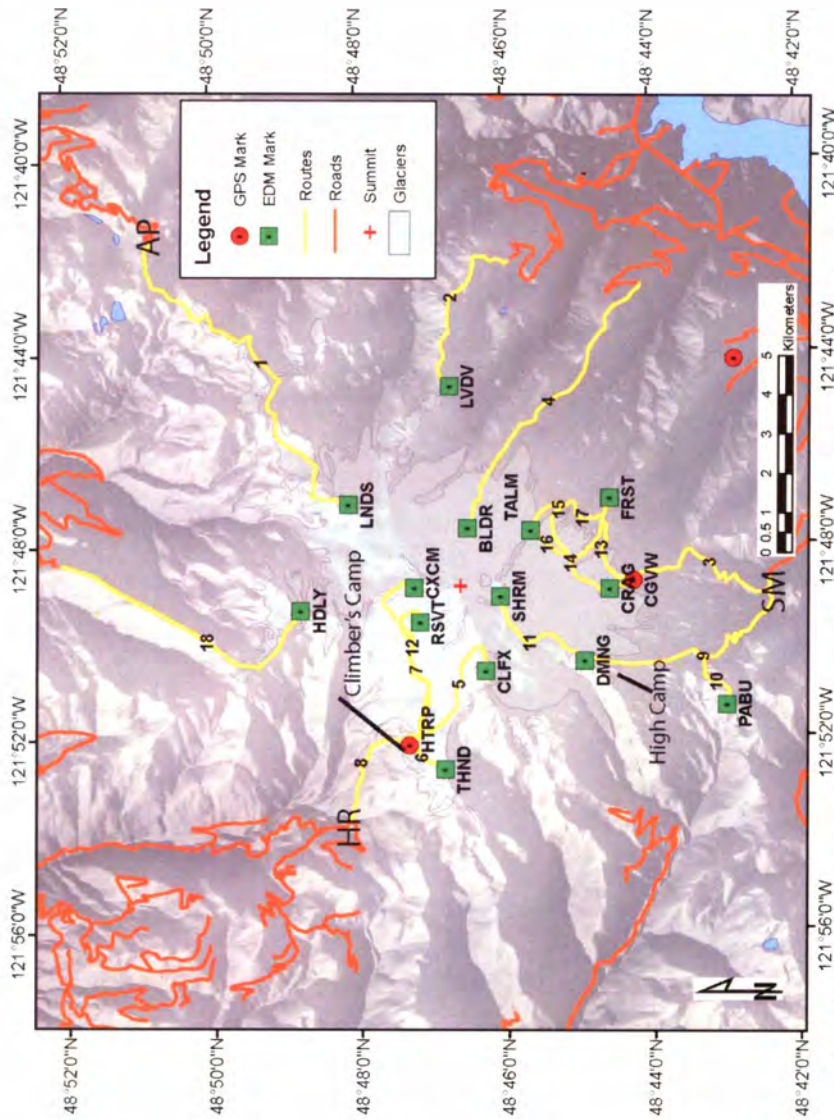
Field Gear

- 1.) Field notebook/pencil
- 2.) Digital camera
- 3.) 6mm rope (10m)
- 4.) Sand bags (3)
- 5.) GPS (handheld)

A note on camping equipment

Lite is right on backcountry travel. Good gear goes a long way to making a tough situation more pleasurable if not preventing discomfort altogether. Experience goes a long way to knowing what is necessary and what is not. With the added weight of the GPS equipment, every gear decision becomes important. Bring what you will need, not what you might need. Nothing more. The one exception is a well stocked backcountry first-aid kit. You probably wont need it but will wish you had one if you do. Unlike the portable espresso maker.

Route Map



The location of EDM (green) and GPS (red) benchmarks on Mount Baker. Routes to mark is given by the yellow lines and referenced by number. Forest service roads are indicated by orange line. Trail heads Artist Point (AP), Heliotrope Ridge (HR), and Schriebers Meadow (SM)

B. Digital resources (on Compact Disc)

B.1. Raw and processed GPS data

B.2. Matlab code used in this thesis

B.3. GIS data

B.4. Copies of figures and thesis

B.5. Field Notes

10. Curriculum Vitae

Brendan E. Hodge

PO Box 2084
Bellingham, WA 98227
Mobile: 360.223.3052
Email: brendan.hodge@gmail.com

Professional Preparation

- 2008 **M.S. Geology**, emphasis in geophysics
Western Washington University, Bellingham, Washington
Advisor: Dr. Juliet Crider
Thesis: Using GPS to characterize surface deformation of an active
 stratovolcano, Mount Baker, Washington
- 2004 **B.S. Geology**, *with honors*
Fort Lewis College, Durango, Colorado
Minor: Geographic Information Systems (GIS)
Thesis: Distribution and orientation of magma tube structures in the south
 dike at Ship Rock, New Mexico

Professional Experience

- 2008 Operations Scientist
GNS Science, GeoNet project
Lower Hutt, Wellington, New Zealand
- 2007 Science Intern
USGS Hawaiian Volcano Observatory (HVO)
Hawaii Volcanoes National Park, Hawaii
- 2005-2007 Research/Teaching Assistant
Western Washington University
Bellingham, Washington
- 2004-2005 GRA Technical Researcher
Los Alamos National Laboratory
Los Alamos, New Mexico
- 2002 GIS Technician
ESC Inc. (Electrical Systems Consultants)
Durango, Colorado

2002 GPS Field Technician
 Landmark Geographic Services
 Durango, Colorado

Instrument Experience

2007 Continuous GPS installation on Mt. Rainier, WA with Cascades Volcano
 Observatory. PI: Dr. Michael Lisowski.
2006-2007 Campaign style GPS and broadband seismometer installation at Mt.
 Baker, WA with WWU.
2007 Seminar on seismometer installation with Guralp representative.
2006 Experience with ground penetrating radar, seismic refraction and magnetic
 surveys.

Laboratory Experience

2007 Analytical elastic dislocation modeling and inversion using MATLAB.
2007 Interferometric synthetic aperture radar (InSAR) processing using
 GAMMA software on Linux.
2005 Geospatial modeling and code development in ArcGIS and
 ArcObjects.

Teaching Experience

2005-2006 Laboratory instructor for introductory geology and physical geology lab
 sessions. Responsible for preparation, presentation and evaluation of
 course curriculum for 90+ students from science and non-science
 backgrounds.
2002 Teaching assistant for survey course involving evaluation of lab
 exercises and field assistance.

Academic Awards and Scholarships

2004 Nominated Sigma Xi associate member
2004 RMAG Neal J. Harr Outstanding Senior Award
2001-2003 Mark Welter Memorial Geology Scholarship
1999 Fort Lewis College Dean's Scholarship

Research Grant Awards

2006 USGS, Jack Kleinman fellowship for volcanic research
2006 Geological Society of America, grants in aid of research
2006 Mazamas, grant for graduate research
2006 WWU Geology Department field research grant

Professional Affiliations

2005 Geological Society of America
2005 American Geophysical Union
2004 Sigma Xi, Associate Member
2004 American Alpine Club

Professional Publications and Abstracts

Hodge, B.E. and Crider, J.G., 2007
Characterizing magmatic activity at Mount Baker, Washington with inversion of slope distance data. American Geophysical Union Fall Conference 2007.

Hodge, B.E. and Crider, J.G., 2007
Edifice contraction from 1981 to 2006 of Mount Baker, Washington: Results from campaign GPS resurvey of EDM network Geological Society of America Abstracts with Programs, v. 39, n. 4, p. 65.